THE CFTR-BASED HIGH-THROUGHPUT SCREENING ASSAY
FOR GPCR MODULATORS

BURANEE YANGTHARA

A THESIS SUBMITTED IN PARTIAL FULFILLMENT
OF THE REQUIREMENTS FOR
THE DEGREE OF DOCTOR OF PHILOSOPHY
(PHYSIOLOGY)
FACULTY OF GRADUATE STUDIES
MAHIDOL UNIVERSITY
2008

THE CFTR-BASED HIGH-THROUGHPUT SCREENING ASSAY FOR GPCR MODULATORS

…………………………........................
Miss Buranee Yangthara
Candidate

……………………………………………
Assoc. Prof. Varanuj Chatsudthipong,
Ph.D.
Major Advisor

……………………………………………
Assistant Prof. Surasak Kantachuvesiri,
MD., Ph.D.
Co-Advisor

……………………………………...
Prof. Alan S. Verkman,
MD., Ph.D.
Co-Advisor

………………………………
Prof.Chairat Shayakul,
MD.
Co-Advisor

……………………………………………
Prof. Chumpol Pholpramool,
Ph.D. (Physiology)
Co-Advisor

………………………………....................
Prof. Banchong Mahaisavariya,
MD.
Dean
Faculty of Graduate Studies

……………………………………………
Assoc. Prof. Varanuj Chatsudthipong,
Ph.D.
Chair
Doctor of Philosophy Programme in
Physiology, Faculty of Science

Thesis
Entitled

THE CFTR-BASED HIGH-THROUGHPUT SCREENING ASSAY FOR GPCR MODULATORS

was submitted to the Faculty of Graduate Studies, Mahidol University
for the Degree of Doctor of Philosophy (Physiology)
on
August 26, 2008

………………………….......................
Miss Buranee Yangthara
Candidate

………………………………………...
Prof. Kriang Tungsanga,
MD.
Chair

………………………………………
Assoc Prof. Varanuj Chatsudthipong,
Ph.D. (Physiology and Biophysics)
Member

………………………………………...
Assistant Prof. Surasak Kantachuvesiri,
MD., Ph.D.
Member

………………………………………
Prof. Chumpol Pholpramool,
Ph.D. (Physiology)
Member

………………………………..
Prof. Banchong Mahaisavariya,
MD.
Dean
Faculty of Graduate Studies
Mahidol University

……………………………….
Prof. Skorn Mongkolsuk,
Ph.D.
Dean
Faculty of Science
Mahidol University

ACKNOWLEDGEMENT

THE CFTR-BASED HIGH-THROUGHPUT SCREENING ASSAY FOR GPCR MODULATORS

BURANEE YANGTHARA   4537109 SCPS/D

Ph.D. (PHYSIOLOGY)

THESIS ADVISOR: VARANUJ CHATSUDIPONG, Ph.D.; ALAN S. VERKMAN, MD., Ph.D.; CHUMPOL PHOLPRAMOOL, Ph.D.; SURASAK KANTACHUVESIRI, MD., Ph.D. AND CHAIRAT SHAYAKUL, MD.

ABSTRACT

G-protein coupled receptors (GPCRs) such as the vasopressin-2 receptor (V_2R) are an important class of drug targets. An efficient high-throughput screening assay was developed for GPCR-induced cAMP elevation using as read-out cAMP activation of cystic fibrosis transmembrane conductance regulator (CFTR) Cl^- channels. Fischer rat thyroid cells expressing CFTR and a halide-sensing yellow fluorescent protein (YFP-H148Q/I152L) were transfected with V_2R. Increased cell Cl^- conductance following agonist-induced cAMP elevation was assayed using a platereader from the cell fluorescence following solution I^- addition. The Z'-factor for the assay was ~0.7 with the V_2R agonist dDAVP (1 nM) as positive control. Primary screening of 50,000 small molecules yielded novel classes of 5-aryl-4-benzoyl-3-hydroxy-1-(2-arylethyl)-2H-pyrrol-2-one (V_2R_{inh} class), a V_2R antagonist, and 2-(acylamino)-3-thiophenecarboxylates (PDE_{act} class), a possible phosphodiesterase activator. The most potent compounds in the V_2R_{inh} class, V_2R_{inh}-02, fully displaced the radiolabeled vasopressin in binding experiments with the IC_{50} of ~70 nM. Through reduction of the cAMP level, the PDE_{act} inhibited not only the dDAVP-, but also cholera toxin-, forskolin-, and dibutylryl cAMP-induced transepithelial currents. Therefore, activation of phosphodiesterase was a suggested mechanism action. The in vitro properties of the V_2R_{inh} and PDE_{act} suggested their potential utility in aquaretic applications, and in conditions with pathologic elevation of cyclic nucleotide levels, respectively.

KEY WORDS: G-PROTEIN COUPLED RECEPTOR / VASOPRESSIN V_2
                        RECEPTOR / CFTR

161 pp.

การคัดกรองหาสารปรับการทำงานของรีเซพเตอร์ที่จับกับจีโปรตีน   โดยอาศัยซีเอฟทีอาร์โปรตีน (THE CFTR-BASED HIGH-THROUGHPUT SCREENING ASSAY FOR GPCR MODULATORS)

บุรณี อย่างธารา   4537109 SCPS/D

ปร.ค. (สรีรวิทยา)

คณะกรรมการควบคุมวิทยานิพนธ์: วรนุช ฉัตรสุทธิพงษ์ Ph.D.; แอลลัน เอส. เวิคแมน MD., Ph.D.; ชุมพล ผลประมูล Ph.D.; สุรศักดิ์ กัณตชูเวศิริ MD., Ph.D. และ ชัยรัตน์ ฉายากุล MD.

บทคัดย่อ

รีเซพเตอร์ที่จับกับจีโปรตีนเช่น เวโซเพรซซิน 2 รีเซพเตอร์ เป็นเป้าหมายที่สำคัญในการผลิตยา วิธีการคัดกรองหาสารปรับการทำงานของ   รีเซพเตอร์ดังกล่าวได้รับการพัฒนาขึ้นในเซลล์ต่อมไทรอยด์ของหนูฟิชเชอร์ที่มี ซีเอฟทีอาร์ เวโซเพรซซิน 2 รีเซพเตอร์ และ โปรตีนเรืองแสงสีเหลือง (เป็นตัววัดคลอไรด์) โดยวัดปริมาณไซคลิกเอเอ็มพีที่เพิ่มขึ้นหลังการกระตุ้นรีเซพเตอร์ซึ่งจะไปมีผลเพิ่มความสามารถในการนำคลอไรด์ผ่าน ซีเอฟทีอาร์(ช่องทางผ่านของคลอไรด์) วิธีคัดกรองนี้ให้ค่าซีไพรมเฟคเตอร์ 0.71 ซึ่งเข้าเกณฑ์การคัดกรองที่ได้มาตรฐานดีมาก การใช้การคัดกรองแบบใหม่นี้กับสารเคมีโมเลกุลเล็กจำนวน 50,000 โมเลกุลพบโมเลกุล 2 ชนิดซึ่งมีฤทธิ์เป็นเวโซเพรซซิน 2 รีเซพเตอร์แอนทาโกนิส (5-aryl-4-benzoyl-3-hydroxy-1-(2-arylethyl)-2H-pyrrol-2-one หรือ V_2R_{inh}) และ สารที่อาจเป็นตัวกระตุ้นฟอสฟอไดเอสเตอเรสหรือเอนไซม์ที่สลายไซคลิกเอเอ็มพี (2-(acylamino)-3-thiophenecarboxylates หรือ PDE_{act}) ตามลำดับ V_2R_{inh} ตัวที่ดีที่สุดสามารถแทนที่เวโซเพรซซินกัมมันตภาพรังสีได้ 50% ที่ความเข้มข้น 70nM ในขณะที่ PDE_{act} ยับยั้งกระแสไฟฟ้าข้ามเซลล์ และ การเพิ่มขึ้นของไซคลิกเอเอ็มพีที่เกิดจาก ดีดีเอวีพี ฟอสโคลิน และ พิษคอเลราได้ รวมทั้งยังยั้งกระแสไฟฟ้าข้ามเซลล์จากไดบิวไทริวไซคลิกเอเอ็มพีได้ ดังนั้นกลไกการออกฤทธิ์ที่เป็นไปได้มากที่สุดจึงน่าจะเป็นการกระตุ้นฟอสโฟไดเอสเตอเรส คุณสมบัติของสารเคมีทั้งสองชนิดดังกล่าวสามารถนำไปประยุกต์ใช้ในการขับน้ำออกจากร่างกาย   และใช้ในโรคหรือสภาวะที่มีการเพิ่มขึ้นอย่างผิดปรกติของไซคลิกเอเอ็มพี

161 หน้า

CONTENTS

CONTENTS (contd.)

CONTENTS (contd.)

LIST OF TABLES

LIST OF TABLES (contd.)

LIST OF FIGURES

Page

FIGURE

LIST OF FIGURES (contd.)

LIST OF FIGURES (contd.)

FIGURE

Page

LIST OF ABBREVIATIONS

5-HT	Serotonin receptor
ABC	ATP-binding cassette
AC	Adenylyl cyclase
ACTH-R	Adrenocorticotropic hormone receptor
ADPKD	Autosomal dominant polycystic kidney disease
AMP	Adenosine monophosphate
AP-1	Activator protein 1
AQP2	Aquaporin 2 water channel
A-R	Adenosine receptor
ARPKD	Autosomal recessive polycystic kidney disease
ATCH	Adrenocorticotropic hormone
ATP	Adenosine triphosphate
AVPR2	Arginine vasopressin receptor 2 gene
BR,	Bradykinin receptor
BRET	Bioluminescence resonance energy transfer
BSA	Bovine serum albumin
cAMP	Cyclic adenosine monophosphate
CCK-B /gastrin	cholecystokinin B/gastrin receptor,
CFTR	Cystic fibrosis transmembrane conductance regulator
cGMP	Cyclic guanosine monophosphate
CLTR	Cysteinyl leuktriene receptor,
CMF-PBS	Calcium and magnesium free phosphate buffer saline
CNG	Cyclic nucleotide gated channel

LIST OF ABBREVIATIONS (contd.)

CRE	cAMP responsive element
CREB	cAMP responsive element binding protein
CTX	Cholera toxin
DAG	Diacyl glycerol
dDAVP	1-deamino-8-D-arginine vasopressin
DI	Diabetes insipidus
DMEM	Dulbecco's Modified Eagle's Medium
EC_{50}	concentration to produce 50% activation
EDG	Endothelial differentiation gene receptor
EDTA	Ethylenediaminetetraacetic acid
ELISA	Enzyme-linked immunosorbent assay
ENaC	Epithelial sodium channel
EP_2-R	E-prostanoid 2 receptor
ETR	Endothelin receptor
FLIPR	Fluorescence Imaging Plate Reader
FRET	Fluorescence resonance energy transfer
FRT	Fisher rat thyroid cells
FSH-R	Follicular stimulating hormone receptor
GCG-R	Glucagon receptor
GDP	Guanosine diphosphate
GFP	Green fluorescence protein
GPCR	G-protein coupled receptor
GPK	G-protein coupled receptor kinase
G-protein	Guanine nucleotide binding protein

LIST OF ABBREVIATIONS (contd.)

GTP	Guanosine triphosphate
H_2R	H_2 histamine receptor
HRP	Horse-raddish peroxidase
HTS	High throughput screening
IC_{50}	concentration to produce 50% inhibition
IgG	Immunoglobulin G
IP	Inositol phosphate
IP_3	Inositol triphosphate
IP-R	Prostacyclin receptor,
LH-R	Luteinizing hormone receptor,
MDCK	Madin-Darby canine kidney cells
MEK/ERK	Mitogen-activated kinase kinase/extracellularly regulated kinase
MR	Muscarinic receptor
NBD	Nucleotide binding domain
NDI	Nephrogenic diabetes insipidus
NFAT	Nuclear factor of activated T cells
NKCC	Sodium-potassium- chloride cotransporter
NKR	Neurokinin
PAR	Protease-activated receptor
PBS	Phosphate buffer saline
PBS-T	Phosphate buffer saline with tween-20
PCR	Polymerase chain reaction
PDE	Phosphodiesterase enzyme

LIST OF ABBREVIATIONS (contd.)

PIP$_2$	phosphatidylinositol. 4,5-bisphosphate
PKA	Protein kinase A
PKC	Protein kinase C
PKD1	Polycystic kidney disease 1 gene
PKD2	Polycystic kidney disease 2 gene
PKHD	Polycystic kidney and hepatic disease
PVN	Paraventricular nucleus
RAAS	Renin-angiotensin-aldosterone system
SE	Standard error
SIADH	Syndrome of inappropriate antidiuretic hormone secretion
SNS	Sympathetic nervous system
SON	Supraoptic nucleus
SPA	Scintillation proximity assay
SSTR	Somatostatin receptor
STa	*E coli* heat-stable toxin
TLC	Thin layer chromatography
TRF	Time resolved fluorescence
UT-A1	Urea transporter A1
V1aR	Vasopressin V$_{1a}$ receptor
V1bR	Vasopressin V$_{1b}$ receptor
V2R	Vasopressin V$_2$ receptor
VIP-R	vasoactive intestinal peptide receptor
YFP	Yellow fluorescence protein
α-AR, β-AR	α-adrenergic receptor, β-adrenergic receptor

CHAPTER I
INTRODUCTION

G-protein coupled receptors (GPCRs) represent the largest and most versatile group of cell surface receptors (Hill, 2006). GPCRs are an important class of targets for identification of clinically useful agonists and antagonists, constituting ~15% of the total 'druggable' genome, ~25% of marketed drugs, and one fourth of the top 100 best selling drugs (Hopkins et al., 2002). GPCRs are coupled to the G-proteins, Gs or Gi, which alters cAMP concentration, or Gq, which increases cytoplasmic calcium concentration. Out of ~800 GPCR genes identified in the human genome, 190 have known functions (Wise et al., 2004), of which ~30 are the targets of available drugs (Chalmers et al., 2002). Among all of the GPCRs, Gs- and Gi-coupled receptors (see Table 1) are valuable as drug targets because they contribute a significant number of receptors to the GPCR family. Particularly, the vasopressin-2 receptor (V_2R), a Gs-coupled receptor, is of considerable interest because its antagonists have aquaretic effects in the kidney for therapy of hyponatremia associated with inappropriately high levels of the antidiuretic hormone vasopressin (Schrier et al., 2006).

The high throughput screening (HTS), a fast and efficient strategy for drug discovery, has been applied successfully in screening for GPCR modulators. An HTS assay is a major determinant of a successful screening, therefore, a number of researches are devoted to constantly improve the assays in throughput, sensitivity, simplicity, and economic feasibility. Several types of functional assays of cAMP concentration have been developed for high-throughput identification of modulators of Gs- or Gi-coupled GPCRs. The three available assay strategies include: (*i*) the competition assay, which is based on competition between endogenous and radiolabeled cAMPs for cAMP antibody binding (William, 2004); (*ii*) the reporter gene assay, where cAMP drives the expression of a reporter gene containing a cAMP response element (Hill, 2001); and (*iii*) the cAMP-dependent protein activity assay, where the cAMP-dependent activity of a target protein is measured (Rich et al., 2005).

Table 1. Examples of GPCRs and their G-proteins.

Gs	Gi/o	Gq/11	G12/13
β_1, β_2, and β_3-AR	α_2-AR	α_1-AR	PAR 1, 2, 3
H_2R	SSTR	CCK-B /gastrin	EDG-R
V_2R	5-HT	H_1R	
VIP-R	M_2R	M_3R	
GCG-R	A_1A-R	$V_{1a}R$	
ACTH-R		A_3A-R	
FSH-R		BR	
LH-R		CLT_1R	
EP_2-R		ET_AR, ET_BR	
$A_{2B}A$-R		NK_1R, NK_2R	
IP		PAR 1, 2, 3	
EDG-R		EDG-R	

β-AR = β-adrenergic receptor, α-AR = α-adrenergic receptor, H_2R = H_2 histamine receptor, VR = vasopressin V_2 receptor, VIP-R = vasoactive intestinal peptide receptor, GCG-R = glucagon receptor, ACTH-R = adrenocorticotropic hormone receptor, FSH-R = follicular stimulating hormone receptor, LH-R = luteinizing hormone receptor, EP_2-R = E-prostanoid 2 receptor, A-R = adenosine receptor, IP = prostacyclin receptor, EDG = endothelial differentiation gene receptor, SSTR = somatostatin receptor, 5-HT = serotonin receptor, MR = muscarinic receptor, BR = bradykinin receptor, CLTR = cysteinyl leuktriene receptor, ETR = endothelin receptor NKR = neurokinin, CCK-B /gastrin = cholecystokinin B/gastrin receptor, and PAR = protease-activated receptor.

The merits and limitations of these assays were described in Chapter III. Briefly, cAMP measurement relies heavily on the competitive immunoassay and the reporter gene assay, both of which require a long incubation time, multiple handling steps, and substrate loading. These requirements reduce the efficiency and increase the operating costs of the screening.

    The objectives of this study are as follows.

        1. Establishing an efficient cell-based HTS assay for cAMP measurement which is *(i)* sensitive, and cost-effective; *(ii)* homogeneous (no multiple handling steps); *(iii)* non-radioactive; *(iv)* miniaturizable (compatible with 96 well plate); and *(v)* economically feasible.

        2. Demonstrating a proof of the assay's concept by performing a HTS of 50,000 drug-like small molecules against vasopressin V_2 receptors, in order to identify a new antagonist. V_2R is chosen as a target because *(i)* it is a Gs-coupled receptor

which is correlated to our objective, *(ii)* none of the currently available antagonists have been discovered by a cell-based assay in HTS, and *(iii)* various important applications of the antagonists in hyponatremia, nephrogenic diabetes insipidus and polycystic kidney disease.

In this study, an efficient assay of GPCR activity for Gs- and Gi-coupled GPCRs was developed, in which cAMP was assayed from halide conductance of the cystic fibrosis transmembrane conductance regulator (CFTR) protein. CFTR halide conductance was increased following cAMP-dependent phosphorylation mediated by protein kinase A. This allowed changes in cAMP levels to be measured indirectly using an intracellular halide influx which was monitored by quenching of the yellow fluorescent protein (YFP-H148Q/I152L), a cellular halide sensor (for detailed characteristics of YFP-H148Q/I152L and its application as a halide sensor, see Appendix A). The principle of the assay was diagrammed in Figure 1. Cells expressing wild-type CFTR and a yellow fluorescent protein-based halide sensor (YFP-H148Q/I152L) were transfected with GPCRs. In the case of the Gs-coupled GPCR V_2R, agonist-induced cAMP elevation activated CFTR, which was assayed from the kinetics of I^- entry into the cells following addition of I^- solution. YFP-H148Q/I152L fluorescence was strongly quenched by I^-, with 50% reduction in fluorescence at 2-3 mM I^- (Galietta et al., 2001a). It was reported previously that the Fischer Rat Thyroid (FRT) cells expressed CFTR and YFP strongly and stably after transfection, and had other properties suitable for high-throughput screening, including low basal halide transport, rapid growth on plastic, and high electrical resistance (Galietta et al., 2001b). The FRT cells expressing YFPs and wild-type or mutant CFTRs were used to identify CFTR activators for potential therapy of cystic fibrosis (Pedemonte et al., 2005) and CFTR inhibitors for potential therapy of secretory diarrheas and polycystic kidney disease (Ma et al., 2002; Muanprasat et al., 2004). Also, in this research, (i) the CFTR-linked GPCR assay as applied to the identification of V_2R antagonists was validated, and (ii) the discovery and the characterization of 5-aryl-4-benzoyl-3-hydroxy-1-(2-arylethyl)-2H-pyrrol-2-one, which was a new competitive V_2R antagonist, and 2-(acylamino)-3-thiophenecarboxylates, a compound that reduced cyclic nucleotide level possibly through activation of phosphodiesterase enzyme, were reported.
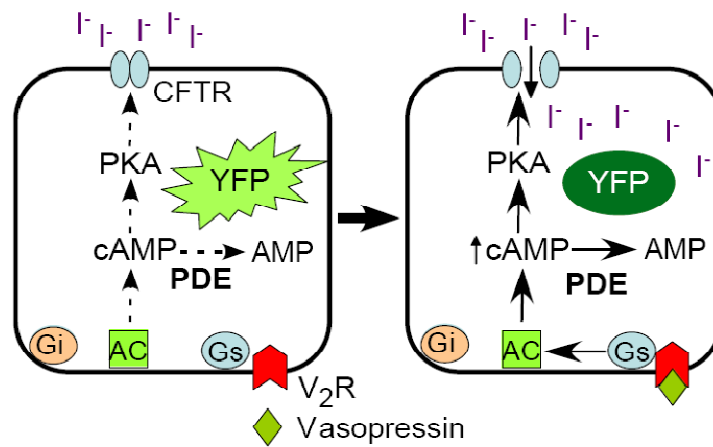
Figure 1.   The principle of the CFTR based cAMP assay for V_2R.   Binding of vasopressin to its receptor, V_2R, increases intracellular cAMP level through G-protein activation.   An increase in cAMP activates PKA, which in turn phosphorylates and opens CFTR chloride channels.   Iodide (I^-) enters the cell and quenchs YFP. V_2R = vasopressin V_2 receptor, Gs = G-protein stimulatory type, Gi = G-protein inhibitory type, PKA = protein kinase A, YFP = yellow fluorescent protein.

CHAPTER II
LITERATURE REVIEW

The literature review presents the background knowledge featuring the importance and impact of G-protein coupled receptors (GPCRs), especially the vasopressin V_2 receptors in normal physiological and pathological processes, and in drug development. This addresses the need to discover GPCR modulators with a novel mode of actions and modulators for the newly de-orphanized receptors with potential clinical applications. Then the drug discovery methods, used historically and currently, are briefly reviewed focusing on a novel high-throughput screening (HTS) which has advanced the pharmacological and academic fields tremendously. HTS assays which are of paramount importance in determining a successful HTS program are reviewed in details exposing the strengths and weaknesses of each available assay. A constant assay improvement is a pre-requisite for further advancement of the field.

G-protein coupled receptors

All GPCRs are transmembrane proteins with 7 closely spaced α-helixes with N- and C-terminals outside and inside the cell, respectively (Jacoby et al., 2006), see Figure 2. The GPCRs are important for hormone and neurotransmitter signaling, and they also act as biosensors for odorants, pheromones, light and extracellular ions. The loss-of-function mutations of GPCRs demonstrate clearly the importance of this receptor family. For example, mutation of endothelin-B receptors results in congenital bowel obstruction or Hirschsprung's disease, mutation of vasopressin V_2 receptors causes the nephrogenic diabetes insipidus due to an inability to concentrate urine, and mutation of parathyroid receptors leads to chondrodysplasia, a disorder involving abnormal breast and bone development (Carrasquillo et.al., 2002; Wysolmerski et.al., 2001). Based on the structural similarity, GPCRs can be divided into rhodopsin, adhesion, frizzled taste, glutamate, and secretin families, of which rhodopsin is the largest with 701 members.
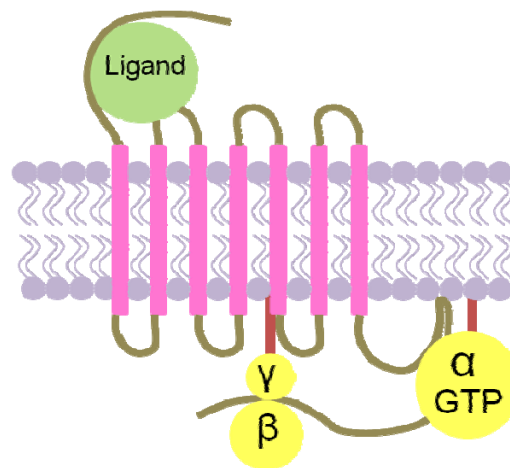
Figure 2.   The GPCR structure (pink cylinders).   The GPCR is shown as being attached to its ligand (green circle) and all 3 subunits of G-protein (yellow circles).

Binding of a ligand to a GPCR causes a change in the receptor conformation t o a form that is able to bind and activate the heterotrimeric guanine nucleotide binding protein (G-protein).   Activation of G-protein initiates a secondary messenger cascade and cellular responses specific to each G-protein subtype.   In the inactivated state, all 3 subunits of the G-protein, α, β, and γ stay united, and the α subunit binds to GDP. After binding to the ligand-receptor complex, the G-protein becomes activated, the GDP on the α subunit is replaced by GTP and finally, the α subunit dissociates from the βγ complex.   The α subunit and the βγ complex stimulate the downstream effector proteins which eventually trigger the cellular responses.   The time consumed by the α subunit to hydrolyze the GTP determines how long the G-protein will remain activated and also how long the subunits will stay apart.   The cycle of the G-protein activities is shown in Figure 3.

Based on the downstream effectors of the α subunit, G-proteins are divided into Gs, Gi/o, Gq/11, and G12/13, each of which initiates a distinct signal transduction cascade, see Figure 4.   The downstream effector of the Gs and Gi/o is adenylyl cyclase (AC) which catalyzes the production of the cyclic adenosine monophosphate (cAMP) from ATP.   The Gs activates while Gi/o inhibits the AC, causing an increase and a decrease in the level of the intracellular cAMP, respectively.   The elevated cAMP releases the catalytic subunits of protein kinase A (PKA) from the inhibition of its
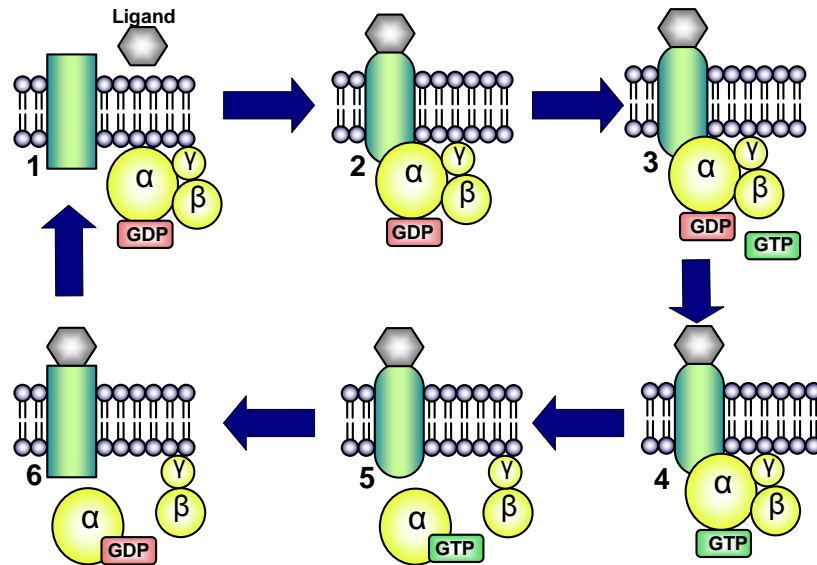
Figure 3. The cycle of G-protein activation. (1) Inactivated G-protein (yellow) with GDP binding to the α subunit. The green cylinders and the gray hexagons represent GPCRs and ligands, respectively. (2) Binding of a G-protein to a ligand-receptor complex. (3) and (4) The GDP on the α subunit is replaced by GTP. (5) A GTP-bound α subunit dissociates from a βγ complex. (6) GTP on the α subunit is hydrolysed to GDP, and G-protein returns to its inactivated state.
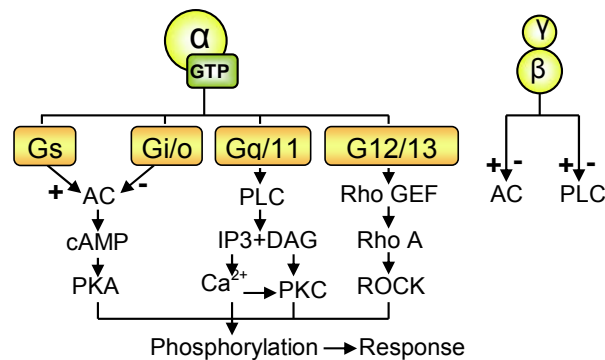
Figure 4. The signal transduction cascades initiated by different types of G-protein (see text for description). A βγ complex also modulates the AC and PLC activities. (AC = adenylyl cyclase, PKA = phospholipase C, PKC = protein kinase C, IP3 = inositoltriphosphate, DAG = diacylglycerol, Rho GEF = Rho guanine nucleotide exchange factor, and ROCK = Rho kinase)

regulatory subunits. The PKA then phosphorylates several downstream effectors

proteins which initiate the cellular responses. Degradation of the cAMP by the

phosphodiesterase enzyme (PDE) to adenosine monophosphate (AMP) reduces cAMP

concentration down to its resting level.

The Gq/11 activates the phospholipase C, an enzyme catalyzing the production

of diacylglycerol (DAG) and inositoltriphosphate (IP$_3$) from phophatidylinositol

bisphosphate (PIP$_2$). DAG and IP$_3$ lead to distinct but interdependent signal

transduction linked by the intracellular calcium. The IP$_3$ increases the intracellular

calcium concentration through opening of the ligand-gated calcium channel located at

the smooth endoplasmic reticulum. The calcium together with DAG activates the

protein kinase C (PKC), which in turn phosphorylates the effector protein in the

MEK/ERK pathway. In addition, calcium is crucial for the functions of many

calcium/calmodulin-dependent proteins.

The G12/13 is the least well characterized G-protein. It is believed to activate

small G-protein, such as Rho, through its influence on the guanine nucleotide

exchange factor (Thomsen et.al., 2005). Each GPCR prefers to couple with different

types of G-protein as shown in Table 1 (Billington et.al., 2003; Berne et.al., 1998).

After a sustained ligand binding, most GPCRs go through sequestration and

down regulation, which are powerful mechanisms to regulate GPCR signaling and

cellular responses, see Figure 5. The ligand induces changes in the receptor

conformation allowing the receptor phosphorylation by G-protein coupled receptor

kinases (GPKs), recruitment of β-arrestin and receptor endocytosis, respectively.

Clathrin-coated pits (for metabotropic glutamate, endothelin, and β$_2$ adrenergic

receptors, etc.) and caveolae (for muscarinic cholinergic receptors, etc.) are two

possible vehicles for receptor endocytosis (Dale et. al., 2001; Carman et.al., 1999;

Dessy et.al., 2000). Some receptors such as endothelin, bradykinin, angiotensin II and

β$_2$-adrenergic receptors use both mechanisms (Bremnes et.al., 2000; Lefkowitz

et.al.,1998). Losses of membranous receptors through endocytosis result in a rapid

desensitization or sequestration without changes in the total number of the receptors.

The endocytosed receptors are then recycled or degraded. Recycling returns the

functional receptors to the cell membrane after the ligand-receptor dissociation in an

early endosome. The receptor degradation by lysosome causes the receptor down
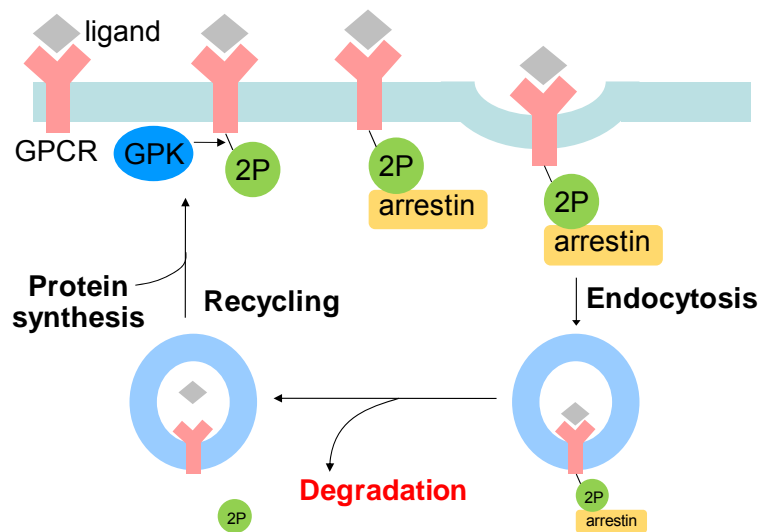
Figure 5. Desensitization of GPCRs through the receptor sequestration and lysosomal degradation. Binding of a ligand to a receptor enables the receptor phosphorylation by G-protein coupled receptor kinase (GPK). The β-arrestin is recruited to the phosphorylated receptor and endocytosis is initiated. The endocytosed receptor is recycled to the plasma membrane or destined to degradation in the lysosome.

regulation, which in contrast to sequestration there is a reduction in the total number of the receptors in the cell. The time consumed for the receptors to reappear at the plasma membrane after the endocytosis depends on the stability of the receptor-β-arrestin complex, and whether the receptors are degraded by lysosome (Shenoy et.al., 2001; Marchese et.al., 2001). The receptor-β-arrestin complex prolongs the sequestration time, while reappearance of the newly synthesized receptor at the plasma membrane is required if the receptor undergoes lysosomal degradation. Different types of GPCRs are desensitized differently via a sequestration- or degradation-predominated mechanism.

Vasopressin and its receptors

    As shown in Figure 6, vasopressin, a nano-peptide hormone, is synthesized and stored in the magnocellular neurons located at the supraoptic (SON) and the

paraventricular (PVN) regions of the hypothalamus (Treschan et.al., 2006). The axons of the neurons extend toward the posterior pituitary gland. When stimulated, the neurons release the stored hormone from its nerve terminals into the blood circulation.

A

cys-tyr-phe-gln-asn-cys-pro-arg-gly-NH$_2$

S — S

B
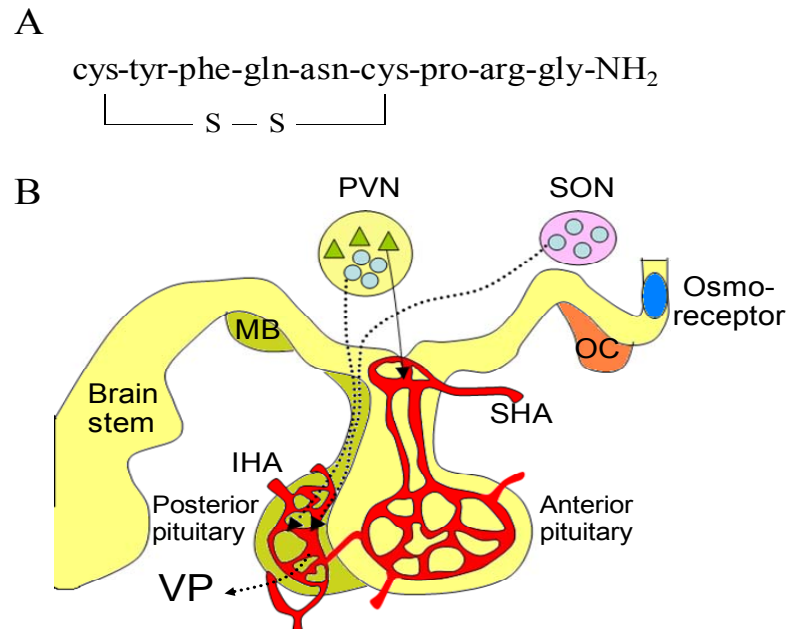
Figure 6. Amino acid compositions of the vasopressin and the neurons involved in vasopressin synthesis and secretion. A. Vasopresin is a nanopeptide hormone with a disulfide bond. B. The anterior and posterior pituitary glands. The surrounding structures are the brain stem, mamillary body (MB) and optic chiasm (OC). Superior and inferior hypophyseal arteries (SHA and IHA, respectively) supply the anterior and posterior pituitary glands, respectively. The short portal artery connects the capillary beds of the two glands. The magnocellular neurons (blue circles), located in the paraventricular (PVN) and supraoptic (SON) nuclei, synthesize and store vasopressin (VP) in the nerve terminals. The neurons send their axons (the dotted lines with the arrow heads) to the posterior pituitary gland. When exposed to the stimuli, vasopressin is released into the systemic circulation. Parvocellular neurons (the green triangles) and the other cells that can synthesize vasopressin, exist only in PVN. The axons of these neurons (the black line with an arrow head) project toward the anterior pituitary gland. The vasopressin from the parvocellular neurons exerts the local effects on the corticotropic cells of the anterior pituitary gland.

The stimuli for vasopressin secretion are (1) an increase in plasma osmolality, and (2) a reduction of the effective intravascular volume which is detected by the osmoreceptors and baroreceptors (carotid sinus, aortic arch, and left atrium), respectively (Bourque et.al., 1997). The regulation of vasopressin secretion is shown in Figure 7. In order to induce a maximal vasopressin secretion, a 2% increase in plasma osmolality or 15–20% reduction in the arterial blood pressure are required, therefore the vasopressin secretion is more sensitive to changes in osmolarity than that of volume (Baylis 1989).
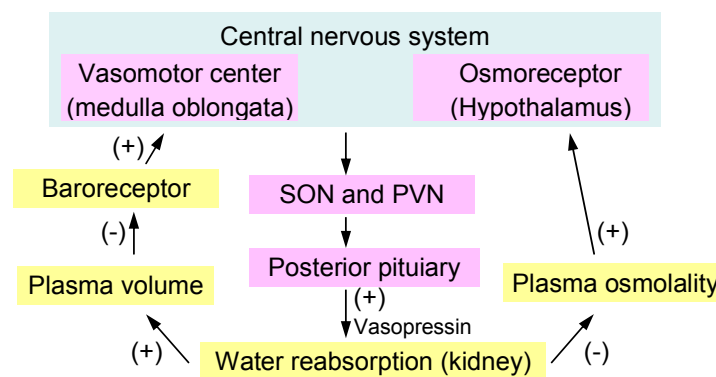
Figure 7. Regulation of vasopressin secretion. The stimuli for vassopressin secretion are plasma hyperosmolality and a low effective circulartory volume. An osmoreceptor in the hypothalamus detects an increase in the plasma osmolality and stimulates vasopressin secretion from the neurons in supraoptic (SON) and paraventricular (PVN) nuclei. An increase in plasma vasopressin concentration leads to renal water conservation which in turn corrects the plasma osmolality. Through baroreceptors, a decrease in the effective circulatory volume stimulates vasopressin secretion, and other mechanisms, namely the sympathetic nervous system and the renin-angiotensin-aldosterone system, both of which are not shown in the diagram, in an attempt to maintain the appropriate blood pressure.

A vasopressin receptor is a member of the GPCR family. It has the basic structure of GPCRs, ie with a disulfide bond between the two cysteine residues of the second and third extracellular domains, the glycosylation on the extracellular

asparagine residues, and the pamitoylation on the cysteine residues 341 and 342 in the carboxyl tail of the receptor as shown in Figure 8 (Sadeghi et.al., 1997).

The vasopressin receptor is classified, based on its affinity for vasopressin and its signal transduction cascades, into 3 types, ie V_{1a}, V_2, and V_{1b} or V_3 (Barberis et.al., 1998). The vasopressin binds to its receptor 15 A^o away from the extracellular surface at the pocket formed from a ring-like arrangement of the second to the seventh transmembrane domains (Mouillac et.al., 1995). The structure of the N-terminus and the first and the second extracellular loops determine the receptor affinity to vasopressin (Hausmann et.al., 1996).

$V_{1a}R$ and $V_{1b}R$ are coupled to Gq, while V_2R is coupled to Gs. The $V_{1b}R$ is able to activate several other types of G-protein such as Gs, and Gi, depending on the level of the receptor expression and the concentration of vasopressin (Thibonnier et.al., 1997). The $V_{1a}R$ is expressed in the vascular smooth muscle cells, liver, testis, uterus, platelet, adrenal cortex, kidney, spleen, adipocyte, and brain. The V_2R and $V_{1b}R$ are

HUMAN V1 Vascular AVP RECEPTOR
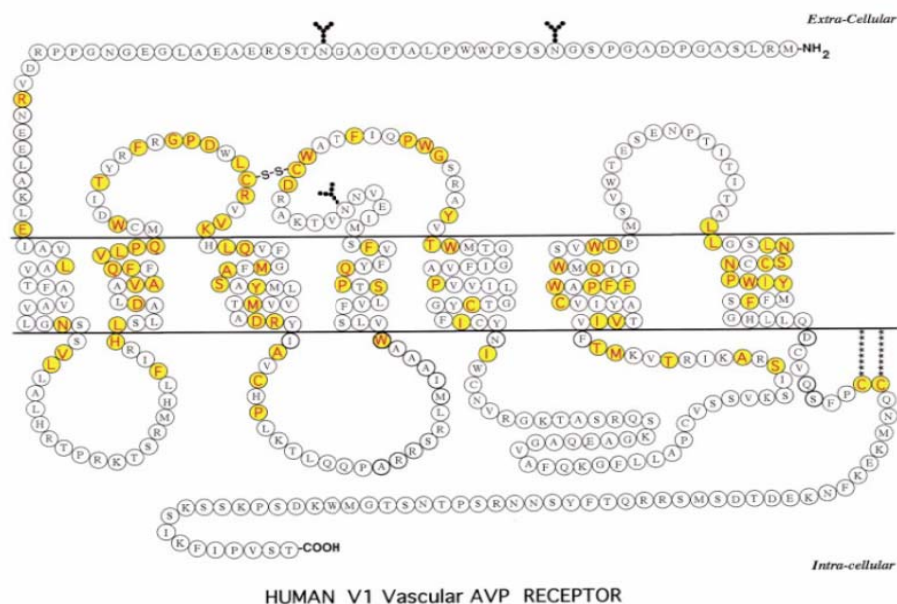
Figure 8. The structure of a vasopressin V_{1a} receptor.

expressed in the principle cells of the renal collecting ducts and in the anterior pituitary cells, respectively. The organ expressions of the vasopressin receptors in correlation with the known physiological functions are summarized in Table 2.

Table 2. Expression of the vasopressin receptors and the correlated physiological functions.

Receptors	Sites of expression	Functions
$V_{1a}R$	vascular smooth muscle	vasoconstriction (Schrier et.al., 1993)
	cardiac myocyte	(+) inotropic effects with low vasopressin and (-) effect with high vasopressin level (Walker et.al., 1988)
	Platelet	platelet aggregation (Filep et.al., 1987)
	Hepatocyte	ureagenesis, and gluconeogenesis (Bankir, 2001)
	Kidney	
	glomerular mesangial cells	contraction and reduction in ultrafiltration coefficient (Bankir, 2001)
	medullary interstitial cells	↑ prostaglandin production (Bankir, 2001)
	vasa recta	↓ inner medullary blood flow (Bankir, 2001)
	cortical and outer medullary collecting duct (luminal)	↑ prostaglandin production (Bankir, 2001)
V_2R	kidney	
	thick ascending limb of Henle's loop	↑ sodium reabsorption (Bankir, 2001)
	entire collecting duct (basolateral)	water permeability (AQP2), ↑ sodium reabsorption (ENaC), ↑ urea permeability (UT-A1)
	endothelial cells	von Willebrand factor secretion (Kaufmann et.al., 2000)
$V_{1b}R$	anterior pituitary cells	stimulate ACTH secretion
	pancreatic β cells	insulin and glucagon secretion

Physiological functions of vasopressin

Vasopressin exerts its effects on several organ systems, namely, cardiovascular, kidney, brain, and hematologic systems.

In the cardiovascular system, $V_{1a}R$ is the receptor responsible for a majority of the vasopressin actions. Sensed by baroreceptors, a decrease in the effective intravascular volume, for example, in the state of shock, stimulates the vasopressin secretion of which role is to maintain the vascular tone and the blood pressure. These actions require a high concentration of the plasma vasopressin (Holmes et.al., 2004). Vasopressin increases the vascular smooth muscle tone via modulation of the ATP sensitive K^+ channels (K_{ATP}) and nitric oxide, and the potentiation of other vasoconstrictor agents (Landry et.al., 2001). In some vascular beds, vasopressin causes the vasodilation which is possibly an action through the endothelial oxytocin receptors (Thibonnier et.al., 1999). The effects of vasopressin on the coronary artery vary depending on the arterial oxygen tension. In the hypoxic state it results in vasodilation, while in the normoxic state vasoconstriction occurs (Boyle et.al., 1990). In addition to the effects on the vascular smooth muscles, a low level of vasopressin exerts the positive inotropic effect on the cardiac myocytes; while at a high level, it triggers the opposite outcome (Walker et.al., 1988). Sustained exposure to a high concentration of plasma vasopressin can also cause the cardiac hypertrophy (Xu et.al., 1999). Vasopressin plays an important role in the renal functions, especially water reabsorption in response to changes in the plasma osmolality, see Figure 9. An increase in the plasma osmolality stimulates vasopressin secretion, and renal water reabsorption, respectively. Because of this action, vasopressin is also known as an antidiuretic hormone. The actions of vasopressin in the kidney are mediated through V_2R and $V_{1a}R$. V_2R is expressed mainly at the basolateral side of the principal cells of the renal collecting duct. The actions mediated by V_2R are as follows.

(1) Along the entire collecting duct, vasopressin increases renal water reabsorption by translocation of the aquaporin 2 (AQP2) water channels to the plasma membrane and by stimulation of the AQP2 mRNA synthesis.

(2) Increasing renal sodium reabsorption by activation of the epithelial sodium channel (ENaC) in the collecting duct, and sodium-potassium-2 chloride transporter (NKCC) in the thick ascending limb of Henle's loop (Bens et.al.,

2001; Bertuccio et.al. 2002; Snyder, 2005).

(3) Stimulation of urea reabsorption via a urea transporter, UT-A1, in the terminal inner medullary collecting duct (Bankir, 2001).
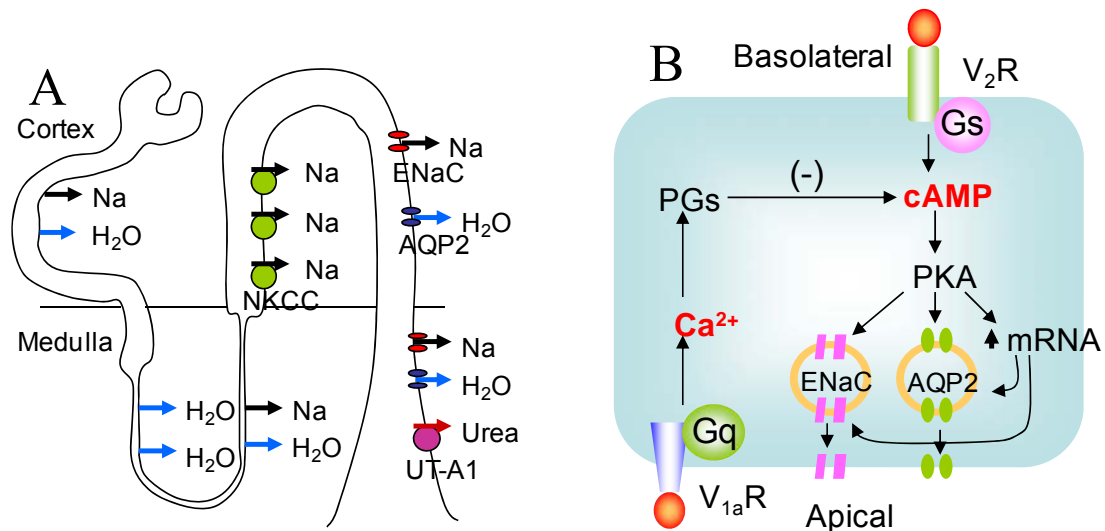
Figure 9. Vasopressin actions in the kidney. A. The transporters and the channels regulated by vasopressin. Vasopressin causes an increase in water permeability, sodium, and urea reabsorptions through AQP2, NKCC, ENaC and UT-A1, respectively. B. In the principal cells of the renal collecting duct, V_2R mediates the membrane translocation and the increase in mRNA synthesis of both ENaC and AQP2, through cAMP. An increase in the intracellular calcium by $V_{1a}R$ induces the PGs production which in turn exerts a negative effect on the cAMP cascade. (ENaC = epithelial sodium channel, UT-A1 = urea transporter A1, AQP2 = aquaporin 2, NKCC = sodium-potassium-2 chloride transporter, and PGs = prostaglandins)

An increase in the reabsorption of sodium and urea contributes to the renal medullar hyperosmolality which establishes an osmotic gradient for water reabsorption. An increase in sodium reabsorption through ENaC increases water reabsorption together with sodium. All of the effects mediated by the V_2R mentioned above employ Gs and cAMP for signal transduction. The rest of the vasopressin actions are through $V_{1a}R$, which are listed below.

(1) Reduction of only the inner medullar blood flow by vasoconstriction of the vasa recta prevents the exits of the solutes from the medullary interstitium and maintains an osmotic gradient for water reabsorption (Cowley, 2000).

(2) Attenuation of the V_2R-mediated effects by stimulation of the prostaglandin synthesis through $V_{1a}R$ at the apical side of the collecting duct and at the medullary interstitial cells. Prostaglandin reduces the level of cAMP by the stimulation of phosphodiesterase, an enzyme responsible for cAMP degradation (Bankir, 2001).

An extrarenal action of vasopressin that facilitates the renal water reabsorption is an increase in the hepatic ureagenesis by $V_{1a}R$. An increase in the level of urea contributes to the medullar osmotic gradient for water reabsorption. Vasopressin also plays a role in the hematological system as a pro-coagulation agent. It induces platelet aggregation via $V_{1a}R$, and through V_2R, stimulates the release of the von Willebrand factor and the factor VIII from the endothelial cells (Ozgonenel et.al., 2006; Kaufmann et.al., 2003). The factor VIII is an important cofactor in the thrombin activation. The functions of the von Willebrand factor are (1) binding to the platelet receptors and facilitating formation of the platelet plugs, and (2) acting as a carrier protein for the factor VIII, therefore preventing it from proteolytic degradation (Vischer et.al., 1999).

In the brain, vasopressin modulates the hypothalamo-pituitary-adrenal axis so that the stress responses meet a physiological demand. Stresses increase vasopressin secretion from the parvocellular and the magnocellular neurons, see Figure 6. Synergistically, vasopressin and corticotrophin releasing hormone, both of which are synthesized from the parvocellular neurons, stimulate the release of corticotrophin (ATCH) from the corticotrope cells in the anterior pituitary gland. The action is mediated by $V_{1b}R$ (Engelmann et.al., 2004).

Vasopressin and the cystic fibrosis transmembrane conductance regulator (CFTR)

The relationship between vasopressin and a CFTR is worth mentioning because it is central to the principle of the assay developed in this research. The CFTR is a voltage-independent epithelial chloride channel, belonging to the family of ATP-binding cassette (ABC) membrane transporters. The CFTR structure consists of two homologous repeats, see Figure 10. Each repeat consists of six transmembrane helixes

and a nucleotide binding domain (NBD). The two repeats are linked together by a large cytosolic regulatory domain. In addition to the chloride, other halides can pass through the CFTR with the conductances of Br≥Cl>I>F. The CFTR is expressed in many epithelial tissues including the intestine, reproductive tract, pancreatic ducts, sweat gland and kidney.

Normally, CFTR is in a closed state. An ATP hydrolysis by NBDs and phosphorylation of the regulatory domain by the cyclic nucleotide-dependent protein kinases (PKA and cGMP-dependent protein kinase) interact to open the channels (Hwang et.al., 1994). The ATP hydrolysis provides an energy source for the transition from closed to open states. However, the phosphorylation of the CFTR regulatory domain determines the efficiency of the ATP hydrolysis by increasing the NBD affinity to ATP, therefore it plays a crucial role in controlling the activation rate of the CFTR. The regulatory domain contains multiple phosphorylation sites for PKA, and the phosphorylation by PKA activates the channel (Cheng et.al., 1991). Agents that increase the cyclic nucleotides, such as the forskolin (cAMP), cholera toxin (cAMP), and heat-stable enterotoxin from *E. Coli* (cGMP) are shown to activate the CFTR (Kirk, 2000). The V_2R specific peptide analogue of vasopressin, dDAVP (1-deamino-8-D-arginine vasopressin), has been shown to stimulate the CFTR chloride current in the mouse renal collecting-duct cells (Chang et.al., 2005). Although there is no information on the signal transduction cascade used by vasopressin to stimulate the CFTR in physiological conditions, cAMP is the secondary messenger employed by vasopressin to stimulate CFTR-induced cystic fluid accumulation in the polycystic kidney disease (Torres VE, 2005.). The physiological roles of vasopressin-induced CFTR activation are studied mainly in the kidney where V_2R and CFTR are co-expressed. However, its role is still unclear because of the lack of significant renal impairments in the cystic fibrosis patients and in the CFTR knockout mouse models (Devuyst et.al., 2002).

Dysregulation of the vasopressin axis

Dysregulation of the vasopressin axis results in abnormalities of renal water reabsorption, and consequently of the serum sodium concentrations.

Insufficient vasopressin secretion and mutation of V_2R cause the central diabetes
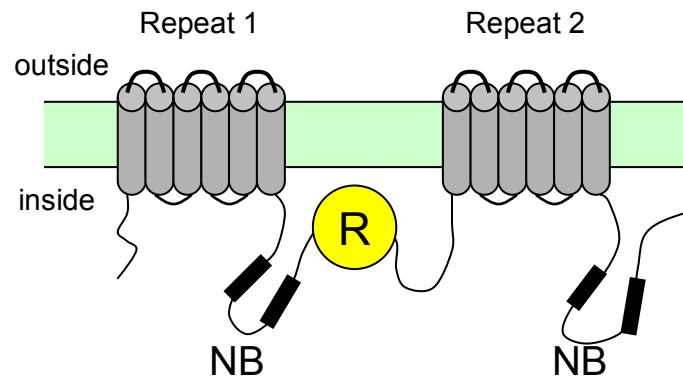
Figure 10. The structure of CFTR. CFTR is composed of two homologous repeats. Each repeat has six transmembrane domains (gray cylinder) and a nucleotide binding site (NB). The regulatory domain (R) is in between the two repeats.

insipidus (DI) and the nephrogenic DI, respectively. Without vasopressin and its functioning receptors, the kidney fails to concentrate the urine resulting in water dieresis, and finally hypernatremia develops. The central DI could be a result of a head trauma, pituitary tumor, or mutation in the prepro-vasopressin-neurophysin gene which encodes vasopressin (Fujiwara et.al., 1995). Treatments of the central DI require administration of the exogenous vasopressin. Mutations of V_2R contribute 90% of the patients with the congenital nephrogenic DI. The gene encoding V_2R (AVPR2) is located in the chromosome Xq28, therefore the disorder is inherited in an x-linked manner (Sands et.al., 2006). Most forms of AVPR2 mutation cause V_2R to fold improperly, and as a consequence the receptor is trapped intracellularly inside the endoplasmic reticulum (Aridor et.al., 1999). The patients can produce urine up to 20 liters per day (Sands et.al., 2006). Unlike the central DI, the mainstay treatment for the nephrogenic DI is adequate water intake, and the exogenous vasopressin is useless under this condition.

As opposed to the DI, a non-osmotic vasopressin release causes hyponatremia (serum sodium<135 mmol/L) as a result of inappropriate renal water conservation. Hyponatremia is a serious and the most common electrolyte disorder in the

hospitalized patients, especially those in an intensive care unit (Wong et.al.,2001; DeVita et.al., 1990). Hyponatremia becomes symptomatic when the serum sodium is less than 125mmol/L or when hyponatremia develops acutely (within less than 48 hr.) and rapidly (Verbalis, 2003). The symptoms of hyponatremia include a headache, nausea, vomiting, muscle cramp, disorientation and depression of reflexes. When severe, it causes seizure, coma, respiratory arrest, brain stem herniation and death (Adrogue et.al., 2000). Chronic slowly developed hyponatremia (>48 hr.) is asymptomatic, because of the brain adaptive mechanism through a cellular loss of electrolytes within a few hours after the onset (Gullans et.al., 1993). However, chronic hyponatremia is an independent predictor of poor prognosis and death for the heart-failure and cirrhotic patients (Borroni et.al., 2000; Kearney et.al., 2002; Lee et.al., 2003). Based on the effects on the extracellular fluid volume, vasopressin-induced hyponatremia is of two types, ie the euvolemic hyponatremia and the hypervolemic hyponatremia.

Euvolemic hyponatremia is a condition of water retention without disturbance in the extracellular fluid volume. It is commonly caused by a syndrome of inappropriate antidiuretic hormone (SIADH) secretion. Central nervous system disorders, certain types of cancer, pulmonary conditions, and drugs can all cause SIADH, see Table 3. The central nervous system disorders, affecting the inhibitory pathways from the brain stem to the hypothalamus, results in hypersecretion of vasopressin (Wong et.al., 2002). Certain types of cancer directly secrete vasopressin independent of the osmotic stimuli. For pulmonary disorders, low blood oxygen and a high carbon dioxide level stimulate a vasopressin release (Wong et.al., 2002). A mechanical ventilator, especially with a positive end expiratory pressure, results in a decrease in the venous return, which triggers the baroreceptor reflex and vasopressin secretion, respectively (Adrogue et.al., 2000).

Hypervolemic hyponatremia occurs with expansion of the extracellular fluid. This type of hyponatremia develops in patients with decompensated congestive heart failure, cirrhosis, and nephrotic syndrome, where the effective circulatory volume is reduced (Verbalis, 2003). An accumulation of the fluid in the interstitial space, resulting from an increase in the intravascular hydrostatic pressure in heart failure and from a decrease in the intravascular oncotic pressure in a nephrotic syndrome, reduces

the effective circulatory volume. For liver cirrhosis, a decrease in the intravascular oncotic pressure, together with vasodilation of the splanchnic vascular bed which in turn reduced the total peripheral vascular resistance, are the cause of arterial under

Table 3. Causes of a syndrome of inappropriate antidiuretic hormone secretion
          (SIADH).

CNS disorders	Pulmonary conditions
mass lesion	pneumonia
inflammation and	lung abscess
demyelinating diseases	bronchiectasis
acute psychosis	tuberculosis
stroke	Positive pressure ventilation
hemorrhage	
trauma	**Drugs**
Cancers	antipsychotics
small-cell lung carcinoma	antidepressants
pharyngeal cancer	anticonvulsants
pancreatic cancer	narcotics
thymoma	hallucinogens
lymphoma	ACE inhibitor
bladder cancer	oxytocin
	sulfonylureas
	clofibrate
	cyclophosphamide
	vincristine

filling (Ishikawa et.al., 2003). In an attempt to maintain the blood pressure, stimulation of the baroreceptors triggers the compensatory mechanisms, including activation of the sympathetic nervous system (SNS), renin-angiotensin-aldosterone system (RAAS), and non-osmotic release of vasopressin, see Figure 11. The SNS and RASS, by themselves, also stimulate vasopressin secretion (Goldsmith et.al., 2005). The compensatory mechanisms increase the renal sodium and water reabsorption, and also increase the peripheral vascular resistance by vasoconstriction. However, with progression of the underlying diseases, the effective circulatory volume continuously declines, and the vicious cycle of compensation carries on, despite the excessive salt and water retention, resulting in expansion of the extracellular fluid and generalized edema (LeJemtel et.al., 2007). The sustained non-osmotic release of vasopressin

causes hyponatremia and contributes to an increase in the peripheral vascular resistance through the $V_{1a}R$ mediated vasoconstriction. This leads to an increase in the cardiac afterload and worsening of the heart-failure conditions (LeJemtel et.al., 2007).
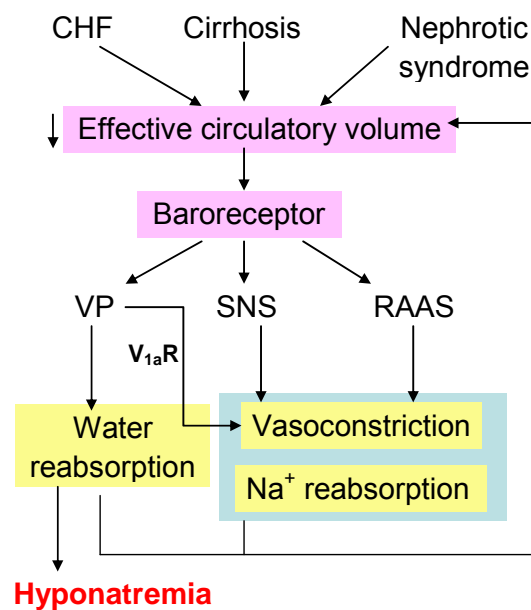
Figure 11. Non-osmotic secretion of vasopressin in hypervolemic hyponatremia. The effective circulatory volume is reduced in a congestive heart failure, cirrhosis and nephrotic syndrome. The stimulated baroreceptors trigger the compensatory responses which are vasoconstriction, and an increase in sodium and water reabsorption through the non-osmotic vasopressin secretion, sympathetic nervous system, and renin-angiotensin-aldosterone system. The vasopressin secretion causes hyponatremia and, through $V_{1a}R$, peripheral vasoconstriction. (VP = vasopressin, SNS = sympathetic nervous system, and RAAS = renin-angiotensin-aldosterone system)

Conservative treatments of hyponatremia include intravenous infusion of the hypertonic normal saline with or without furosemide diuretic, and fluid restriction (<1.0-1.5 L/day) for symptomatic and asymptomatic patients, respectively. However, fluid restriction to less than 800 ml/day increases the serum sodium concentration only 1-2 mEq/L per day, and is poorly tolerated by the patients (Haskal, 2007). Alternative

treatments for patients with persistent hyponatremia, who have poor compliance to fluid restriction regimen, are administration of demeclocycline (a tetracycline analogue), lithium carbonate, and urea (Adrogue et.al., 2000; Goh, 2004; Nguyen et.al., 2005; Verbalis, 2003). Unfortunately, these treatments suffer from significant adverse effects of the renal toxicity and are not widely used (Goh, 2004). The rate of serum sodium correction (not more than 10-12 mEq/L daily) is very important, because a rapid restoration can potentially cause central pontine myelinolysis or pontine demyelination which results in pseudobulbar pulsy and limb paralysis (Sterns et.al., 1986).

Applications of V_2R agonists

A V_2R agonist, which is given as a treatment in the following conditions, is a peptide or a chemical compound that mimics the endogenous vasopressin actions on V_2R.

    1. Central diabetes insipidus (DI)**.**

        The patients with the central DI requires administration of the exogenous vasopressin to restore urine concentrating ability.

    2. Coagulation disorders.

        Because of its pro-coagulation effects, vasopressin has long been used in many bleeding disorders as shown in Table 4 (Kasper, 1984; Franchini, 2007). In 1977, dDAVP was used for the first time as a bleeding prophylaxis for patients with mild to moderate haemophillia receiving dental extraction (Mannucci, 1977). A major advantage of using a vasopressin agonist in coagulation disorders over the intravenous administration of blood components is absence of the risk of blood-borne infections. The dDAVP is superior to vasopressin because it has no vasopressor effects (mediated through $V_{1a}R$) which reduce the cardiovascular side effects of the treatment.

        Haemophillia A is an x-linked genetic disorder with the factor VIII deficiency, where dDAVP is effective only in patients with mild to moderate diseases (Franchini, 2007). The von Willebrand's disease is a bleeding disorder with abnormality of von Willebrand's factor both quantitatively (types 1 and 3), and qualitatively (type 2). The patients with this disease develop symptoms similar to those of haemophillia A, because an absence of von Willebrand's factor leads to a dramatic increase in the proteolytic degradation of the factor VIII. An administration of dDAVP benefits only

in type 1 where the von Willebrand's factor is not completely deficient, and in some of type 2 with mild functional defects (Ozgonenel et.al., 2006).

Applications of V$_2$R antagonists

Contrary to the case of an agonist, a V$_2$R antagonist is a peptide or a chemical compound that inhibits V$_2$R-mediated vasopressin actions which benefit the following

Table 4. Bleeding disorders that benefit from dDAVP administration.

Inherited bleeding disorder	Acquired bleeding disorder

▪ von Willebrand's disease
▪ mild to moderate haemophillia A
▪ congenital platelet dysfunction
  storage pool deficiency
  primary secretion defect
  Bernard-Soulier syndrome
  Hermansky-Pudlak syndrome
  May-Hegglin anomaly
▪ Vascular disorder
  Ehlers-Danlos syndrome
  Marfan syndrome
  Heterozygous factor XI deficiency
	▪ acquired von Willebrand syndrome
	▪ acquired haemophillia A
	▪ uremia
	▪ hepatic cirrhosis
	▪ anti-platelet drug (aspirin, ticlopidine)
	▪ heparin
	▪ thrombocytopenia

diseases or conditions.

1. Hyponatremia

An obvious application of V$_2$R antagonists is in the treatment of the euvolemic and hypervolemic hyponatremia, discussed in the previous section (SIADH, congestive heart failure, and liver cirrhosis). However, the antagonist is contraindicated in the hypovolemic hyponatremia which mostly results from the conditions such as severe diarrhea and vomiting, because it can further reduce the effective circulatory volume. According to several clinical trials which will be discussed in details in the next section, the antagonist is shown to effectively induce free water excretion both in normal subjects and in hyponatremic patients. It is

superior to the conventional hyponatremia treatments, because it directly eliminates the cause of hyponatremia related to non-osmotic vasopressin secretion. And, in contrast to the intravenous infusion of hypertonic saline and diuretics, it induces water diuresis with minimal effects on the electrolyte balance (aquaretic effect). For severe hyponatremia, it is also superior to water restriction which is relatively ineffective and low in compliance.

2. The polycystic kidney disease

The polycystic kidney disease is a common renal genetic disorder which results in 5% of all end-stage renal failure cases (Gabow, 1993; Grantham 1993). A polycystic kidney is composed of multiple cysts originated from the proliferation and excessive fluid secretion from the dedifferentiated tubular epithelial cells. The autosomal dominant polycystic kidney disease (ADPKD), the third most common cause of the end-stage renal failure in the U.S.A., is a result of PKD1 or PKD2 mutation, whereas mutation in the PKHD1 gene is responsible for an autosomal recessive form (ARPKD) (Torres et.al., 2005). The PKD and PKHD genes are encoded for polycystins and fibrocystin, respectively. Both proteins are implicated in translation of the mechanical (urine flow) or chemical stimuli into the intracellular calcium fluxes (Praetorius et.al., 2001; 2004; Wang et.al., 2004). However, the mechanism how the disturbance in the calcium fluxes causes tubular dedifferentiation and cyst formation is not completely understood (Torres et.al., 2005). An increase in the intracellular cAMP level is observed in most polycystic kidney models and could be a result of

(1) A decrease in the intracellular calcium which leads to a decrease in the activity of the calcium-dependent PDE (PDE1), and an increase in the activity of the calcium inhibitable adenylyl cyclase (AC6) (Torres et.al., 2005); and

(2) An elevated plasma concentration of vasopressin as a consequence of the intrinsic urine concentrating defect, commonly found in polycystic kidney diseases (Torres et.al., 2005).

The intracellular cAMP contributes to the cyst formation through stimulation of the cellular proliferation and the fluid secretion via the CFTR chloride channels

(Torres et.al., 2005). In the animal model, administration of a vasopressin antagonist is shown to reduce the cAMP level and inhibit the disease development and progression significantly (Wang et.al.,2005).

3. Congenital nephrogenic diabetes insipidus caused by mutation in the AVPR2 gene

The V_2R antagonist is shown to increase the plasma membrane expression of a mutant V_2R by acting as a molecular chaperone which binds to a partially folded receptor and prevents it from immature destruction (Morello et.al., 2000). The antagonist acts from inside the cells, because a non-cell permeable analogue has no chaperone effects. However, the antagonist can rescue only the mutation that causes V_2R to be trapped intracellularly without having a dramatic functional defect.

Development of non-peptide V_2R antagonists

Initially peptide vasopressin antagonists are developed by modification of the vasopressin structure. However, the development is hampered by the properties of the peptide itself, namely (1) high developmental costs, (2) difficulty in drug formulation, (3) low bioavailability, and (4) its partial agonist activity. Therefore, there is an apparent need for a non-peptide antagonist, and the first one discovered by a random screening of several thousands chemical compounds at Otsuka Pharmaceutical, is a $V_{1a}R$ antagonist, OPC-21268 (Yamamura et.al., 1991). Unfortunately, this compound is not as potent in humans as in rats (Burrell et.al., 1994). By the same company, the first V_2R antagonist, OPC-31260, is derived from chemical modifications of the OPC-21268 structure (Yamamura et.al., 1992). The chemical structures, IC_{50} and Ki of OPC-31260 which is already in a nano-molar range, and other non-peptide antagonists mentioned in this topic, are shown in Table 5. Four years later, another pharmaceutical company, Sanofi-Aventis, finds a new structurally unrelated V_2R antagonist, SR-121463, also by a random screening. Both OPC-31260 and SR-121463 display a competitive antagonist property. Since then, because of its vast possible applications, several new V_2R antagonists with improved Ki and IC_{50} are released by many pharmaceutical companies. However, the designs are based on modifications of the OPC-31260 structure, and there has been no new and unrelated structure

discovered to date.   In addition to a selective V_2R antagonist, a dual V_{1a}/V_2R antagonist (VPA-985) which has relatively similar affinities for both of the receptor types, is developed.   The dual antagonist is expected to be better than the selective V_2R antagonist for heart-failure patients, because inhibition of $V_{1a}R$ results in vasodilation and reduction of the cardiac after-load, respectively (Goldsmith, 2006).

At present, many vasopressin antagonists are extensively studied and enter clinical trials for various applications as already mentioned above, see Table 6. All of the antagonists are well tolerated and able to increase the free water excretion, urine flow rate, and serum sodium concentration in healthy subjects and in patients with hyponatremia resulting from various causes.   In the congestive heart failure, the antagonists reduce the pulmonary capillary wedge pressure and the right atrial pressure, both of which indicate a decrease in fluid congestion.   However, the impact of the antagonists on the mortality rate in heart-failure patients is still needed to be clearly defined. In December 2005, the dual V_{1a}/V_2R antagonist, YM-087 (the generic name: Conivaptan, trade name: Vaprisol), was the first to be approved by the American Food and Drug Administration for hospitalized patients with euvolemic

Table 5. V_2R antagonists: structures, potencies, and developers.
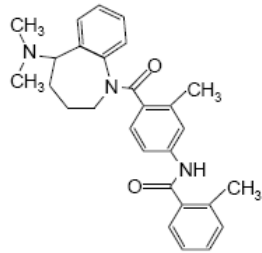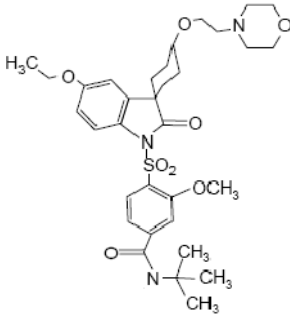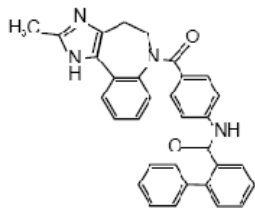
Structures			
Names	**OPC-31260**	**Satavaptan (SR-121463)**	**Conivaptan (YM087)**
Labs	Otsuka	Sanofi-Aventis	Astellas
Year	1992	1996	1997
Ki(nM) $V_{1a}R$, V_2R		304, 2.75	4.30*, 1.91*
IC$_{50}$ (nM) $V_{1a}R$, V_2R	$1.2 \times 10^{3*}$, 14.0*		3.38, 0.18
References	Yamamura et.al., 1992	Thibonnier et.al., 2001	Thibonnier et.al., 20

Table 5(continued). V_2R antagonists: structures, potencies, and developers.
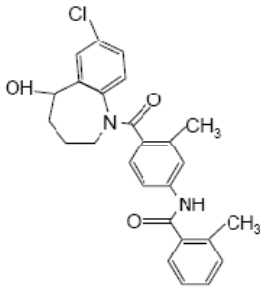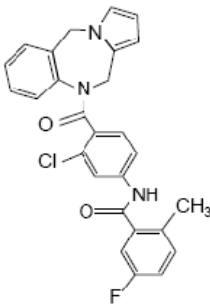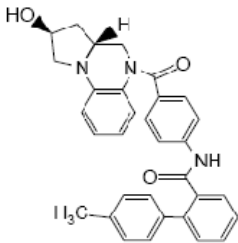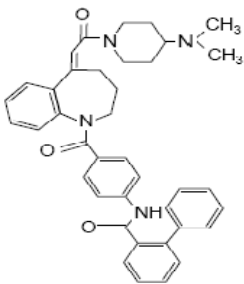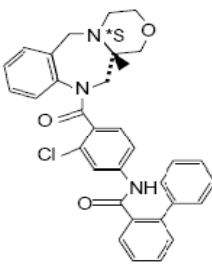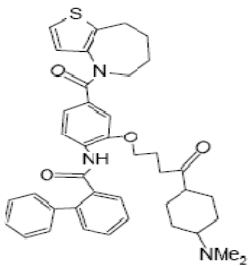
Structures			
Names	**Tolvaptan (OPC-41061)**	**Lixivaptan (VPA-985)**	**VPA-343**
Labs	Otsuka	CardioKine	Wakamoto
Year	1998	1998	1999
Ki (nM) $V_{1a}R$, V_2R	12.3, 0.43		
IC$_{50}$ (nM) $V_{1a}R$, V_2R		230, 1.2	110*, 0.77*
References	Yamamura et.al., 2001	Albright et.al., 1998	Naito et.al., 2000

Table 5(continued). V_2R antagonists: structures, potencies, and developers.

Structures			
Names	**YM-471**	**RWJ-351647**	**JTV-605**
Labs	Yamanouchi	Johnson&Johnson	Japan Tobacco
Year	2000	2004	2004
Ki (nM) $V_{1a}R$, V_2R	0.62, 1.19	24, 1	
IC$_{50}$ (nM) $V_{1a}R$, V_2R			
References	Shimada et.al., 2000	Matthews et.al., 2004	Cho et.al., 2004

The data obtained from rat vasopressin receptors.

Table 6. Clinical trials for V$_2$R antagonists**.**

Conivaptan				
Objective	**Type of study**	**N/Dose (mg)**	**Results**	**Ref.**
pharmacokinetic and pharmacodynamic	open-label, crossover	N= 6/ Dose=60 oral or 50 IV	↑urine flow rate, ↓ U$_{osm}$, oral bioavailability 44%	Burnier, 1999
hemodynamic effects in CHF	randomized, perspective, placebo-controlled	N=143 (NYHA class III, IV)/ Dose=10, 20, or 40 IV	↓PCWP and Right atrial pressure	Udelson 2001
ADVANCE	double-blinded, multicenter	N=345		Russell, 2003
efficacy in hyponatremia	placebo-controlled	N=84/ Dose=20 IV for 30 min, then 40 or 80 IV per day	↑S$_{Na}$, well tolerated	Ghali, 2006
efficacy in euvolemic hyponatremia	placebo-controlled, randomized, double-blinded	N=74/ Dose=40 or 80 oral	increase S$_{Na}$, well tolerated	Zeltser, 2007

Satavaptan				
Objective	**Type of study**	**N/Dose (mg)**	**Results**	**Ref.**
effects in SIADH	long term, double-blinded, open-label	N= 34/ Dose=25, 50	correction of S$_{Na}$, well tolerated	Soupart, 2006

IV = intravascular, Uosm = urine osmolality, CHF = congestive heart failure, NYHA = New York heart association class, PCWP = pulmonary capillary wedge pressure, ADVANCE = a dose evaluation of vasopressin antagonist in CHF patients undergoing exercise and, S$_{Na}$ = serum sodium

Table 6(continued). Clinical trials for V_2R antagonists.

Tolvaptan				
Objective	**Type of study**	**N/Dose (mg)**	**Results**	**Ref.**
effects in CHF	randomized, double-blinded	N=127/ Dose=30, 45, or 60 daily	↓BW and edema,↑S_{Na}	Gheor-g-hiade, 2003
ACTIV in CHF	multi-center, placebo-controlled, randomized, double-blinded, parallel group	N= 319	Association between ↑S_{Na} and ↓mortality	Gheor-ghiade, 2004
EVEREST (in hospitalized and worsening CHF)	multi-center, randomized, placebo-controlled, double-blinded, parallel group, dose ranging	N=2260 (in April, 2005)/ Dose=30, 60, or 90	↓ 60 days mortality only in CHF with severe congestion and renal impairment	Gheor-g-hiade, 2005
ECLIPSE	multi-center, randomized, placebo-controlled	N=181 (NYHA class III, IV)/ Dose=15, 30, 60	↓PCWP, no effects on systolic BP, systemic and pulmonary vascular resistance, or cardiac index	Lemm e-ms, 2006
SALT	multi-center, randomized, double-blinded, placebo-controlled	N=448/ Dose=15-60 per day	↑S_{Na}, well tolerated	Schrie r, 2006
Tolvaptan VS Fluid restriction in hyponatremia	multi-center, prospective, randomized, active-controlled, open-labelled	N=28/ Dose=10-60 per day or fluid restriction 1200 ml/day	Tolvaptan was more effective with no difference in adverse effects.	Gheor-g-hiade, 2006

BW = body weight, ACTIV in CHF = acute and chronic therapeutic impact of vasopressin antagonist in congestive heart failure, EVEREST = efficacy of vasopressin antagonism in heart failure: outcome study with Tolvaptan, ECLIPSE = effect of Tolvaptan on hemodynamic parameter in subjects with heart failure, BP = blood pressure, and SALT = studies of ascending levels of Tolvaptan in hyponatremia

Table 6(continued). Clinical trials for V_2R antagonists.

Objective	Type of study	N/Dose (mg)	Results	Ref.
Lixivaptan				
pharmacodynamic in patients with ascites	placebo-controlled, randomized, double-blinded	N= 5/ Dose=25,50, 100, 200, 300 oral	dose dependent aquaretic response	Guyader,2002
efficacy in hyponatremia	multi-center, randomized, placebo-controlled	cirrhosis= 33, CHF=6, SIADH=5/ Dose= 25, 125, 250	⬆ Free water clearance, ⬆ S_{Na}, ⬆ S_{osm}	Wong, 2003
efficacy in cirrhotic hyponatremia	multi-center, randomized, double-blinded	N=60/ Dose=100-200 per day	normalized S_{Na}, ⬇ Uosm and body weight	Gerbes, 2003
aquaretic effect in CHF	placebo-controlled, randomized, double-blinded	N=42 (NYHA class II, III) / Dose= 10, 30, 75, 150, 250, 400 oral	increase urine volume, well tolerated	Abraham, 2006

S_{osm} = serum osmolality

hyponatremia. Conivaptan is currently in trials for applications in congestive heart-failure (Russell et.al., 2003). Tolvaptan (OPC-41061) is also in clinical trials for its applications in heart failure, hyponatremia, cirrhosis, and polycystic kidney disease. Lixivaptan (VPA-985) and Satavaptan (SR-121463) are tested primarily for hyponatremia and cirrhosis.

V$_2$R is an important drug target, because of its various important applications. This is evidenced by an interest manifested by several pharmaceutical companies toward its development. However, currently there are only two main antagonist structures derived from random screening and structural modifications. The assay used in andom screening is of radioactive ligand binding category which is not compatible for identifying a newer generation of the V$_2$R modulators, such as an allosteric antagonist. Therefore, it is not surprising that all of the currently known V$_2$R

antagonists have competitive antagonistic activity. An allosteric antagonist binds to a receptor at a different site from that of the endogenous ligand, and some of its attractive characteristics are as follows.

a. Unlike the competitive antagonist, the presence of high endogenous ligand concentration has minimals effects on the allosteric antagonist binding.

b. Even though all of the receptors are occupied, some of the allosteric antagonists do not inhibit the receptors completely, therefore the toxicity from the receptor over-inhibition is impossible.

c. Allosteric antagonists can have higher receptor specificity than their competitive counterparts. Because the ligand binding sites of different GPCR subtypes, binding to the same endogenous, have a certain level of similarity, targeting these sites yields limited receptor specificity. Allosteric antagonists bind to a distinct site in the receptor which does not directly involve in the endogenous ligand binding. The site thus has more structural diversity and can be targeted with higher specificity.

An application of the recent drug discovery technology, namely high throughput screening, employing a cell-based assay in screening for V_2R modulators, has a promising potential in revealing a novel structure with a new mode of actions, other than the rigid competition. According to the second attractive characteristic of the allosteric antagonist mentioned above, one of the possible clinical benefits of the allosteric V_2R antagonist is its improved ability and ease to control the rates of serum sodium correction in hyponatremia, independently of dose adjustments. This benefit improves safety of hyponatremia treatments and could possibly reduce morbidity and mortality resulting from conventional treatments.

Drug discovery

Of the four possible druggable molecules (protein, polysaccharides, lipid and nucleic acid), proteins are the greatest target, because the compounds for targeting them have high specificity, low toxicity, and high potency (Hopkins et.al, 2002). Half of the experimental and marketed drug-target proteins are of 5 categories, viz GPCRs, kinases, proteases, nuclear receptors, and ion channels (Hopkins et.al., 2002).

There are 3,051 druggable protein targets identified from the human genome (Hopkins et.al., 2002), and 15% are GPCRs. The GPCRs are valuable drug targets, as evidenced by an observation that GPCRs are targeted by 25% of the hundred top-selling drugs, because (1) this receptor family contains numerous members, either orphans (excluding the sensory GPCRs, a hundred out of approximately 800 GPCR genes exist without known ligands) or of known functions; (2)they are shown to involve in several physiological and pathological processes, including those of the nervous, cardiovascular, respiratory, renal, and reproductive systems; and (3) the expressions of GPCRs mostly are tissue specific which allow GPCR modulation a high level of specificity (Klabunde T, 2002). The field of GPCR drug discovery is continuously expanding, because of the newly emerging de-orphanized receptors with potential clinical applications, and the need for GPCR modulators with a novel mode of actions, such as allosteric modulators.

There are two main strategies in drug development, ie the structure-based drug design and the random screening of diverse chemical compounds against the targets of interest. The structure-based development requires beforehand extensive information on the target structures, thus the drug discovery rate is hindered dramatically. This requirement, together with emergence of many new potential drug targets as a result of completion of the human genome project, causes the time consuming nature of the structure-based strategy to be no longer acceptable. Even though the random screening bypasses the rate-limiting step of acquiring a target structure, it is laborious and can be equally time consuming, because thousands of chemical compounds have to be tested manually at a sluggish rate of 20-50 compounds per week (Pereira et.al., 2007). In an attempt to markedly reduce the time used in random screening, an automated technology with robotic assistance, called high throughput screening (HTS), is developed in which hundreds or even thousands of chemical reactions are run at the same time. The screening rate increases from 20-50 compounds per week to 1,000-10,000 compounds per week (Pereira et.al., 2007). The early development of HTS was in the period of 1984 to 1995, but the conceptual application began from 1995 to 2000 (Pereira et.al., 2007). Nowadays, the technology has advanced dramatically with many users worldwide both in the pharmaceutical businesses and in the academic sector, representing clearly its advantages over the traditional methods.

Because of its popularity, numerous HTS assay formats are invented and some are even commercially available.

The heart of HTS is the throughput or the ability to screen as many compounds as possible against a target of interest in a short period of time. A carefully designed assay together with automation grants a desired level of throughput. An HTS assay should be simple and homogeneous. Steps, such as centrifugation, shaking, heating and cooling, should be avoided as much as possible because they require expensive automation systems and special equipment, resulting in unnecessary high operating costs. It is important and challenging to maintain the assay simplicity while maximize its sensitivity which enhances active compound identifications, enables further miniaturization, and increases the assay throughput. Taken together, the factors distinguishing an HTS assay from a traditional manual random screening assay are (1) simplicity of the assay protocol, the less steps the better; (2) automated reagent handling; (3) microtiter plates of size ranging from 96-, 384-, or 1,536-well are used as an assay container; (4) small assay volume usually <100μl; and (5) a small amount of compound used per reaction, see Table 7. Furthermore, the characteristics of an ideal HTS assay are (1) sufficient sensitivity, (2) reproducible, (3) correlation between controls and known pharmacology of the target, and (3) economically feasible. After an assay has been established its performance can be assessed statistically, using a Z' factor which is defined as follows.

$$Z' = 1 - \frac{3(\sigma_{max} + \sigma_{min})}{|\mu_{max} - \mu_{min}|}$$

The μ_{max} and μ_{min}, and σ_{max} and σ_{min} represent, respectively, the means and standard deviations of the two control groups. The Z' factor takes into account of both the means and the standard deviations of data, therefore it is a suitable parameter for assessing an assay performance (Iversen, 2006). The values of Z' factor range from 0 to 1, and the accepted range representing a good assay is 0.5-1.

Table 7. Distinct characteristics and advantages of HTS over traditional random screening.

Parameter	Traditional screening	HTS
Protocol	can be complex with several steps	few and simple steps
Assay volume	0.1-1 ml	50-100 μl
Assay format	single tube	96-, 384-, or 1,536-well plate
Reagent handling	manual	Robotic
Compound used	5-10 mg	1μg
Number of compounds	20-50/week	1,000-10,000/week
Compound diversity	limited number and diversity	unlimited number and diversity

HTS assays for GPCRs

The HTS has been applied successfully in screening for several GPCR modulators. A number of researches are devoted to improve its assay's throughput, sensitivity, simplicity and economic feasibility in order to enable HTS to identify a novel modulator **as**as fast and economical as possible. Generally, there are two types of HTS assays for GPCRs, ie a ligand binding assay, and a functional or cell-based assay. The latter is more popular and more widely utilized because of its superior characteristics as will be discussed below.

1. **Ligand binding assays.**

Many of the traditional random screening programs employ this assay either in an intact cell expressing native or recombinant receptors or in a receptor membrane preparation (Bylund et.al., 2004). The assay relies on competition between the compounds being screened and the labeled ligand in binding to the GPCR of interest. The displacement of the labeled ligand by the compound reduces the intensity of the signal detected from the labeling after a careful washing step. Labeling (a source of detectable signals), is mostly done with radioactive molecules, such as ^{125}I, and ^{3}H. The ^{125}I gives better signal intensity and specificity compared with those of ^{3}H, therefore less number of the receptors are required in a binding reaction. However, ^{125}I has a short half-life and high radioactivity, which makes equipment contamination a serious concern. Although the ligand binding assay is the only assay that can

demonstrate direct ligand-receptor interactions, it has several disadvantages as follows: (1) a requirement of radio-labeled ligands which render studies of the orphan receptors impossible; (2) a need to extensively characterize the ligands, in order to determine the best labeling site; (3) inability to distinguish between agonists and antagonists; (4) less sensitivity to allosteric compounds which could be a potent modulator despite a weak binding affinity; and (5) high costs of radioactive waste management which reduces the economic feasibility of the assay (Eglen et.al., 2007). To overcome the last disadvantage, fluorescent labeling is developed (Nouel et. al., 1997). However, the difficulty in attaching a complex fluorescent group to a ligand without disturbing its original properties and the fact that this technology is available only for peptide ligands limits its use.

   2. **Functional or cell-based assays.**

       This assay simply measures various outcomes of GPCR modulation in a form of changes in signal transduction or in the cellular responses. Therefore, when compared with the ligand binding assay which relies solely on the binding affinity, the major advantages of the functional assay are its ability to distinguish between agonists and antagonists, higher sensitivity in detection of the allosteric modulators, and similarity to an in vivo environment. Taken together, it is not surprising that the functional assay has become a dominant assay for HTS (Rees, 2002). Different parameters representing GPCR activity are measured in each assay. The more downstream the parameters are from the ligand-receptor complex the more sensitive the assay becomes, due to signal amplification.

Various measurement platforms are available for each parameter, namely radioactivity, photon absorption, and photon emission. A popular method for radioactivity detection is the scintillation proximity assay (SPA^{TM}) in which the scintillants coated on beads or plates become activated only when the radio-labeled molecules are adequately close to the scintillants by binding to the surface of the beads or plates, see Figure 12A. Despite its simplicity, the photon absorption or colorimetric method is not sufficiently sensitive for the assay miniaturization, therefore its use is relatively limited (Fan, et.al.,2007). The photon emission, namely fluorescence and chemiluminescence, is the most widely used platform world wide because of its high

sensitivity and compatibility with assay miniaturization (Fan, et.al.,2007). For fluorescence, the molecule emits light after receiving a photon excitation, while chemiluminescent emission acquires excitation energy from exothermic chemical reactions. The fluorescent signal is therefore higher in intensity when compared with that of chemiluminescence, because the intensity of the excitation photons can be adjusted accordingly to obtain the best emission outcomes. However, an increase in the undesirable background occurs at the expense of the adjustment of excitation intensity. An advantage of the chemiluminescence technology is a very low or absence of the luminescence background, because it does not need excitation photons. Bioluminescence is a luminescent emission catalyzed by some specific enzymes in a living organism. The examples of such enzymes exploited in HTS assays are:
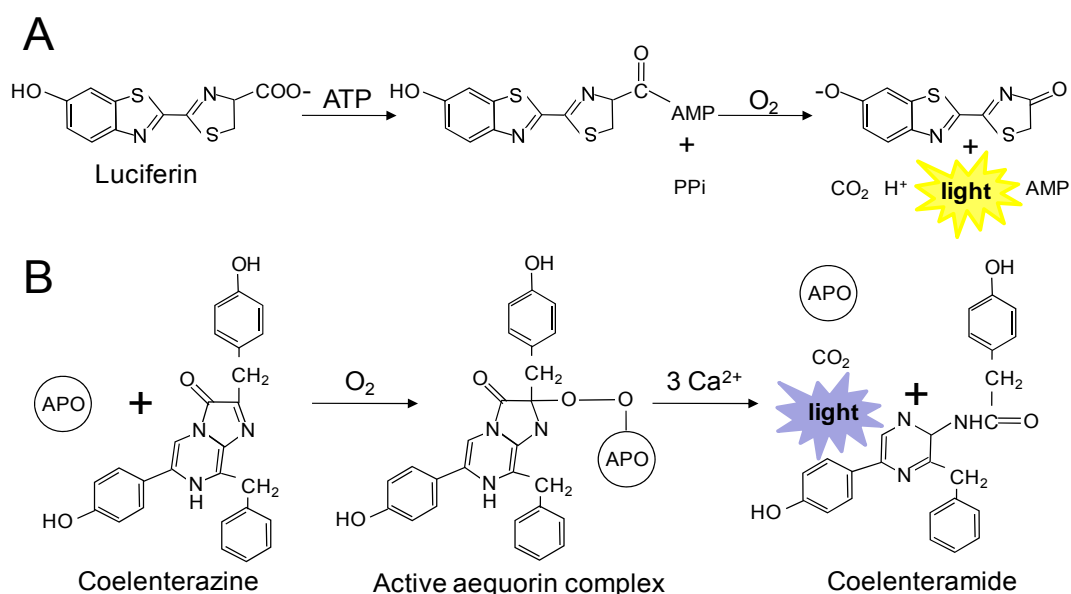
Figure 12. Bioluminescence reactions catalyzed by luciferase and aequorin enzymes. A. A luciferase reaction, which requires luciferin, ATP and O_2, yields yellow light emission, together with CO_2, H^+, and AMP. B. In the presence of O_2, aequorin (APO), a calcium sensitive enzyme, forms a complex with its substrate, coelenterazine. A subsequent catalytic reaction, which yields blue light emission, coelenteramide and CO_2, requires 3 calcium molecules.

(1) Firefly (*Photinus pyralis*) luciferase, see Figure 12A.   Its substrate is luciferin and the reaction gives the yellow green light of 560-nm wavelength (de Wet et.al., 1987).

(2) Renilla (*Renilla reniformis*) luciferase. The reaction with coelenterazine as a substrate emits blue light with the spectral maximum of 480 nm (Lorenz et.al., 1991).

(3) Aequorin from *Aequorea victoria*, a jelly fish. This enzyme is calcium sensitive and utilizes coelenterazine as a substrate. The reaction emits blue light with the spectral maximum of 480 nm, see Figure 12B (Shimomura et.al., 1962).

The constantly advancing fluorescence technology is divided into several sub-platforms which differ in their applications and sensitivity. In addition to the simple fluorescent intensity measurement, other platforms available for HTS are:

(1) Time-resolved fluorescence (TRF). This technique employs special fluorescent molecules, lanthanide (europium, samarium, terbium and holmium), which have longer fluorescent emission time (hundreds of microseconds) compared with other fluorescent molecules (nanoseconds). When lanthanide is excited briefly, it emits light which decays slowly; while the light emitted from the other background fluorescent molecules has completely decayed long before and becomes immeasurable, see Figure 13C. Therefore, the main advantage of the TRF is its low background noise.

(2) Fluorescence polarization. The polarized light excites only the fluorophores parallel to its plane. Fluorophores alone can rotate freely at a fast rate, while a complex between fluorophores and proteins is heavier and rotates sluggishly, giving it a better chance of being excited by the polarized light, see Figure 13D.

(3) Fluorescence-resonance energy transfer (FRET). As shown in Figure 13B, when two fluorescent molecules are close together at an approximate distance of 10 nm, a photon emission from one molecule (a donor) can excite the other (an acceptor). This method is mainly used to study the protein interactions.

(4) Bioluminescence-resonance energy transfer (BRET). This is a hybrid between bioluminescence and fluorescence technologies. The underlying principle is similar to that of FRET, with replacement of one of the two fluorescent molecules with the enzyme catalyzing a bioluminescence reaction, see Figure 13B.
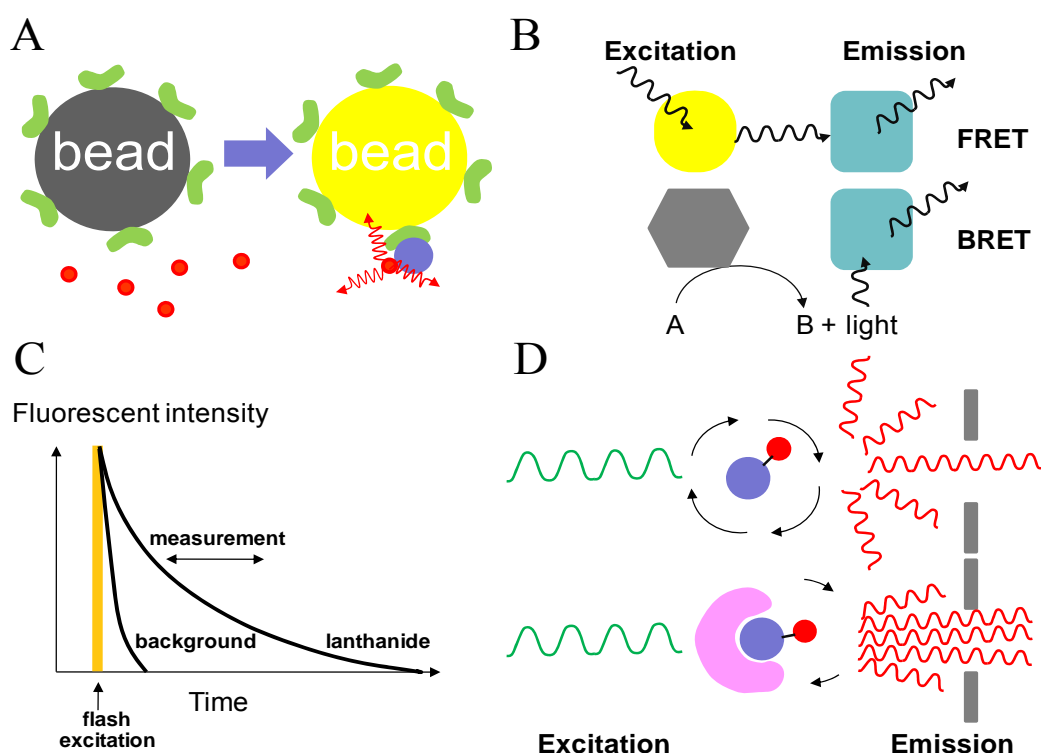
Figure 13. Measurement platforms for the radioactivity and the fluorescence assays. A. Scintillation proximity assay. The radioactive molecules (red circles) that are not bound to the targets of interest (blue circle) are not sufficiently close to the bead to activate it. B. The fluorescence-resonance energy transfer (FRET), and the bioluminescence-resonance energy transfer (BRET) assays. FRET is an energy transfer between two fluorescent molecules, while BRET is an energy transfer between a luminescence molecule and a fluorescence molecule. C. The time-resolved fluorescence (TRF). After being briefly excited, lanthanide emits photons for a longer period of time compared with other fluorescent molecules. The measurement, scheduled at the period after which the background fluorescent has completely decayed, improves the signal-to-noise ratio of the assay. D. Fluorescence polarization. A small molecule (blue circle) attached to a fluorophore (red circle) can rotate freely due its light weight. This results in less probability for the polarized light to induce excitation. With an increasing weight by the attachment of the third pink molecule, the rotation rate is reduced, and the polarized light has a greater chance to excite the fluorophore.

The following sections are reviews of each functional assay according to the position of the measured parameters in the signal transduction cascade.

2.1 Assays measuring G-protein activities.

At a G-protein level, the parameters that represent GPCR activation are (i) an increase in the G-protein binding affinity to GTP as assessed by the binding of [^{35}S]GTPγS, a non-hydrolyzable radioactive-labeled GTP analogue, to the membrane preparation containing the GPCR and the G-protein of interest; and (ii) an increase in the G-protein GTPase activity, of which the available assay is not compatible with HTS (Milligan, 2003). A non-radioactive GTPγS is developed by PerkinElmer in the form of Europium-GTPγS, and the assay platform for this molecule is the TRF. Theoretically, this assay can detect the GPCR activation regardless of the type of the

G-protein they are coupled to, but Gq has a low GDP/GTP exchange rate which renders this assay insensitive to a Gq-coupled receptor. In addition, a majority of the G-proteins expressed in most cells are Gi/o, therefore this assay is the most suitable with the Gi/o-coupled receptors (Thomsen et.al., 2005). A GPCR-Gα fusion protein is developed in an attempt to overcome the lack of the G-protein expression in the cell line (Milligan et.al., 2001). However, the fusion could interfere with the normal pharmacology of the receptors. The background noise of the GTPγS binding assay is high, because GTPγS can bind to every G-protein in the cells, especially the small G-proteins, such as Rho (De Lapp, 2004).

2.2 Inositol phosphate (IP) accumulation assay for Gq-coupled receptors.

The IP produced from the Gq-coupled receptor activation can be measured in two assay platforms. Firstly, the radioactive platform, the metal ions immobilized on the SPA^{TM} beads capture [^{3}H]IP at the phosphate group (Liu et.al., 2003). Secondly, the Cisbio Company releases the IP-One HTRF$^{®}$ assay which is compatible with the fluorescence technology, see Figure 14. The essential components of the assay are the IP$_1$ coupled to a fluorescent acceptor molecule, and a europium-conjugated antibody against the IP$_1$. Without the cellular IP$_1$, the two components of the assay bind together, and FRET can occur between the europium

and the fluorescent acceptor molecules. The presence of the cellular IP_1 inhibits FRET by binding competitively to the europium-conjugated antibody.

2.3 The calcium assay for Gq-coupled receptors.

The commercial availability of convenient calcium sensitive dyes, Fluo-3, Fluo-4, and Calcium-3, results in their popularity in HTS, see Figure 15. Upon binding to calcium, these dyes emit fluorescent light at different spectra. The dye requires intracellular loading which takes time and could be difficult in the cell line expressing a high level of transporters, which prevents the dye accumulation. The Fluorescence Imaging Plate Reader (FLIPR®) is an instrument developed specifically for HTS using the calcium-sensitive dye assay.

For calcium measurement in a bioluminescent platform, aequorin, a calcium- sensitive enzyme, is a recent technology developed by Euroscreen. When
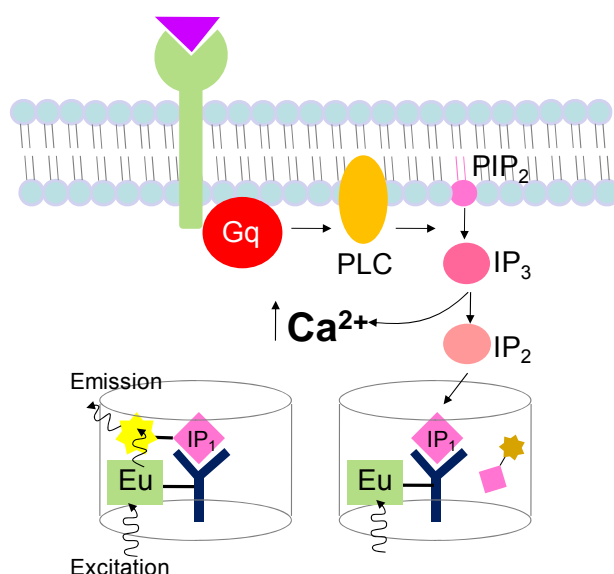
Figure 14. The inositol phosphate accumulation assay in the fluorescence platform. Activation of a Gq-coupled receptor results in an increase in the intracellular calcium and the inositol phosphate accumulation. The assay relies on competition between the intracellular Inositol monophosphate (IP_1) and the fluorophore-labeled IP_1 in binding to an IP_1 antibody conjugated to Europium (Eu). Binding of the labeled IP_1 to the antibody brings florophore in close proximity to Eu which allows FRET to occur. Replacement of the labeled IP_1 with the cellular IP_1 eliminates FRET.

three Ca^{2+} ions bind to an active aequorin complex, comprising of a 22,000-dalton apoaequorin protein, the molecular oxygen and the luminophore coelenterazine are oxidized to coelenteramide with a concomitant release of carbon dioxide and blue light, see Figure 13B (Head et.al., 2000). Even though dye loading is not required, a major disadvantage of this assay is a long incubation time (4-18 hours) (Thomsen et.al., 2005).

In addition to direct measurement of the intracellular calcium concentration the assays which are involved in the calcium-induced reporter gene expression are also available in both the luminescence and the fluorescence platforms. The frequently used reporters are the green fluorescent protein (GFP), β-galatosidase, β-lactamase, alkaline phosphatase, and luciferase (William C, 2004). The level of the intracellular calcium influences the gene expression through the responsive elements, in the promoter of the reporter gene, of the activator protein 1(AP1) or the Nuclear factor of the activated T cells (NFAT). This assay is very sensitive because the measured parameter (reporter gene expression) is located the most downstream in the signal transduction cascade. A major pitfall of the assay is its long incubation time, in
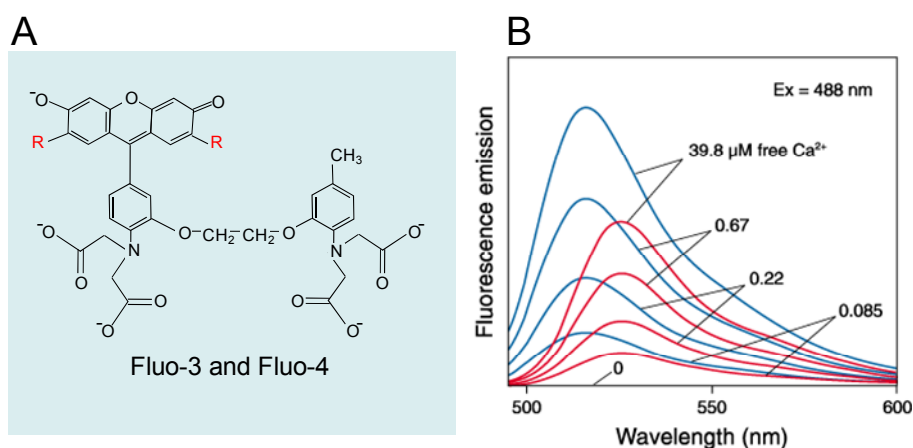
Figure 15. Calcium-sensitive dyes. A. The structure of Fluo-3 and Fluo-4. R-group is Cl and F for Fluo-3, and Fluo-4, respectively. B. Fluorescence emission of Fluo-3 (red) and Fluo-4 (blue) is influenced by the calcium concentrations (Both Figures are from the Invitrogen product inserts).

order to allow transcription and translation, which could result in GPCR desensitization.

2.4 The cAMP assay for Gs- and Gi/o-coupled receptors

The commercially available methods used to detect the intracellular cAMP are mainly ELISA-based and adapted to various platforms ranging from the radioactivity to luminescence, see Table 8 (Gabriel et.al., 2003). The assay is based on competition between the intracellular cAMP and the labeled cAMP in binding to an anti-cAMP antibody. The type of cAMP labeling determines the platform of the assay. The disadvantage of the immunoassay is the use of the antibody which is expensive, requiring a washing step and a long incubation time.

An elevation of the intracellular cAMP changes the level of gene transcription, through activation of a CREB (cAMP regulatory element binding protein) which in turn binds to the CRE (cAMP regulatory element) in the promoter. Therefore, the reporter gene assays can be applied to measure the intracellular cAMP levels as well as in calcium measurement. The advantages and disadvantages of this assay are similar to those of the calcium reporter gene assay.

The cAMP biosensor assay makes use of the cyclic nucleotide-gated channel (CNG) which is directly gated by a cAMP (Reinscheid et.al., 2003). An increase in the cAMP level causes an influx of calcium into the cell through CNG. The intracellular calcium can be measured using a wide variety of calcium sensitive dyes mentioned previously. The assay has advantages over the ELISA-based and the

Table 8. Commercially available ELISA-based cAMP assays

Assay name	Manufacturer	Labeled cAMP	Platform
SPA^{TM}	GE Healthcare	[^{125}I] SPA	Radioactive
FlashPlate^{TM}	Perkin Elmer	[^{125}I] SPA	Radioactive
AlphaScreen^{TM}	Perkin Elmer	Biotinyl-cAMP	Luminescence
Fluorescence polarization	Perkin Elmer Molecular Devices GE Healthcare	Fluorophore labeled-cAMP	Fluorescence polarization
HTRF cAMP	Cisbio	Fluorophore labeled-cAMP	Time resolved fluorescence
HitHunter^{TM}	Applied Biosystem	ED-cAMP	Fluorescence and Luminescence

reporter gene assays because it requires neither an antibody nor a lengthy incubation time. However, the dye loading step is unavoidable.

Compound libraries.

Compounds are an important part in HTS. The compounds in a library can be derived from chemical syntheses or from natural products. For a synthetic library, an efficient HTS requires a large number of compounds with sufficient diversity which is used to be a limitation for HTS users in the academic sector due to the lack of a large scale synthetic capacity. Fortunately, because of the rapidly growing HTS society, new industries in compound production have emerged just to supply the need. Some of the important compound library suppliers are AslnEx, ChemDiv, ChemBridge, Timtec, Bionet, ChemStar, Enamine, Interbioscreen, Labotest, and Maybridge, etc. The compounds are provided in solutions or powder, in vials, or plates. The price per library of 5,000-10,000 compounds is approximately $10,000 (Dove, 2007). In general, a manual synthesis, except for being slower, results in more diversified compound library when compared with a synthesis assisted by an automation system (combinatorial chemistry). However, in view of having lower compound diversity and faster compound production, the compound library derived from an automation-assisted synthesis is more advantageous in screening for more potent analogues of the known active compounds. Many natural products from plants, microorganisms and animals are known for their pharmacological applications, in fact, 60%-70% of the drugs for cancer and infectious diseases are from natural resources (Newman et.al., 2003). Table 9 presents examples of the drugs discovered from the natural compound libraries. At present, the natural product libraries are not as widely used as the synthetic counterpart because of difficulties in obtaining them. However, there is an ongoing effort to invent and implement new technologies to overcome the obstacles (Lam, 2007). The advantages of a natural product library are (1) unmatched structural diversity and complexity, (2) largely unexplored, and (3) usually composed of compounds with desirable pharmacokinetic properties.

HTS instrumentations

The instruments and integrated software are at the heart of HTS automation. Automated devices replace manual efforts in liquid handling and measurement processes. A robot arm transports samples between the automated devices, and the whole system is orchestrated by a software. A functioning HTS room should contain the following: (1) a 2x2 meter or larger work table which supports most of the other devices containing a motorized track for the robotic arm; (2) a liquid handler station, a device for aspirating and dispensing liquid to or from the samples, which comprises a pod that can be attached to disposable plastic pipette tips; (3) a plate reader compatible with the assay platform; (4) a carousel for placement of the compound or cell plates; (5) a carbon dioxide incubator; (6) other accessories such as a shaker, barcode reader, washer, micro-plate centrifuge, and a plate sealer; (7) a robotic arm; and (8) a computer for the system coordination and data collections. Figure 16 illustrates an example of the HTS room and its components.

Table 9. Drugs developed from natural compounds.

Drugs	Natural compounds	Indications
Caspofungin	Pneumocandin B	Antifungal
Pimecrolimus	Ascomycin	Atopic dermatitis
Telithromycin	Erythromycin	Antibacterial
Amrubicin hydrochloride	Doxorubicin	Anticancer
Biapenem	Thienamycin	Antibacterial
Fulvestrant	Estradiol	Anticancer
Daptomycin	Daptomycin	Antibacterial
Extenatide	Incretin	Anti-diabetic
Zicontide	MVIIA	Pain management

Conclusion

Completion of the human genome project has brought about numerous possible drug targets. To match the number of the emerging targets with an appropriate rate of drug discovery, the HTS has widely replaced the sluggish structure-based drug discovery and the traditional random screening. The compound libraries, the assay design, and a level of automation determine a successful HTS.

GPCR is one of the successful drug targets as evidenced by the significant contributions of their modulators in the marketed drugs. The field of GPCR drug

discovery is still expanding because hundreds of the orphan GPCRs existing in the human genome are largely unexplored for their potential clinical applications. In response to a vast interest in the GPCR modulators, several HTS assays are invented and continuously improved towards a new level of sensitivity, throughput, and economic feasibility. These improvements are necessary for the discovery of the modulators with novel properties, as fast and economical as possible.

The V_2R antagonist which is discovered by the traditional random screening using a ligand binding assay is a good example of the successful GPCR modulators with various applications. All of the available antagonists are derived from the only two distinct structures and they are competitive antagonists. The use of HTS strategy, especially together with the functional assay, should reveal a new V_2R antagonist structure with a mode of action that is not previously recognized by the ligand binding assay.
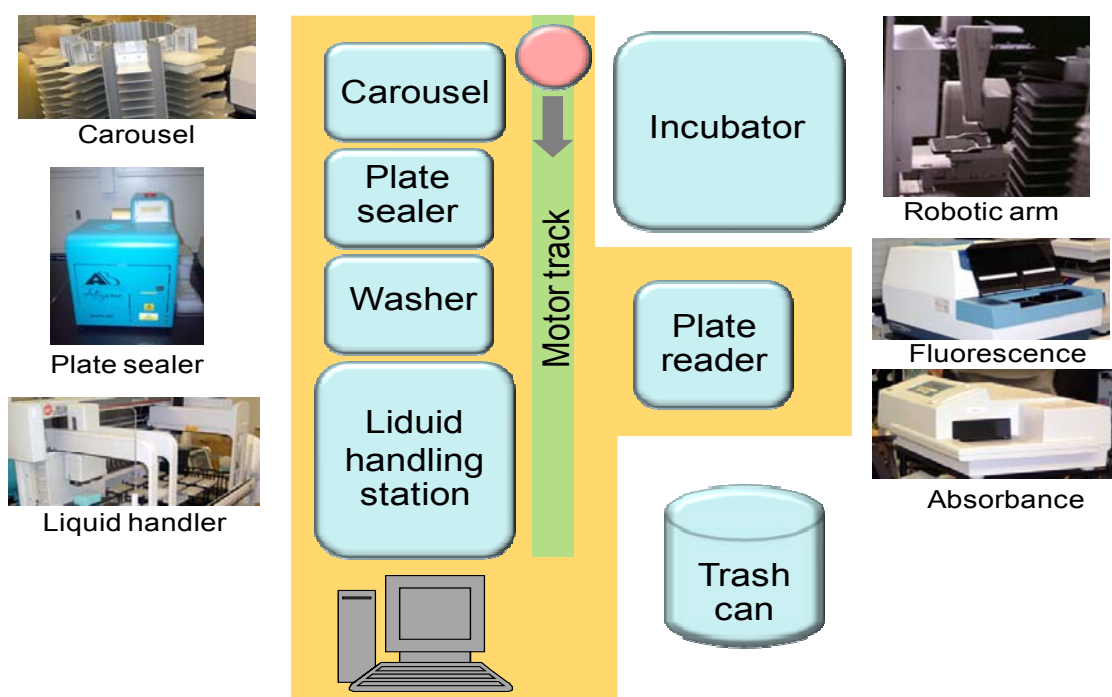
Figure 16. An example of a HTS room. Several automated devices such as the plate readers and the liquid handler are arranged strategically in the room to ensure the robotic arm accessibility. The whole system is coordinated by a specialized software.

CHAPTER III
MATERIALS AND METHODS

1. An overview of the method

It should be noted that all of the following experiments, except the chemical analyses and syntheses were carried out by the candidate.

Cell selection: The Fisher rat thyroid (FRT) cells were chosen for the screening because we reported previously that (1) they expressed CFTR and YFP strongly and stably after transfection, (2) they had properties suitable for high-throughput screening, including low basal halide transport, and rapid growth on plastic, (3) their high electrical resistance allowed active compound validation with Ussing chamber short-circuit current measurement, and (4) they, similar to the renal tubular cells, were of an epithelial origin which was preferable for V_2R expression (Galietta et al., 2001).

Establishing a cell line expressing the human V_2R: The FRT cells, already expressing CFTR and YFP-H148Q/I125L (Ma et.al., 2002), were stably transfected with the N-terminal cmyc-tagged human wild type or mutant V_2Rs. The small cmyc tag did not alter the V_2R functions and was previously used in several studies (Morello et.al., 2000; Andersen-Beckh et.al., 1999; Terrillon et.al., 2004). The colonies with the transgene expression were identified by the immunocytochemical and immunoblot staining with an anti-cmyc antibody which was essential, because none of the commercially available V_2R antibodies worked well. Then, the colony with the most homogeneous V_2R expression was selected for a further study. The FRT cells, expressing mutant V_2R (W164S) which was folded incorrectly and trapped inside the cells, served as a control for the assay validation, and they could be used in a future HTS for molecular chaperones, a treatment for the nephrogenic diabetes insipidus.

Validation of the cell line for its ability to detect the V_2R activation: The increase in halide conductance resulting from dDAVP was assessed through the YFP fluorescence, using a fluorescence plate reader and a direct chloride current

measurement in the Ussing's chambers. V_2R was confirmed to mediate an increase in the conductance by demonstrating (1) the failure of dDAVP to induce responses in the cell line with W164S V_2R or without V_2R, and (2) the inhibition of the dDAVP-induced responses in the cell line expressing the wild type V_2R by the V_2R antagonists, namely [1-β-mercapto-β, β-cyclopentamethylenepropionyl[1], O-ET-TYR[2], VAL[4], ARG[8]]-vasopressin and SR-121463. The contribution of CFTRs in a dDAVP-induced increase in halide conductance was evidenced by inhibition of the responses by CFTR $_{inhibitor}$-172.

Optimization of the assay: Different dDAVP concentrations and incubation times for the assay were tested in order to identify the optimal conditions for HTS yielding the best achievable Z′ factor.

A high-throughput screening for the V_2R antagonists: Fifty thousands small molecules in a four-compounds-in-one-well mixture were screened for the compounds that were able to antagonize dDAVP-induced V_2R activation. In approximately 10 hours, six thousands and four hundreds compounds were tested with the cells in a 96-well plate in one round of HTS. The YFP fluorescent intensity was measured by a fluorescence plate reader, and the screening was assisted by an automated system.

Elimination of false positives with a secondary screening: The identified active four-in-one-well mixtures were screened for the second time using the YFP fluorescent intensity and the short-circuit current measurement to eliminate false positives. Then, the individual compound in the mixture was verified for its antagonist activity and inhibition potency.

Structure-activity relationships and the compound syntheses: Several analogues of the active compound were screened for their antagonist activity which would lead to an understanding of the structure-activity relationship of the compound class. The active compound and some of its potent analogues were then synthesized by chemists to obtain enough quantities for further experiments.

Target identification: The CFTR-based assay for V_2R antagonists was a pathway screen concerning activation/inhibition of the whole signal transduction cascade, therefore the possible targets of the active compounds included V_2R, Gs, Gi, AC, PDE, PKA, CFTR, and the phosphatase enzyme, see Figure 1. The compound that was able to inhibit the V_2R-induced cellular responses (cAMP elevation, and an

increase in halide influx), but that failed to do the same for the Gs-coupled receptors and the β_2 adrenergic receptors, was a V_2R antagonist. The CHO-K1 cells transiently expressed the β_2 adrenergic receptors were used to evaluate the ability of the compound to inhibit the cAMP elevation after the isoproterenal-induced receptor activation. Using the short-circuit current measurement, the compound inhibition of the isoproterenol-induced chloride current was observed in the Calu-3 cells which endogenously expressed the β_2 adrenergic receptors. The compound was ultimately classified as a V_2R antagonist when it displaced the radio-labeled vasopressin from the V_2R in the radioactive ligand binding assay. By the same method, comparison between binding affinities of the compound to V_{1a}-R and to V_2R was also studied. The radioactive binding assay was carried out in the intact FRT cells stably expressing the V_{1a}-R or V_2R receptor. The diagrammatic version of the overview was shown in Figure 17.
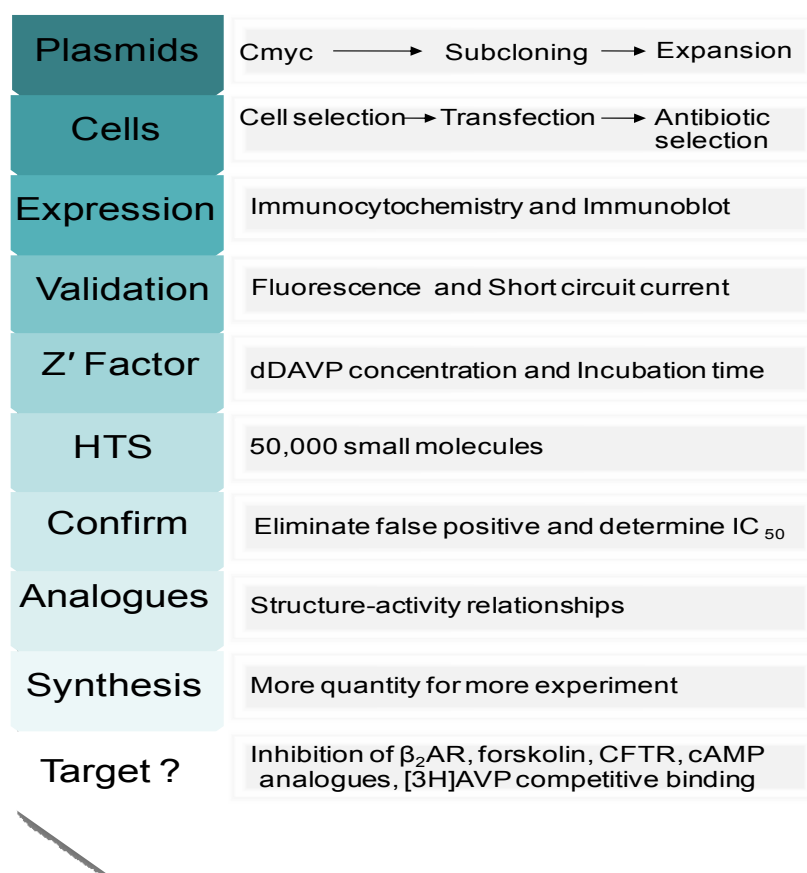
Figure 17. An overview of the method.

2. Materials

Table 10. The materials used in the research.

Reagents and Equipments		Sources
Plasmids	Plasmids encoding human wild type and mutant (W164S) V_2Rs	Dr. Daniel Bichet (University of Montreal)
	Plasmids containing HA-tagged human β-adrenergic	UMR cDNA Resource Center
	Plasmids containing HA-tagged human V_{1a} R	UMR cDNA Resource Center
	pCDNA3.1 Hyg$^+$	Invitrogen
PCR	Taq polymerase enzyme	Invitrogen
	Custom PCR primers	UCSF cell culture facility
	10mM dNTP mix	Invitrogen
	Thermocycler GeneAmp PCR System 9700	Applied Biosystems
Electrophoresis	Certified^{TM} Molecular Biology agarose	Bio-Rad
	TAE buffer (tris/ acetic acid/ EDTA)	Bio-Rad
	Lambda DNA/*Hin*dIII Markers	Promega
	UltraPure^{TM} 10mg/ml Ethidium Bromide	Invitrogen
	FisherBiotech Horizontal Electrophoresis Systems	Fisher Scientific
Kit	QIAquick Gel Extraction Kit	Qiagen
	QIAprep spin miniprep plasmid extraction kit	Qiagen
	cAMP Parameter assay kit	R&D Systems
Enzymes	XhoI	New England Biolab
	XbaI	New England Biolab
	T4 DNA ligase	Invitrogen
Baterial culture	One shot® chemically competent E Coli.	Invitrogen
	LB broth, LB Amp plates	Teknova
	S.O.C. medium	Invitrogen

Table 10(continued). The materials used in the research.

Reagents and Equipments		Sources
Cells	FRT	UCSF cell culture facility
	MDCK	UCSF cell culture facility
	CHO-K1	UCSF cell culture facility
	T84	UCSF cell culture facility
	Calu-3	UCSF cell culture facility
Cell Culture	F-12 Modified Coon's Medium	Sigma
	F-12 Ham's Nutrient mix medium	UCSF cell culture facility
	MEM Eagle & Earle's BSS medium	UCSF cell culture facility
	10X MEM	Gibco
	Fetal bovine serum	Hyclone
	Glutamine	UCSF cell culture facility
	Sodium bicarbonate	UCSF cell culture facility
	Essential amino acid	UCSF cell culture facility
	Sodium pyruvate	UCSF cell culture facility
	Penicillin/Streptomycin	UCSF cell culture facility
	0.05% Trypsin with 0.5 mM EDTA	UCSF cell culture facility
	PBS	UCSF cell culture facility
	PBS Ca2+ and Mg2+ Free (CMF-PBS) with 0.04% EDTA	UCSF cell culture facility
	HEPES	UCSF cell culture facility
	Purecol	Inamed Corporation
Cell culture vessels	75 cm^2 Flask, 175 cm^2 flask	Corning
	24 well plate	Corning
	Clear bottom black 96 well plate	Costar
	Snap well filter	Costar 3801
	Lipofectamine™ 2000	Invitrogen
Cell Transfection Selective antibiotics Immuunoblot	Opti-MEM I medium	Invitrogen
	Ampicillin, Hygromycin	Roche
	Zeocin	Invitrogen
	Bovine serum albumin (BSA)	Sigma-Aldrich
	Protease inhibitor cocktail	Sigma-Aldrich
	Bio-Rad DC kit	Bio-Rad
	NuPAGE® Electrophoresis system	Invitrogen
	SeeBlue® Pre-Stained standard	Invitrogen
	PVDF membrane	Sigma-Aldrich
	ECL Plus™ Western Blotting Detection	Amersham
	Hyperfilm™	Amersham

Table 10(continued)**.** The materials used in the research.

Reagents and Equipments		Sources
Antibodies	Rabbit anti-cmyc	Roach
	Horse-raddish peroxidase (HRP)-conjugated anti-rabbit IgG	Cell Signaling Technology
	Cy3-conjugated anti-rabbit IgG	Zyme
Chemicals	dDAVP	Ferring Pharmaceuticals
	[1-β-mercapto-β, β-cyclopentamethylenepropionyl[1], O-ET-TYR[2], VAL[4], ARG[8]]-vasopressin	Sigma-Aldrich
	[^{3}H]AVP	Perkin Elmer
	Forskolin	Sigma-Aldrich
	Cholera toxin	Sigma-Aldrich
	E Coli. heat stable toxin	Sigma-Aldrich
	SR-121463B	Sanofi-Aventis
	SR-49059	Sanofi-Aventis
	Isoproterenol	Sigma-Aldrich
	Propanolol	Sigma-Aldrich
	NaI	Sigma-Aldrich
	NaCl	Sigma-Aldrich
	KCl	Sigma-Aldrich
	KH_2PO_4	Sigma-Aldrich
	$CaCl_2$	Sigma-Aldrich
	$MgCl_2$	Sigma-Aldrich
	Na-HEPES	Sigma-Aldrich
	Na-glutamate	Sigma-Aldrich
	HTS compound library[†]	ChemDiv
Equipment	Vertical diffusion chamber	Costar
	DVC-1000 voltage-clamp apparatus	World Precision Instruments
	CO_2 incubator	
	Water bath	
	Spectrophotometer	
	FluoStar Optima plate reader	BMG Lab Technologies
	Biomek FX Liquid Handling Workstation	Beckman
	LabSystems Multidrop Dispenser	ThermoLabsystems
	ALPS 300 Automated Laboratory Plate Sealer	ABGene
	Hotel carousel for plates and tip boxes	Beckman
	Plate Washer Elx405	Bio-Tek instrument

† The compound library was selected based on its diversity and drug-like characteristics according to the rule of five (Lipinski et al., 1997).

3. The experiments

3.1 Plasmids

The N-terminus cmyc-tagged V_2Rs were created by the PCR introduction of the cmyc sequence to the plasmids encoding the human wildtype and the mutant (W164S) V_2Rs, see Appendix B. The PCR products were subcloned into the plasmid pCDNA3.1Hyg+ at the XbaI and the HindIII restriction sites to give the plasmids wV_2R-Hyg (wildtype) and mV_2R-Hyg (mutant), see Appendix C. The cDNAs were confirmed by a sequence analysis (the Fisher Lab, the University of California, San Francisco).

3.2 Cell culture and transfection

The Fisher rat thyroid cells expressing the CFTR and YFP-H148Q/I152L, as described previously (Maunprasat et al., 2004), the CHO-K1 cells, and the T84 cells were cultured in the F-12 Modified Coon's Medium, F-12 Ham's Nutrient mix, and the 1:1 mixture of DMEM high glucose and the F-12 medium, respectively. Calu-3 and the MDCK cells were maintained in the MEM Eagle & Earle's BSS medium. All the media were supplemented with10% fetal bovine serum, 100 units/ml of penicillin, and 100 µg/ml of streptomycin. The medium for the FRT cells was supplemented with 2 mM glutamine, 1.5 g/l $NaHCO_3$, 500 µg/ml zeocin, and 500 µg/ml geneticin. The media for Calu-3 and the MDCK cells were supplemented with 2 mM glutamine, 0.11 mg/ml sodium pyruvate, 1.5 g/l $NaHCO_3$ and the non-essential amino acids. The cells were grown at 37 ^{o}C in 5% CO_2 / 95% air. For a summary on the cell culture media, see Appendix D.

For a stable transfection, cells at ~80% confluence were transfected with wV_2R-Hyg, HA-tagged human V_{1a}R, or mV_2R-Hyg using Lipofectamine 2000 according to the manufacturer's instructions, see Appendix E. Twenty-four hours after the transfection the cells were selected for 2 weeks with 350 µg/ml hygromycin for the V_2R, or with 750 µg/ml geneticin for the V_{1a}R. The remaining colonies were grown at the clonal density and screened for the receptor expression by the immunofluorescence

and the immunoblot analyses. Stably transfected cell lines were maintained in the same medium as that used for the selection. The transient transfection of the CHO-K1 cells with the HA-tagged human β_2-adrenergic receptor was carried out in a manner similar to the stable transfection. The cells were used 48 hours after the transient transfection.

3.3   Immunofluorescence and immunoblot analyses

The cells were grown on glass coverslips for 48 hours before staining. For cmyc immunostaining, non-permeabilized cells were washed three times with the phosphate buffered saline (PBS); incubated for one hour with the anti-cmyc antibody (1:1000) in the PBS containing 1% bovine serum albumin; washed three times with the PBS; and fixed for 10 min in 4% paraformaldehyde. After three washes with the PBS, the cells were incubated for 1 h with Cy3-conjugated anti-rabbit IgG, washed and mounted for the fluorescence microscopy. Immunostaining of permeabilized cells was similarly carried out, except that cells were permeabilized with 0.1% Triton-X100 in the PBS prior to fixation, and blocked for 15 min in the PBS containing 1% BSA.

For immunoblot, see Appendix F for details, the cells were homogenized in 250 mM sucrose, 1 mM EDTA and 1% protease inhibitor cocktail. The homogenate was centrifuged at 5000g for 10 min and the supernatant was assayed for the protein concentration using a Bio-Rad DC kit. The proteins (20 µg/lane) were resolved by SDS-PAGE (NuPAGE 4-12% Bis-Tris gel; Invitrogen) and transferred to a PVDF membrane. The PVDF membrane was blocked overnight in 5% skimmed milk in the PBS containing 1% Tween-20, washed three times, and incubated for 2 h with the anti-cmyc antibody (1:1000). The membrane was washed three times, incubated for 1 h with the HRP-conjugated anti-rabbit IgG, washed, and then detected by the enhanced chemiluminescence.

3.4   YFP fluorescence measurement of the I⁻ influx

The transfected FRT cells were plated in black-walled, 96-well plates with a transparent plastic bottom (Corning-Costar), cultured overnight or till confluence, washed three times with the PBS, and treated with the specified compounds in the final volume of 60 µl. The YFP-H148Q/I152L fluorescence was measured using a

commercial plate-reader (FluoStar Optima; BMG Lab Technologies) equipped with the custom excitation and emission filters (500 nm and 544 nm, respectively, Chroma). When inside the plate reader, the fluorescence signal from the cells was measured before and after the PBS/I$^-$ (PBS with 100 mM Cl$^-$ replaced by I$^-$; the details on PBS/I$^-$ preparation are in Appendix H) addition for a total of 14 seconds. One hundred microliters of the PBS/I$^-$ was added to the cells by a built-in injector programmed to inject the PBS/I$^-$ 2 seconds after the measurement started.

3.5   Short-circuit current measurement

The cells were cultured on the Snapwell filters until confluence (transepithelial resistance >500 ohms). The apical membrane current was measured in the Ussing chamber with 3ml Ringer's solution bathing the basolateral surface, and 3 ml of Half-Ringer's solution bathing the apical surface. The compositions of Ringer's solution were: 130 mM NaCl, 2.7 mM KCl, 1.5 mM KH$_2$PO$_4$, 1 mM CaCl$_2$, 0.5 mM MgCl$_2$, 10 mM Na-HEPES, 10 mM glucose, pH 7.3. The same for Half-Ringer's solution, except that 65 mM NaCl was replaced with Na gluconate, and the CaCl$_2$ was increased to 2 mM. The details on the Ringer and the Half-Ringer preparations are in Appendix J. For a short- circuit current measurement of the T84 cells, Ringer solution was used in both the apical and basolateral surfaces. The chamber was bubbled continuously with air. The apical membrane current was measured using a voltage-clamp apparatus. The currents were visualized and recorded in a computer using the Chart5 software for PC. For a detailed protocol, see Appendix I.

3.6   High-throughput screening

The compound library for screening contained 50,000 chemically diverse and drug-like small molecules. The stock compounds were stored in 96-well plates at 2.5 μM in DMSO in a -20°C freezer. The compounds occupied 80 wells with the remaining 16 wells containing only DMSO (for positive and negative controls). The compounds were thawed at the room temperature for 30 minutes before the actual screening begins. Screening was done using an automated apparatus (Beckman Coulter) containing a CO$_2$ incubator, carousels for compound plates and pipette tip boxes, plate washer, liquid handling station, and two plate readers. Robotic operations

were controlled by the SAMI software (version 3.3, Beckman Coulter).

For high-throughput screening, the cells expressing the human wildtype V_2R were plated in 96-well plates using the LabSystems Multidrop Dispenser, see Appendix G for the details on the HTS cell culture. After an overnight growth to confluence, the cells were washed with the PBS, and dDAVP (1 nM) was added together with the test compounds (20 μM). The first and last columns of each plate were used for positive (PBS) and negative (dDAVP, no test compound) controls. The I^- influx was assayed as described in the above after a thirty-minute incubation at 37 ^{o}C in a CO_2 incubator.

3.7   Data analysis

The I^--influx, $\left(dI^-/dt\right)_{t=0^+}$, was computed from the initial slope of the fluorescence-vs-time curve, which was approximated by a 3rd-order polynomial regression, after normalization for the total fluorescence, ie the initial fluorescence minus the background fluorescence (Muanprasat et al., 2004). The percent inhibition was computed using the following formula.

$$\% \; Inhibition = 100 \times \frac{(negative \; control \; fluorescence - compound \; fluorescence)}{(negative \; control \; fluorescence - positive \; control \; fluorescence)}$$

The positive and negative control values denoted $\left(dI^-/dt\right)_{t=0^+}$ obtained from the first and last columns of each plate. The primary screening data were subjected to a histogram analysis for 'hit' selection.

EC_{50} and IC_{50} were calculated from a Hill slope model using the KaleidaGraph program as follows.

$$y = bot + (top - bot)/\{1 + (x/IC_{50})^{Slope}\}$$

Where y is the percent activity and x is the corresponding concentration. The fitted IC_{50} or EC_{50} parameter is defined as the concentration giving a response half way between the fitted top and bottom of the curve.

3.8   Synthesis procedures for V_2R_{inh}-02

2,4-Dioxo-4-phenyl-ethylbutylate **1**. A solution of anhydrous benzene (50 ml) and acetophenone (1.2 g, 0.010 mol) was added to the suspension of NaH in oil (60%;

0.8 g, 0.020 mol), and the mixture was stirred for 30 min. To the solution of diethyl oxalate (2.19 g, 0.015 mol), benzene (10 ml) was added dropwise, and the reaction mixture was stirred for 6 h. The mixture was filtered over Celite and purified by the chromatography to give 2,4-dioxo-4-phenyl-ethylbutylate **1** (1.76 g; 85% yield).

4-benzoyl-5-(4-fluorophenyl)-3-hydroxy-1-(4-hydroxyphenylethyl)-2,5-dihydro-2-pyrrolone (V_2R_{inh}-02). Tyramine (93 mg, 0.675 mmol) and 4-fluorobenzaldehyde (84 mg, 0.675 mmol) were heated to 110 ^{o}C for 10 min. The water was removed during the reflux with a cotton swab. Compound **1** (135 mg, 0.614 mmol) was added dropwise in dioxane (5 ml) and stirred overnight at 100 ^{o}C. The 2-pyrrolone was purified by the column chromatography and re-crystallized to give V_2R_{inh}-02 (153 mg, 60 % yield). ^{1}H NMR (400 MHz, CD_3OD): δ 7.72 (d, J = 7.6 Hz, 2H), 7.59 (t, J = 7.2 Hz, 1H), 7.48 (d, 8.0 = Hz, 2H), 7.24 (m, 2H), 7.10 (t, J = 8.8 Hz, 1H), 7.03 (d, J = 8.6 Hz, 2H), 6.81 (d, J = 8.6 Hz, 2H), 5.26 (s, 1H), 3.91 (m, 1H), 3.36 (s, 1H), 2.97-2.68 (m, 2H), 2.71 (m, 1H). LC-MS: m/z 418.1 $[M+ H]^+$ (Nova-Pak C_{18} column, 99%, 200-400 nm).

3.9   The cAMP measurement

The cells were grown in 24-well plates, treated with the test compounds as indicated, lysed by sonication, centrifuged to remove the cell debris, and assayed for cAMP according to the manufacturer's instructions, see Appendix K. For the CHO-K1 cells, 24 hours after transfection with the β_2 adrenergic receptors, the cells were trypsinized and plated onto 24-well plates overnight before carrying out the cAMP assay.

For a functional competition study where reduction of cAMP concentration was measured in the V_2R expressing FRT cells after stimulation by different concentration of dDAVP in the presence of various concentrations of V_2R_{inh}-02 (Figure 30A), the slope of the Schild plot and Ki of V_2R_{inh}-02 were calculated from the following equation using the KaleidaGraph program.

$$\log(dose\ ratio - 1) = \log \{[B] - \log(K_i)\}$$

The dose-ratio is the EC_{50} in the presence of antagonist divided by the

EC_{50} in the absence of antagonist (the EC_{50} values were calculated in the same way as previously described in 3.7). [*B*] and Ki is a concentration and a dissociation constant of V_2R_{inh}-02, respectively.

3.10 The receptor binding assay

The radiolabeled vasopressin binding was measured in the intact FRT cells stably expressing the human V_2R or $V_{1a}R$. The confluent cells in the 24-well plates were washed twice with the ice-cold binding buffer (PBS containing 0.1% glucose, and 0.2% bovine serum albumin). The cells were incubated for 2 hours at 4 ^oC with the specified concentrations of V_2R_{inh}-02 and the binding buffer containing 1 nM [^3H]AVP, washed twice with the ice-cold PBS, and lysed in 0.1 N NaOH containing 0.2% SDS. Then the radioactivity of the cells was measured with a scintillation counter, of which values were for the specific binding plus the non-specific binding. Approximately simultaneously, the same procedure, except that V_2R_{inh}-02 was replaced by dDAVP (for V_2R) or SR 49059 (for $V_{1a}R$), was repeated for the cells in the remaining wells; and the resulting measured radioactivity values were for the non-specific binding that were to be subtracted from those obtained previously in order to obtain the radioactivity values for the specific binding.

3.11 Synthesis procedures for PDE$_{act}$ class.

Thin layer chromatography was performed on the Merck aluminum sheets containing silica gel 60 F_{254}. ^1H NMR was recorded on a Varian 400 MHz spectrometer using TMS as the internal standard. Liquid chromatorgraphy and electrospray mass spectral data were obtained on a Waters integrated LC-MS. See Figure 30 for the synthetic schemes.

Methyl (E/Z) 2-cyano-3-tolyl-pent-2-enoate (3): Methyl cyanoacetate (0.5 gm, 0.0033 mol) and 4'-methylpropriophenone (0.33 gm, 0.0033 mol) were dissolved in 20 ml of dry benzene to which ammonium acetate (0.051 gm, 0.00067 mol) and 0.2 ml of acetic acid were added. The mixture was refluxed azeotropically using a Dean-Stark apparatus until water formation ceased. The reaction mixture was cooled, dried over sodium sulfate and concentrated in vacuo. The residue was purified by flash

chromatography (silica gel, hexane:EtOAc) to a pale yellow oil. ^{1}H NMR (400 MHz, δ, CDCl$_3$): 7.35 − 6.8 (m, Arom-H, 8H), 3.84/3.64 (2s, -OCH$_3$, 6H, *Z/E*), 3.08/2.83 (2q, -CH$_2$, 4H, *E/Z*), 2.35/2.36 (2s, -CH$_3$ of tolyl. 6H), 1.03/1.02 (2t, -CH$_3$, 6H).

Methyl 2-amino-5-methyl-4-p-tolylthiophene-3-carboxylate (4): A stirred solution of methyl 2-cyano-3-tolyl-pent-2-enoate (0.2 gm, 0.00087 mol) in a mixture of dry THF-MeOH (10 ml) was treated with sulfur (0.033 gm, 0.0010 mol) and diethylamine (0.076 gm, 0.108 ml, 0.00104 mol) at the ambient temperature. The reaction mixture was stirred at 35-40 ºC until the starting material disappeared by thin layer chromatography (TLC). The reaction mixture was then concentrated in vacuo and the residue was purified by flash chromatography to get the product 4 as pale yellow solid. ^{1}H NMR (400 MHz, δ, CDCl$_3$): 7.11 (d, Arm-H, 2H), 7.03 (d, Arm-H, 2H), 5.82 (bs, -NH$_2$, D$_2$O exchangeable), 3.45 (s, -OCH$_3$, 3H), 2.34 (s, *p*-tolyl, 3H), 2.00 (s, -CH$_3$, 3H).

Exo-Bicyclo[2.2.1]heptane-2,3-dicarboxylic anhydride (6): exo-Bicycyclo[2.2.1]hept-5-ene-2,3-dicarboxylic anhydride (1 gm, 0.006 mol) was dissolved in dry THF (45 ml) and placed in a standard parr bottle. 5% palladium on charcoal (approximately 100 mg) was added and hydrogenation was carried out at 2.2 bar until the H$_2$ uptake ceased. The catalyst was removed by filtration, the reaction mixture was concentrated under reduced pressure and the petroleum ether and hexane were added to obtain the product **6** as crystalline white solid (yield 96%). Mp 78-79 ºC; ^{1}H NMR (400 MHz, δ, CDCl$_3$): 2.90 (s, -CH, 2H), 2.84 (s, -CH, 2H), 1.25-1.78 (m, -CH$_2$, 6H).

3-(3-(methoxycarbonyl)-5-methyl-4-p-tolylthiophen-2-ylcarbamoyl)endo-bicyclo[2.2.1]heptane-2-carboxylic acid (7): A mixture of methyl 2-amino-5-methyl-4-*p*-tolylthiophene-3-carboxylate and *endo*-bicyclo[2.2.1]heptane-2,3-dicarboxylic anhydride were heated to melting to give the crude product **7**. The mixture was dissolved in a minimum quantity of chloroform, and precipitated with hexane (yield 56-60%). ^{1}H NMR (400 MHz, δ, CDCl$_3$): 11.30 (bs, -COOH, 1H), 7.15 (d, Arm-H, 2H), 7.01 (d, Arm-H, 2H), 3.50 (s, -COOCH$_3$, 3H), 3.24 (d, -CH, 1H), 3.02 (d, -CH,

1H), 2.65 (d, -CH, 2H), 2.39 (s, *p*-tolyl, 3H), 2.11 (s, -CH$_3$, 3H), 1.4 – 1.8 (m, -CH$_2$, 6H).

3-(3-(methoxycarbonyl)-5-methyl-4-p-tolylthiophen-2-ylcarbamoyl)exo-
bicyclo[2.2.1]heptane-2-carboxylic acid (8): A mixture of methyl 2-amino-5-methyl-4-*p*-tolylthiophene-3-carboxylate and *exo*-bicyclo[2.2.1]heptane-2,3-dicarboxylic anhydride were heated to melting to give the crude product **8**. The mixture was dissolved in a minimum quantity of chloroform, and precipitated with hexane (yield 56-60%). ^{1}H NMR (400 MHz, δ, CDCl$_3$): 1.32 (bs, -COOH, 1H), 7.15 (d, Arm-H, 2H), 7.02 (d, Arm-H, 2H), 3.50 (s, -COOCH$_3$, 3H), 2.82 (dd, -CH, 1H), 2.68 (bs, -CH, 1H), 2.58 (bs, -CH, 1H), 2.38 (s, *p*-tolyl, 3H), 2.26 (d, -CH, 1H), 2.09 (s, -CH$_3$, 3H), 1.2 – 1.8 (m, -CH$_2$, 6H).

3.12   Intestinal fluid secretion

Mice (CD1 strain, 25-35 g) were deprived of food for 24 hours but given 5% dextrose water. Following the anesthesia with Avertin, see Appendix L, generally 4 mid-jejunal loops (10-15 mm each) were created using suture as described (Oi et.al., 2002; Hitotsubashi et.al., 1992). One hundred μl of the PBS, CTX, STa, CTX or STa (with or without PDE$_{act}$-04) were injected into the loops. The intestine was returned to the abdominal cavity and the incision closed with suture. The mice were allowed to recover from the surgery. Six hours later, the intestinal loops were removed, and the net fluid accumulation was quantified by measurement of loop-to-length ratios. Mice were euthanized by an anesthetic overdose. For a detailed description of the procedure see Appendix M.

3.13   An MDCK cell model of PKD

The MDCK cells were mixed with collagen (Purecol), MEM, 10 mM HEPES pH 7.4, 100 units/ml penicillin, and 100 μg/ml streptomycin, and plated at 300 cells per well in 24-well plates. After 2-hour incubation in a CO$_2$ incubator at 37 ^{o}C, the cell culture media containing the indicated concentrations of forskolin were added on top of the cells containing collagen gel. The media were changed twice daily. Small cysts developed by 4 days, at which time PDE$_{act}$-04 was added, and the culture

continued for 7 more days. The phase-contrast light micrographs of cyst were obtained on a confocal microscope at 10x magnification every two days. The cyst growth was quantified using the NIH-Image J software. For a detailed protocol see Appendix N.

CHAPTER IV
RESULTS

Expression of the wild-type and the mutant V$_2$Rs in the FRT cells

Stably transfected FRT cell lines were generated that co-expressed the human wild-type CFTR, YFP-H148Q/I152L, and cmyc-tagged wild-type V$_2$R or the mutant V$_2$R-W164S. The cmyc-tag was inserted at the external-facing V$_2$R N-terminus. The wild-type V$_2$R showed a plasma membrane distribution by cmyc staining, see Figure 18A, whereas no membrane staining was seen in the non-transfected cells or the cells expressing V$_2$R-W164S that had a defect in cellular processing with retention at the endoplasmic reticulum (Oksche et al., 1996). An immunoblot analysis with the cmyc antibody showed the bands at ~40 kDa, corresponding to the non-glycosylated and glycosylated V$_2$Rs, and at 64 kDa which correlated to receptor aggregates, see Figure 18B, (Innamorati et al., 1996; Sadeghi et al., 1997). These results indicated stable surface expression of the wild-type V$_2$R in FRT cells.

Forskolin, an adenylyl cyclase activator, and dDAVP, a V$_2$R-selective vasopressin receptor agonist (Chang et al., 2005), increased the cytoplasmic cAMP concentration; and hence activated the CFTR. The CFTR activity was assayed from the kinetics of the decreasing YFP-H148Q/I152L fluorescence following external I$^-$ addition. Forskolin treatment increased the CFTR activity in the wild-type, mutant and non-transfected cells, whereas dDAVP increased the CFTR activity only in the cells expressing the wild-type V$_2$R, see Figure 19A. The increased CFTR activity in response to forskolin or dDAVP was inhibited by the CFTR blocker CFTR$_{inh}$-172 (Ma et al., 2002a). Inhibition of the dDAVP-stimulated I$^-$ influx was found with the partial V$_2$R agonist [1-β-mercapto-β, β-cyclopentamethylenepropionyl[1], O-ET-TYR[2], VAL[4], ARG[8]]-vasopressin (Sigma) and the V$_2$R antagonist SR121463B (Sanofi Pharmaceutical) (Serradeil-Le Gal et al., 1996; Manning et al., 1997).
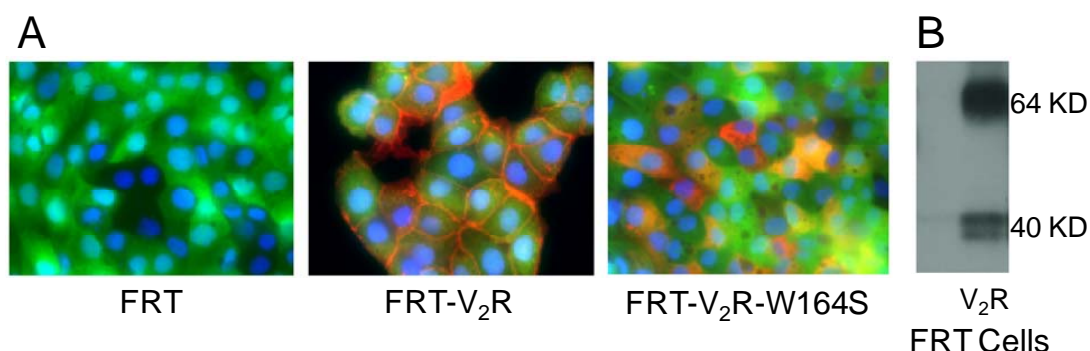
Figure 18. Immunocytochemical and Immunoblot staining of FRT cells. A. Staining of non-transfected FRT cells, the FRT cells stably expressing the wild-type human V_2R (FRT-V_2R), and the FRT cells stably expressing the W164S mutant or V_2R (FRT-V_2R-W164S). Anti-cmyc staining is shown in red, with the YFP in green and the nuclei (DAPI) in blue. B. Immunoblot of a crude protein extract from the FRT (left lane), and FRT-V_2R (right lane) cells.

The concentration-activation data were summarized in Figure 19B. The EC_{50} for the CFTR activation by dDAVP of ~ 0.1 nM was less than that observed in the V_2R radioligand binding experiments, but comparable to that reported in other functional assays (Saito et al., 1996). Figure 20 showed that the forskolin and the dDAVP caused a concentration-dependent increase in the apical membrane Cl^- current in the FRT cells expressing the wild-type V_2R, providing a direct measure of the CFTR function. In each case, the current was fully inhibited by $CFTR_{inh}$-172. These results confirmed a functional cell surface expression of the wild-type V_2R in the stably transfected FRT cells.

High-throughput screening

To establish a screening assay using the V_2R-transfected cells, we first investigated the possible effects of the agonist-induced receptor desensitization and internalization, which for the GPCRs depended on the incubation time and the agonist concentration (Robben et al., 2004). Figure 21 showed the incubation time- and concentration-dependent reduction in the cellular response to dDAVP, as assayed by the CFTR activation. At 1 μM dDAVP, the response was maximal but decreased rapidly with time. Similar maximal responses were found for 1 and 10 nM dDAVP,

but with little time-dependent desensitization. For the primary screening, 1 nM of
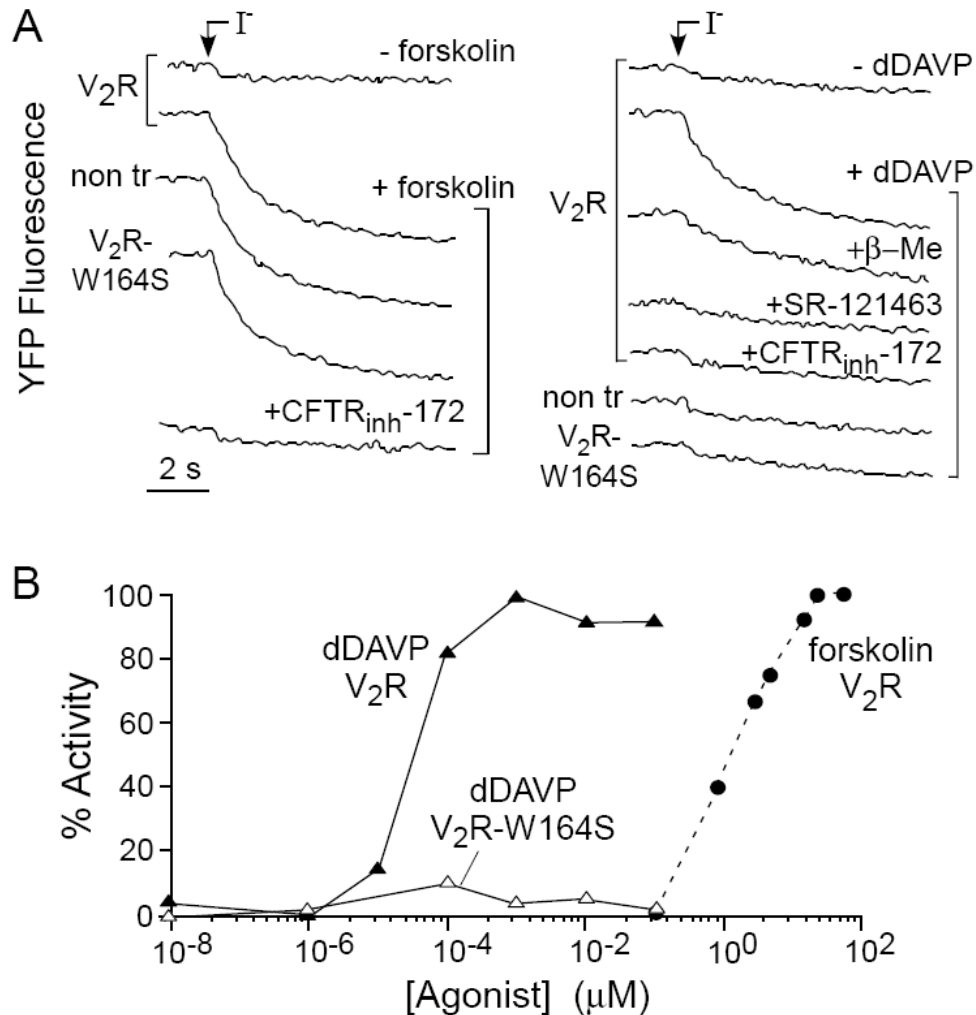
Figure 19. Functional characterization of FRT-V_2R-expressing FRT cells. A. YFP fluorescence following I⁻ addition in the FRT, FRT-V_2R, and FRT-V_2R-W164S cells. The cells were pre-incubated with 20 μM forskolin (left) or 1 nM DAVP (right) for 20 minutes prior to the I⁻ addition. The indicated inhibitors were present before and during measurement: CFTR$_{inh}$-172 (20 μM); [1-β-mercapto-β, β-cyclopentamethylenepropio-nyl[1], O-ET-TYR[2], VAL[4], ARG[8]]-vasopressin (β-ME, 10 μM); SR-21463A (10 μM). B. Percentage maximal activity (from the initial fluorescence slopes following I⁻ addition) as a function of the forskolin and dDAVP concentrations in the FRT-V_2R and FRT-V_2R-W164S cells (Best representation of 3 experiments).
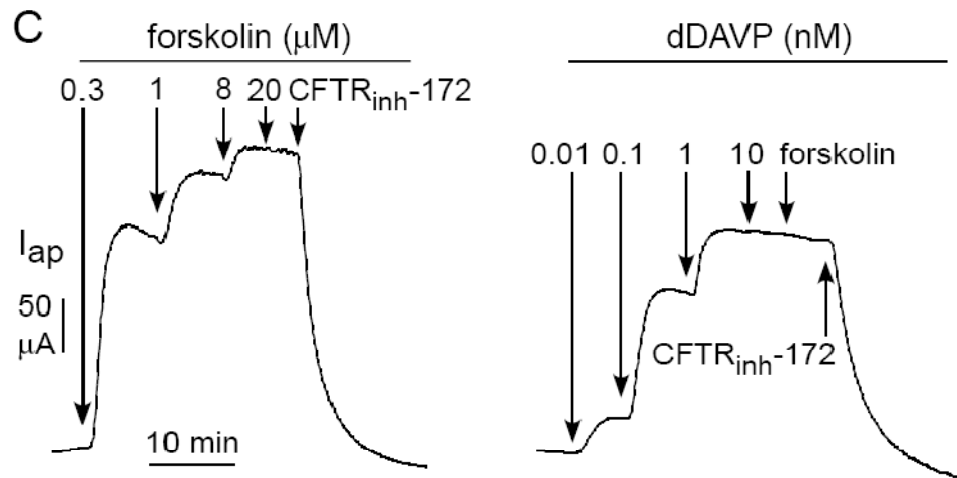
Figure 20. Forkolin- and dDAVP-induced apical membrane current in the FRT-V$_2$R cells. Forskolin and dDAVP concentration-response data in the FRT-V$_2$R cells were measured as the apical membrane current (Iap) in the short-circuit current measurements. Where indicated, 20 µM CFTR$_{inh}$-172 was added. The tracings shown were the representative data from 3 separate sets of experiments.
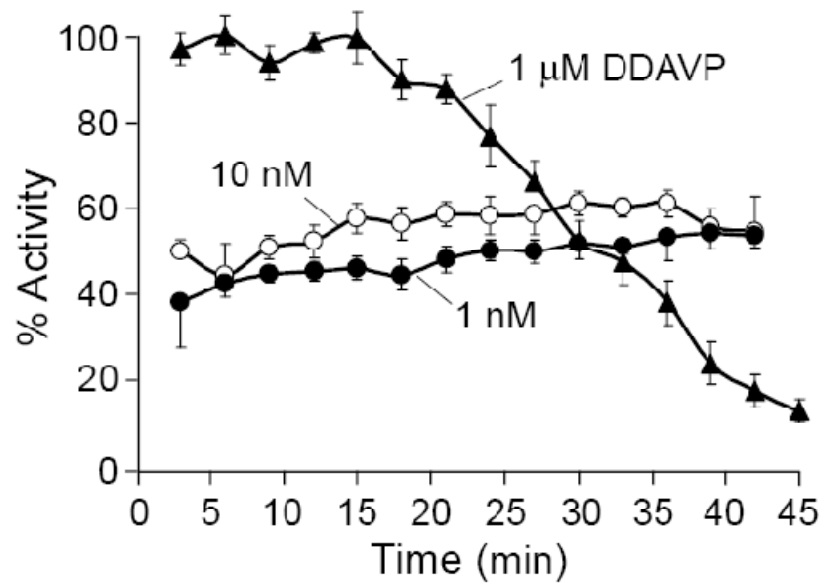
Figure 21. The concentration- and time-dependent nature of dDAVP-induced V$_2$R activation. A time course of V$_2$R desensitization assayed by I$^-$ influx in the FRT-V$_2$R cells exposed to the indicated dDAVP concentrations (n=3, mean±SE).

dDAVP was used to maximize the detection sensitivity of the weakly active, small-molecule competitive antagonists.

The assay suitability for high-throughput screening is evaluated by an experimental determination of the Z'-factor, a quantitative measure of the assay's 'goodness' that depends on the difference between the mean values of the positive and negative control signals, and also their standard deviations (Seethala et al., 2001). Figure 22 (left) shows the original fluorescence data from the individual wells of 96-well plates, incubated for 30 minutes with PBS or 1 nM dDAVP. The distribution of the initial I^- influx rates in the individual wells, $\left(dI^-/dt\right)_{t=0^+}$, shows well-separated positive and negative controls (Figure 22, right), giving a Z'-factor of 0.71. A Z'-factor greater than 0.5-0.6 is considered excellent such that a single primary screening is predicted to be informative in identifying 'hits'.
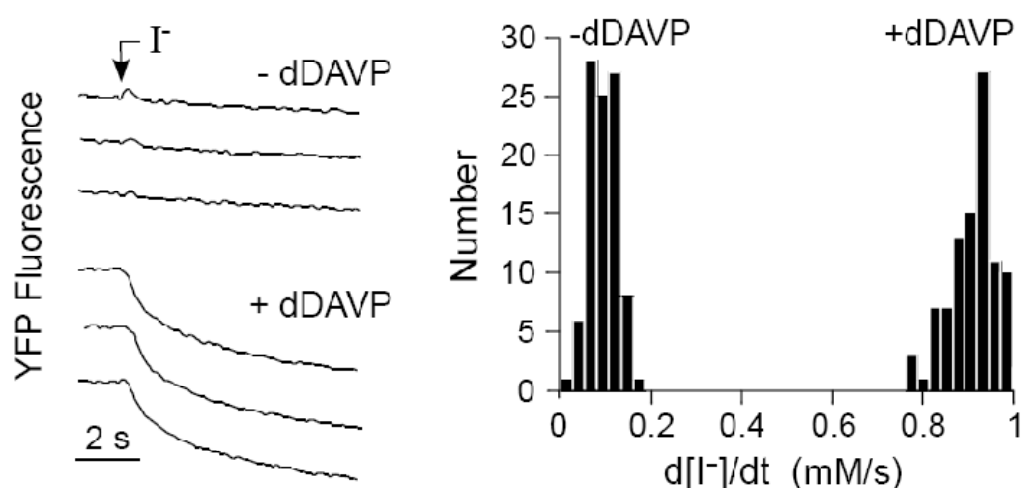
Figure 22. Suitability of the assay for high-throughput screening. Left panel, YFP fluorescence of the FRT-V$_2$R cells pre-incubated with 0 or 1 nM dDAVP for 30 minutes with I$^-$ added as indicated. On the right panel, a histogram distribution of the I$^-$ influx rates, d[I$^-$]/dt, determined from the initial fluorescence slopes.

Primary screening of 50,000 small molecules was carried out using the FRT cells expressing the wild-type human V$_2$R, CFTR and YFP-H148Q/I152L. The cells were incubated with 1 nM dDAVP and the test compounds (20 μM final concentration) for 30 minutes prior to the fluorescence assay of the I$^-$ influx. Figure

23 (left) showed the representative original data for positive and negative controls, along with an example of the active test compound. Figure 23 (right) summarized the percent inhibition as a frequency histogram. The majority of the compound groups (12456 groups of 4 different compounds) did not reduce the $d[I^-]/dt$ significantly (< 30% inhibition at 20 μM). Two hundred and seventy-two compound groups were classified as weak inhibitors (30-90% inhibition), and 27 groups were considered strong inhibitors (> 90% inhibition).

The 'strong' inhibitor groups identified in the primary screening were further evaluated to confirm their inhibition activity at low micromolar concentrations and to identify the individual compounds responsible for the activity out of the groups-of-four used in the primary screening. Two potent classes of compounds were found, one of which was a V_2R antagonist (Figure 24), as judged by their selective inhibition of the dDAVP-induced cAMP production (see below). The V_2R antagonist was of the 5-aryl-4-benzoyl-3-hydroxy-1-(2-arylethyl)-2H-pyrrol-2-one chemical class, which was not structurally similar to other known V_2R antagonists (the OPC 31260 and SR 121463A structures shown in Figure 24). Another (non-V_2R antagonist) hit identified in the screening, aryl-3-alkoxycarbonyl-2-(acylamino)thiophenes, was to be discussed in the later section.
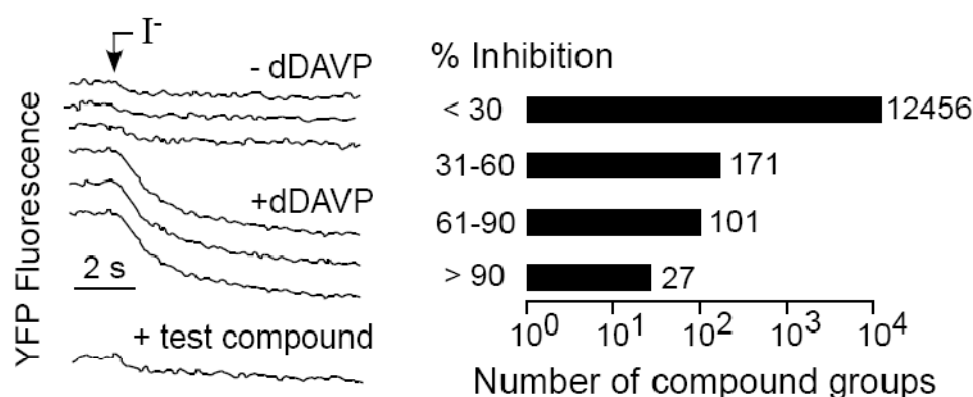
Figure 23. The results from HTS of 50,000 compounds. Left panel, examples of positive and negative control fluorescence data from the individual wells in the primary screening, along with an example of the 'active' test compound. On the right panel, the histogram distribution of inhibitions in percent from the screening of 50,000 small molecules in groups of four.

An analysis of the V_2R_{inh} structure-activity relationship (SAR)

SAR analysis was done by screening a small set of 35 commercially available
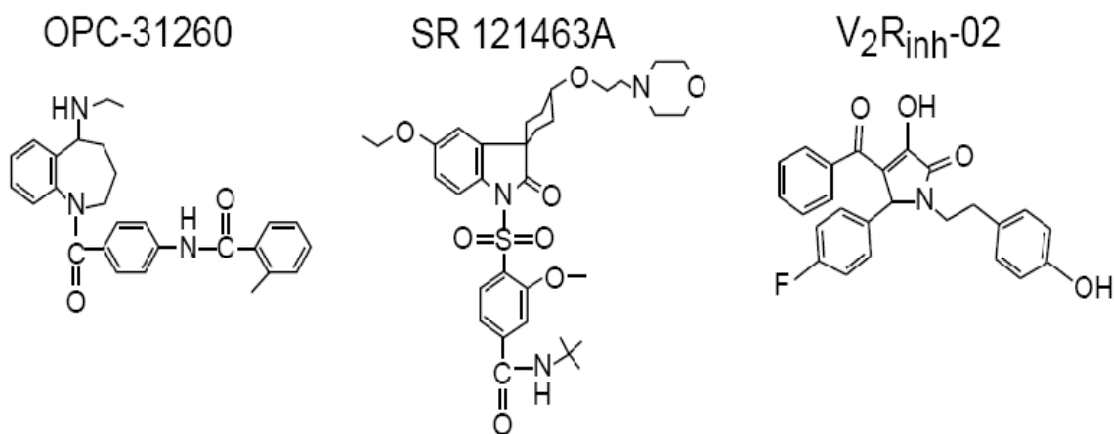
Figure 24. The structure of V_2R_{inh}-02 shown with the previously identified V_2R antagonists, OPC-312260 and SR-121463A.

2,5-dihydro-2-pyrolone analogs. Tables 11 and 12 listed the V_2R inhibition data of the active and inactive compounds; and Figure 25 (left) summarized the SAR analysis in terms of the functional groups conferring the V_2R antagonist activity. At position R_1, 4-substituted phenyl conferred the greatest inhibition; the inhibition was lost when R_1 was methyl or furanyl. Notably, V_2R_{inh}-13, which contained a thiophenyl ring at R_1, was also active. The greatest diversity in the collection of the 2-pyrrolone analogs was in R_2. The activity was seen primarily for the 4-halogen or 4-nitro substituted phenyl. Exceptions to this were the two 2-fluorophenyl derivatives [V_2R_{inh}-04 and V_2R_{inh}-11] and the 3-nitrophenyl derivative [V_2R_{inh}-08]. Phenyl substitutions at R_2 that led to inactive compounds were generally electron donating substituents including methoxy, hydroxy, and alkyl. Methyl formate esters and other heterocycles were not tolerated at R_2, including furyl, thiophenyl, and 3-pyridinyl rings. R_3 as phenyl and 4-hydroxy phenyl gave active compounds; and the 3,4-dimethoxyphenyl and the 4-hydroxy-3-methoxyphenyl analogs were inactive. The 4-hydroxylphenyl derivative gave the greatest inhibition potency, with the most potent compound being 4-benzoyl-5-(4-fluorophenyl)-1,5-dihydro-3-hydroxy-1-[2-(4-hydroxyphenyl)ethyl-2H-pyrrol-2-one (V_2R_{inh}-02). This compound was synthesized in a pure form on a large scale and

further characterized.
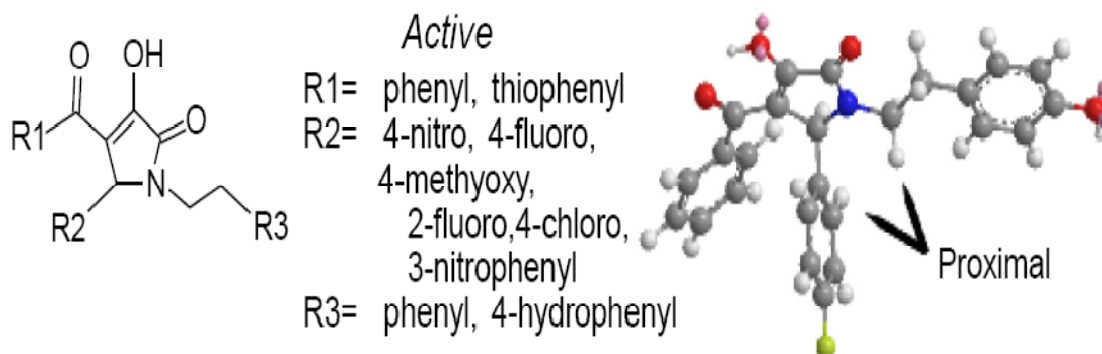
Figure 25. The structure-activity relationship of V_2R_{inh}-02 (left). A summary of the structure-activity relationship data for 35 compounds (left panel), see also Table 11. On the right, the predicted 3-dimensional structure of V_2R_{inh}-02.

Table 11. The structure-activity relationship of the active V_2R antagonists.

Compounds	R1	R2	R3	% inhibition at 20 μM
V_2R_{inh}-01	Ph	4-NO_2–Ph	Ph	20
V_2R_{inh}-02	Ph	4-F-Ph	4-OH-Ph	100
V_2R_{inh}-03	4-Me-Ph	4-OMe-Ph	Ph	50
V_2R_{inh}-04	4-OMe-Ph	2-F-Ph	Ph	41
V_2R_{inh}-05	4-OMe-Ph	4-Cl-Ph	Ph	82
V_2R_{inh}-06	4-OMe-Ph	4-NO_2–Ph	Ph	10
V_2R_{inh}-07	4-OMe-Ph	4-OMe-Ph	Ph	45
V_2R_{inh}-08	4-Cl-Ph	3-NO_2-Ph	Ph	40
V_2R_{inh}-09	4-Cl-Ph	4-NO_2–Ph	Ph	60
V_2R_{inh}-10	4-Br-Ph	2-F-Ph	Ph	71
V_2R_{inh}-11	4-Br-Ph	4-Cl-Ph	Ph	72
V_2R_{inh}-12	4-Br-Ph	4-NO_2-Ph	Ph	35
V_2R_{inh}-13	thiophenyl	4-Cl-Ph	Ph	62

Ph = phenyl, Br = bromo, Cl = chloro, F = fluoro, OMe = methoxy, and NO_2 = nitro.

Table 12. Inactive analogues of V_2R antagonists.

Compound	R1	R2	R3
V_2R_{inh}-14	Benzoyl	2-NO_2-Ph	Ph
V_2R_{inh}-15	Benzoyl	4-OMe-Ph	3,4-di-OMe-Ph
V_2R_{inh}-16	4-Me-Benzoyl	3-NO_2-Ph	Ph
V_2R_{inh}-17	4-OMe-Benzoyl	2-NO_2-Ph	Ph
V_2R_{inh}-18	4-OMe-Benzoyl	3-NO_2-Ph	Ph
V_2R_{inh}-19	4-OMe-Benzoyl	2,4-di-OMe-Ph	Ph
V_2R_{inh}-20	4-OMe-Benzoyl	2-Cl-Ph	Ph
V_2R_{inh}-21	4-Br-Benzoyl	2-Cl-Ph	Ph
V_2R_{inh}-22	4-Br-Benzoyl	3-NO_2-Ph	Ph
V_2R_{inh}-23	4-Br-Benzoyl	2,4-di-OMe-Ph	Ph
V_2R_{inh}-24	4-Br-Benzoyl	3,4-di-OMe-Ph	Ph
V_2R_{inh}-25	Ethanoyl	Ph	Ph
V_2R_{inh}-26	Ethanoyl	4-Me-Ph	Ph
V_2R_{inh}-27	Ethanoyl	4-OMe-Ph	Ph
V_2R_{inh}-28	Ethanoyl	4-OH-Ph	3,4-di-OMe-Ph
V_2R_{inh}-29	Ethanoyl	4-F-Ph	3,4-di-OMe-Ph
V_2R_{inh}-30	Ethanoyl	3-F-Ph	3,4-di-OMe-Ph
V_2R_{inh}-31	Furan-2-CO	3,4-di-OMe-Ph	3,4-di-OMe-Ph
V_2R_{inh}-32	Furan-2-CO	Pyridine-3-yl	3,4-di-OMe-Ph
V_2R_{inh}-33	Furan-2	Thiophene-2-yl	3,4-di-OMe-Ph
V_2R_{inh}-34	5-Me-Furan-2-CO	Thiophene-2-yl	3,4-di-OMe-Ph
V_2R_{inh}-35	Furan-2-CO	Furan-2-yl	3,4-di-OMe-Ph

Ph = phenyl, Br = bromo, Cl = chloro, CO = Carbonyl, F = fluoro, Me = Methyl,

OMe = methoxy, and NO_2 = nitro.

Synthesis and characterization of V_2R_{inh}-02

The synthesis of V_2R_{inh}-02 was accomplished in two steps as follows. The dioxoethyl butylate1 was synthesized by the reaction between the enolate of acetophenone and the diethyloxylate to give 2,4-dioxo-4-phenyl-ethylbutylate1**,** see Figure 26. Following the reaction of 4-bromobenzaldehyde and tyramine to form the imine, addition of 2,4-dioxo-4-phenyl-ethylbutylate1 in dioxane gave V_2R_{inh}-02, see Figure 26, which was purified by crystallization. Its pKa was 4.76 as measured by the spectrophotometric titration (absorbance 346 nm) of 100 μM V_2R_{inh}-02 in aqueous solution containing the citric acid, sodium acetate, HEPES, sodium borate, tris, and sodium carbonate (each of 5 mM) titrated to the indicated pH using HCl and NaOH. Deprotonation of the hydroxyl group on the pyrrolone ring occurred at low pH, such

that V_2R_{inh}-02 contained a single negative charge at the physiological pH. The aqueous solubility of V_2R_{inh}-02 in PBS was 377 µM as measured by the optical absorbance of a saturated solution after appropriate dilution. The high aqueous solubility of V_2R_{inh}-02 was a consequence of its polarity and charge.

The V_2R_{inh}-02 identity was confirmed by ^{1}H NMR and mass spectrometry. Purity was determined to be 99% by the liquid chromatography. Figure 25 (right) showed the predicted 3-d structure of V_2R_{inh}-02, based on the energy minimization computations. An interesting finding from the ^{1}H NMR spectra was the magnetic non-equivalence of the two CH_2 groups of the 1-(4-hydroxyphenethyl) fragment. From the computed structure, it might be concluded that this magnetic non-equivalence was due to the proximal 4-fluorophenyl group interacting with H on the -CH_2-N group, accounting for the AA'BB' splitting pattern and the downfield chemical shift ~3.9 ppm of the proximal proton. This interpretation was supported by the published structure data for 5-aryl-1-benzyl-2,5-dihydro-2-pyrrolones (Aliev et al., 2003).
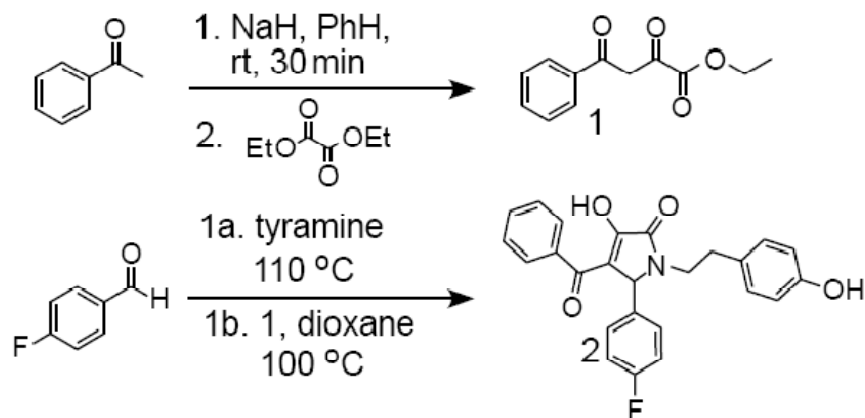
Figure 26. A synthesis of V_2R_{inh}-02: 4-benzoyl-5-(4-fluorophenyl)-1,5-dihydro-3-hydroxy-1-[2-(4-hydroxyphenyl)ethyl-2H-pyrrol-2-one. See the text for description.

The V_2R_{inh}-02 was first tested for its inhibitory potency in the apical membrane current measurements of the CFTR Cl$^-$ channel activity. Figure 27 showed V_2R_{inh}-02 concentration-dependent inhibition of the Cl$^-$ current induced by 1 nM dDAVP, with IC$_{50}$ of appriximately 0.5 µM.
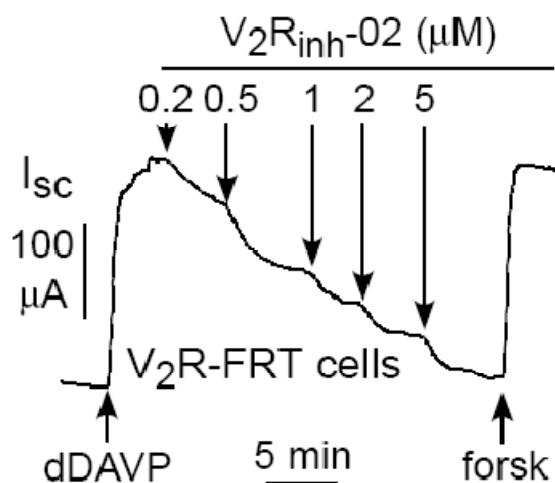
Figure 27. Inhibition of dDAVP-induced chloride current in V_2R-FRT cells by V_2R_{inhi}-02. Twenty μM of forskolin was added where indicated. The tracing shown was the representative data from 3 separate sets of experiments.

Several possible steps in the signal transduction cascade for the CFTR activation could be modulated by V_2R_{inh}-02, including (i) V_2R; (ii) G-proteins, Gs or Gi; (iii) adenylyl cyclase; (iv) phosphodiesterase; (v) protein kinase A; and (vi) CFTR. The failure of V_2R_{inh}-02 to inhibit the forskolin-induced Cl^- current, as seen in Figure 27, indicated that V_2R_{inh}-02 was unlikely to act on Gi, adenylyl cyclase, or more distal components of the signal transduction cascade. To distinguish the action of V_2R_{inh}-02 as a V_2R antagonist versus a Gs-inhibitor, the short-circuit current was measured in the Calu-3 cells which natively expressed the β_2-adrenergic Gs-coupled receptor. Figure 28 (left) showed inhibition of the isoproterenol-induced short-circuit current in the Calu-3 cells by the β_2 antagonist propranolol. V_2R_{inh}-02 did not inhibit the isoproterenol-induced response in the Calu-3 cells (Figure 28, right). Taken together, these findings suggested that V_2R_{inh}-02 was a V_2R antagonist.

Measurements of the cAMP concentration were made in the V_2R expressing the FRT cells in order to verify the action of V_2R_{inh}-02 at the vasopressin-2 receptor. Figure 29A (left) showed dDAVP concentration-response data for elevation of cAMP
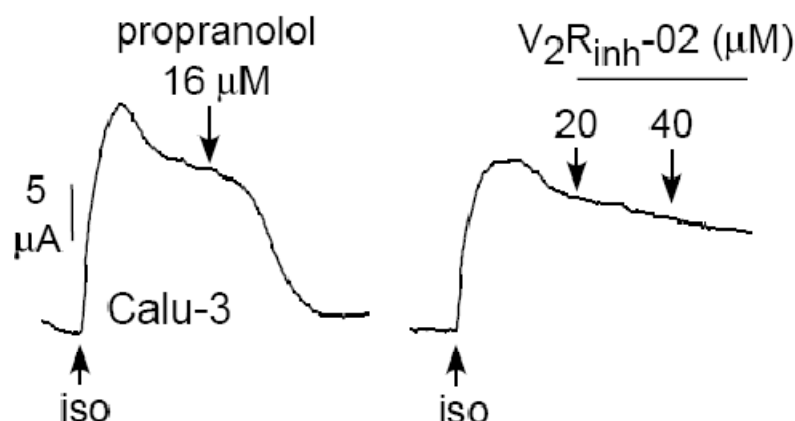
Figure 28. Inhibition of the isoproterenol-stimulated short-circuit current in the Calu-3 cells by the indicated concentrations of propranolol and V_2R_{inh}-02. The tracings shown were the representative data from 3 separate sets of experiments.

concentration. V_2R_{inh}-02 inhibition of cAMP concentration following the stimulation by 1 nM dDAVP was shown in Figure 29A (right). The IC_{50} was ~60 nM. To verify the action of V_2R_{inh}-02 on the V_2R, the cAMP concentration was measured in the β_2-receptor transfected CHO cells, see Figure 29B. The cellular cAMP was increased by isoproterenol as expected. The increased cAMP concentration was inhibited by propranolol but not by SR 121463B or V_2R_{inh}-02, supporting the V_2R inhibition by V_2R_{inh}-02.

V_2R_{inh}-02 is a competitive V_2R antagonist

Figure 30A showed a functional 'competition study' in which the V_2R_{inh}-02 reduction of cAMP concentration was measured in the V_2R expressing FRT cells after stimulation by different concentrations of dDAVP. The apparent IC_{50} increased greatly with increasing dDAVP concentrations, indicative of a competitive binding mechanism. A Schild plot was shown in the inset to Figure 30A where [V_2R_{inh}-02] was plotted against the dDAVP dose-ratio (Kenakin, 1997). The slope of 1.3 of the fitting line was consistent with a competitive inhibition mechanism with the calculated K_i of approximatlely 70 nM.
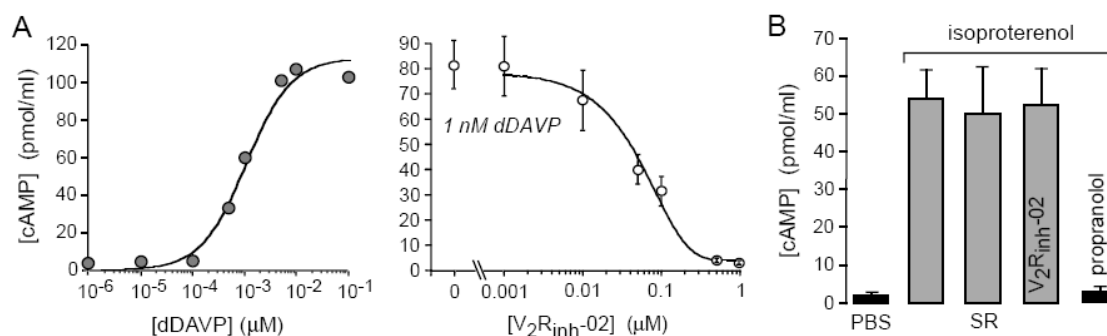
Figure 29. The effects of V_2R_{inh}-02 on cAMP concentration. A. (Left) cAMP concentration vs dDAVP concentration in the FRT-V_2R cells after 20-minute incubation with various concentrations of dDAVP. (Right) Reduced cAMP following V_2R_{inh}-02. *The cells* were incubated for 20 minutes with 1 nM dDAVP and various concentrations of V_2R_{inh}-02 (mean ± SE, n=3). B. cAMP concentration in the CHO cells transiently transfected with the human β2-adrenergic receptor. The cells were incubated for 20 minutes with 0.01 μM isoproterenol in the presence of 20 μM SR-121463A, V_2R_{inh}-02, or propranolol. The data were shown as mean ± SE, n=3.

Binding displacement assays were done to prove V_2R_{inh}-02 competition with vasopressin at the V_2R. Cell-associated radiolabeled vasopressin was measured after binding to the V_2R expressing FRT cells. The V_2R selective binding component was determined by subtracting the non-specific binding(the radioactivity in the presence of a high concentration of non-radioactive dDAVP) from the total radioactivity. As summarized in Figure 30B, V_2R_{inh}-02 at 1 μM reduced the cell-associated radioactivity to near zero with 50% competition at ~70 nM, supporting a competitive V_2R_{inh}-02 binding mechanism. To investigate the V_2R binding selectivity versus $V_{1a}R$ binding selectivity, similar binding displacement experiments were carried out in the FRT cells stably expressing $V_{1a}R$. Fifty percent competition of V_2R_{inh}-02 to [^{3}H]AVP was observed at ~5 μM (Figure 30B), indicating that the affinity of V_2R_{inh}-02 to V_2R was ~70 times that of V_2R_{inh}-02 to $V_{1a}R$.
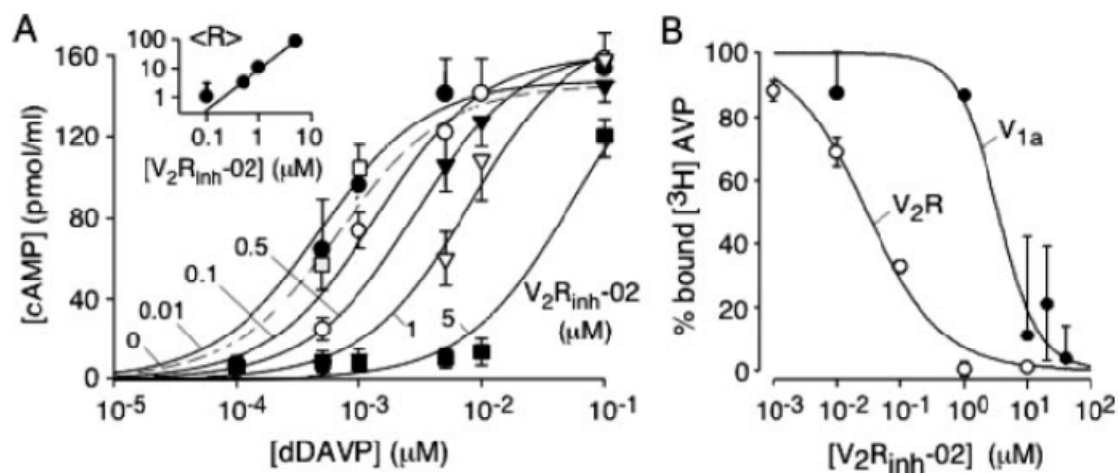
Figure 30. Competitive binding and vasopressin receptor subtype selectivity of V_2R_{inh}-02. A. A competition study showing the cAMP concentration in the FRT-V_2R cells as a function dDAVP concentrations in the presence of different concentrations of V_2R_{inh}-02 (mean ± SE, n=3). Inset: a Schild plot with a slope of 1.3 and the extrapolated K_i of 70 nM. B. [³H]AVP binding displacement assays were done in the intact FRT cells stably expressing V_2R or $V_{1a}R$. The cells were incubated for 2 hours with 1 nM [³H]AVP in the presence of different concentrations of V_2R_{inh}-02. The cell-associated radioactivity after incubation and washing (mean ± SE, n=3). Non-specific binding is subtracted. See Chapter IV: Materials and Methods for more details.

Synthesis of chiral 2-(acylamino)-3-thiophenecarboxylates

In addition to the 5-aryl-4-benzoyl-3-hydroxy-1-(2-arylethyl)-2H-pyrrol-2-one (V_2R_{inh} class) which was characterized in details above, another class of the compound identified from the HTS was aryl-3-alkoxycarbonyl-2-(acylamino)thiophenes or PDE_{act}. The syntheses of the original hits identified from the HTS, chiral 2-(acylamino)-3-thiophenecarboxylates (PDE_{act}-04) and its analogues (PDE_{act}-03) were achieved by condensing bicyclo[2.2.1]heptane-2,3-dicarboxylic anhydride with 5-methyl-4-substituted aryl-3-alkoxycarbonyl-2-aminothiophenes. A representative synthetic strategy for PDE_{act}-03 was shown in Figure 31. The α,β unsaturated nitrile 3 was isolated as an *E/Z*-isomeric mixture and obtained by heating 4'-methyl propiophenone and methyl cyanoacetate in benzene using a Dean-Stark apparatus for constant water separation in the presence of glacial acetic acid and catalytic ammonium acetate. ¹H NMR of 3 clearly showed the mixture of *E/Z* isomers with two

distinct singlets at 3.84 and 3.64 ppm, corresponding to a methyl group of methyl ester along with two separated quartets for a methylene group and the multiplet for the rest of the methyl groups and aromatic protons. Knoevenagel condensation product 3 was subsequently cyclized with sulfur and diethylamine to yield 4. A complete disappearance of the condensation product 3 was observed when the reaction was carried out at 35-40ºC, suggesting that isomerization from E to Z occurred at an elevated temperature enabling the reaction of the E-isomer, which was a major condensation product. ^{1}H NMR showed a para substituted pattern in the aromatic signals along with the broad singlets of amine protons at 5.82 ppm. Three prominent singlets in the aliphatic region at 3.45, 2.34 and 2.00 ppm corresponding to the methyl ester, p-tolyl and methyl, respectively, confirmed the formation of 4. The key synthon $Endo$-bicyclo[2.2.1]heptane-2,3-dicarboxylic anhydride was purchased from Aldrich (mp 163 ºC) and used as such, and the contrary, exo-bicyclo[2.2.1]heptane-2,3-dicarboxylic anhydride which was synthesized by saturation using the catalytic hydrogenation of exo-bicyclo[2.2.1]hept-5-ene-2,3-dicarboxylic anhydride, showed the melting point at 78-79º. ^{1}H NMR of $endo$ and exo-bicyclo[2.2.1]heptane-2,3-dicarboxylic anhydrides also showed the corresponding differences in signals. Condensation of 4 with either $endo$ or exo bicyclo[2.2.1]heptane-2,3-dicarboxylic anhydride was achieved in the melting reaction which yielded $endo$ or exo-PDE$_{act}$-03, respectively.

Structure-activity analysis of 2-(acylamino)-3-thiophenecarboxylates

To define the structure-activity relationship, 144 synthetic analogs of PDE$_{act}$-04 and the compound identified from the HTS were screened in the functional assay using the YFP fluorescence intensity as a read-out (Tables 13, and 14). Figure 32 summarized the structural features of the active aryl-3-alkoxycarbonyl-2-(acylamino)thiophenes. The active compounds contained the p-tolyl, 3,4-dimethylphenyl or ortho/para chlorophenyl substituents at R$_4$, methyl at R$_5$, methoxy or ethoxy at R$_3$, and 3-bicyclo[2.2.1]heptyl-2-carboxylic acid at R$_2$ of the thiophene nucleus. The activity was abolished or substantially reduced with substitutions at R$_2$ including N,N-dimethylaminomethyl, methyl, chloromethyl, 2-carboxyphenyl, mono, di and trisubstituted nitrophenyl, substituted methoxyphenyl, 3-chloro-benzthiophenyl,

pyridine-3-yl, coumaryl, tetrahydrofuryl, 1,4-benzodioxyl, substituted carboxy cyclohexenyl, substituted halophenyl, thiophene-2-yl, isoindolinyl-1,3-dione, anilino and furanyl.
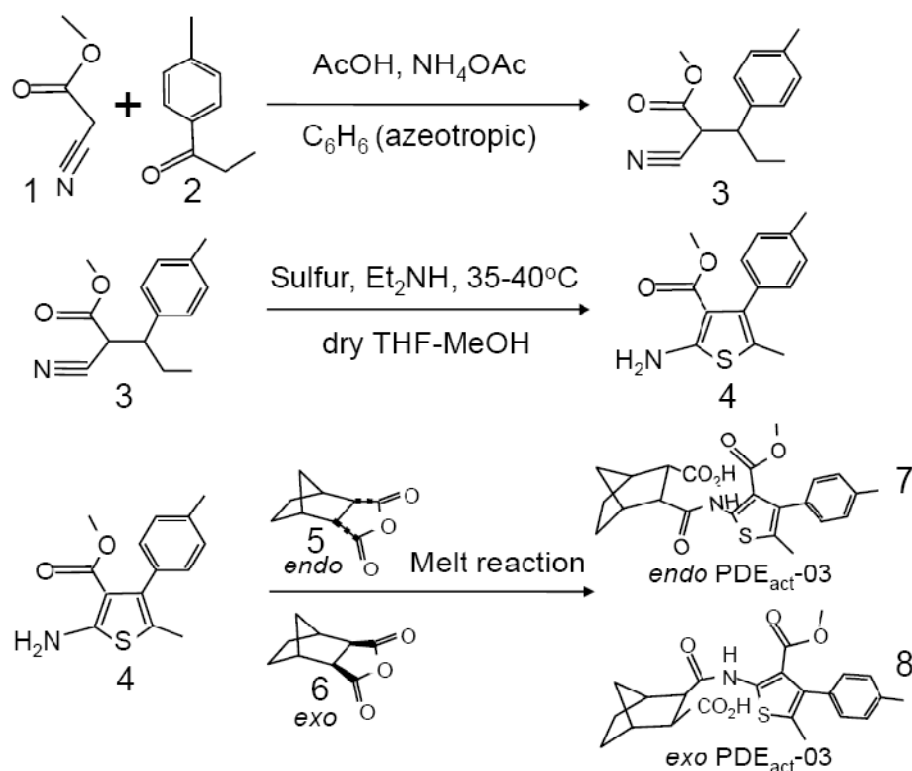
Figure 31. Synthetic schemes for PDEact-03. See the text for description.
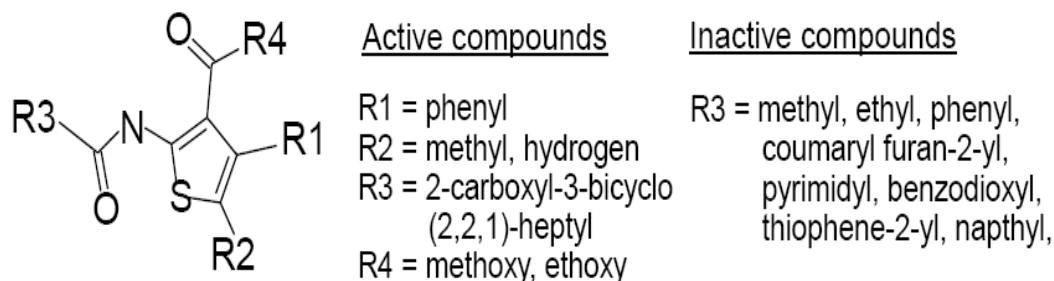
Figure 32. Structure-activity relationships of 2-(acylamino)-3-thiophenecarboxylates.

Table 13. Active analogues of PDE$_{act}$-04.

Compound	R1	R2	R3	R4	IC$_{50}$ (µM)
PDE$_{act}$-01	2-Cl-Ph	Me	2-COOH-3-Bicyclo(2,2,1)-Heptyl	OMe	15
PDE$_{act}$-02	3,4-di-Me-Ph	Me	2-COOH-3-Bicyclo(2,2,1)-Heptyl	OMe	4
PDE$_{act}$-03	4-Me-Ph	Me	2-COOH-3-Bicyclo(2,2,1)-Heptyl	OMe	4
PDE$_{act}$-04	4-Cl-Ph	Me	2-COOH-3-Bicyclo(2,2,1)-Heptyl	OEt	8
PDE$_{act}$-05	3,4-di-Me-Ph	Me	2-COOH-3-Bicyclo(2,2,1)-Heptyl	OEt	6

Ph = Phenyl, Me = Methyl, OMe = Methoxy, OEt = Ethoxy, COOH = Carboxyl, and

Cl = Chloro

Table 14. Inactive analogues of PDE$_{act}$-04.

Compound	R1	R2	R3	R4
PDE$_{act}$-06	Ph		Me	OEt
PDE$_{act}$-07	Ph		Cl-Me	OEt
PDE$_{act}$-08	Ph		OMe-Me	OEt
PDE$_{act}$-09	Ph		OPh-Me	OEt
PDE$_{act}$-10	Ph		SPh-Me	OEt
PDE$_{act}$-11	Ph		N,N-di-Me-Amino-Me	OEt
PDE$_{act}$-12	Ph		Pyrrolidine-N-Methylene	OEt
PDE$_{act}$-13	Ph		1-Me-Et	OEt
PDE$_{act}$-14	Ph		1,1-di-Me-Et	OEt
PDE$_{act}$-15	Ph		3-COOH-1-Propanyl	OEt
PDE$_{act}$-16	Ph		3-COOH-1-Propanyl	OEt
PDE$_{act}$-17	Ph		Cyclopropanyl	OEt
PDE$_{act}$-18	Ph		2-COOH-3-cyclohexenyl	1-Me-OEt
PDE$_{act}$-19	Ph		Ph	OEt
PDE$_{act}$-20	Ph		2-Cl-Ph	OEt
PDE$_{act}$-21	Ph		2-F-Ph	OEt
PDE$_{act}$-22	Ph		2-OMe-Ph	OEt
PDE$_{act}$-23	Ph		2-COOH-Ph	OEt
PDE$_{act}$-24	Ph		3-OMe-Ph	OEt
PDE$_{act}$-25	Ph		4-Cl-Ph	OEt
PDE$_{act}$-26	Ph		4-NO$_2$-Ph	OEt
PDE$_{act}$-27	Ph		4-Ph-Ph	OEt
PDE$_{act}$-28	Ph		3,5-di-NO$_2$-Ph	OEt
PDE$_{act}$-29	Ph		3,4,5-tri-OMe-Ph	OMe
PDE$_{act}$-30	Ph		2-Cl-4,5-di-F-Ph	OEt

Table 14 (continued). Inactive analogues of PDE$_{act}$-04

Compound	R1	R2	R3	R4
PDE$_{act}$-31	Ph		3-Cl-Benzthiophenyl	OEt
PDE$_{act}$-32	Ph		Pyridine-3-yl	OEt
PDE$_{act}$-33	Ph		1,2,4-Triazolepyrimidyl	OEt
PDE$_{act}$-34	Ph		Coumaryl	OEt
PDE$_{act}$-35	Ph		Tetrahydrofuryl	OEt
PDE$_{act}$-36	Ph		Furan-2-yl	OMe
PDE$_{act}$-37	Ph		1,4-benzodioxyl	OEt
PDE$_{act}$-38	4-Me-Ph		Me	OEt
PDE$_{act}$-39	4-Me-Ph		Cl-Me	OEt
PDE$_{act}$-40	4-Me-Ph		OMe-Me	OEt
PDE$_{act}$-41	4-Me-Ph		SPh-Me	OEt
PDE$_{act}$-42	4-Me-Ph		Ph-Me	OEt
PDE$_{act}$-43	4-Me-Ph		Et	OEt
PDE$_{act}$-44	4-Me-Ph		Pentanyl	OEt
PDE$_{act}$-45	4-Me-Ph		2-COOH-3-Cyclohexenyl	OEt
PDE$_{act}$-46	4-Me-Ph		2-COOH-3-Cyclohexenyl	1-Me-OEt
PDE$_{act}$-47	4-Me-Ph		3-Br-Ph	OEt
PDE$_{act}$-48	4-Me-Ph		4-F-Ph	OEt
PDE$_{act}$-49	4-Me-Ph		4-Ph-Ph	OEt
PDE$_{act}$-50	4-Me-Ph		Pyridine-3-yl	OEt
PDE$_{act}$-51	2,4-di-Me-Ph		3-Br-Ph	OEt
PDE$_{act}$-52	3,4-di-Me-Ph		Me	OEt
PDE$_{act}$-53	3,4-di-Me-Ph		OMe-Me	OEt
PDE$_{act}$-54	3,4-di-Me-Ph		Tetrahydrofuryl	OEt
PDE$_{act}$-55	4-OMe-Ph			OEt
PDE$_{act}$-56	4-OMe-Ph		Me	OEt
PDE$_{act}$-57	4-OMe-Ph		OMe-Me	OEt
PDE$_{act}$-58	4-OMe-Ph		Et	OEt
PDE$_{act}$-59	4-OMe-Ph		1-Me-Et	OEt
PDE$_{act}$-60	4-OMe-Ph		Propanyl	OEt
PDE$_{act}$-61	4-OMe-Ph		Cyclohexanyl	OEt
PDE$_{act}$-62	4-OMe-Ph		Ph	OEt
PDE$_{act}$-63	4-OMe-Ph		3-NO$_2$-Ph	OEt
PDE$_{act}$-64	4-OMe-Ph		4-Me-Ph	OEt
PDE$_{act}$-65	4-OMe-Ph		4-(1,1-di-Me-Et)Ph	OEt
PDE$_{act}$-66	4-OMe-Ph		4-Cl-Ph	OEt
PDE$_{act}$-67	4-OMe-Ph		Thiophene-2-yl	OEt
PDE$_{act}$-68	4-OMe-Ph		Pyridine-3-yl	OEt
PDE$_{act}$-69	4-OMe-Ph		Tetrahydrofuryl	OEt
PDE$_{act}$-70	3,4-di-OMe-Ph			OEt
PDE$_{act}$-71	3,4-di-OMe-Ph		Me	OEt
PDE$_{act}$-72	3,4-di-OMe-Ph		OMe-Me	OEt
PDE$_{act}$-73	3,4-di-OMe-Ph		Et	OEt

Table 14(continued). Inactive analogues of PDE_{act}-04.

Compound	R1	R2	R3	R4
PDE_{act}-74	3,4-di-OMe-Ph		1-Me-Et	OEt
PDE_{act}-75	3,4-di-OMe-Ph		1,1-di-Me-Et	OEt
PDE_{act}-76	3,4-di-OMe-Ph		2-Cl-Et	OEt
PDE_{act}-77	3,4-di-OMe-Ph		Ph	OEt
PDE_{act}-78	3,4-di-OMe-Ph		2-OMe-Ph	OEt
PDE_{act}-79	3,4-di-OMe-Ph		2-F-Ph	OEt
PDE_{act}-80	3,4-di-OMe-Ph		Thiophene-2-yl	OEt
PDE_{act}-81	3,4-di-OMe-Ph		Pyridine-3-yl	OEt
PDE_{act}-82	3,4-di-OMe-Ph		Pyridine-4-yl	OEt
PDE_{act}-83	3,4-di-OMe-Ph		Furan-2-yl	OEt
PDE_{act}-84	3,4-di-OMe-Ph		Tetrahydrofuryl	OEt
PDE_{act}-85	3,4,5-tri-OMe-Ph		Ph	OEt
PDE_{act}-86	4-OEt-Ph			OEt
PDE_{act}-87	4-OEt-Ph		Me	OEt
PDE_{act}-88	4-OEt-Ph		OMe-Me	OEt
PDE_{act}-89	4-OEt-Ph		Et	OEt
PDE_{act}-90	4-Br-Ph		SPh-Me	OEt
PDE_{act}-91	4-Br-Ph		2-COOH-3-Cyclohexenyl	1-Me-OEt
PDE_{act}-92	4-Br-Ph		Ph	OEt
PDE_{act}-93	4-Br-Ph		4-Me-Ph	OEt
PDE_{act}-94	4-Br-Ph		2-COOH-Ph	OEt
PDE_{act}-95	4-Br-Ph		3-Cl-Ph	OEt
PDE_{act}-96	4-Br-Ph		3-NO_2-Ph	OEt
PDE_{act}-97	4-Br-Ph		4Ph-Ph	OEt
PDE_{act}-98	4-Br-Ph		Furan-2-yl	OEt
PDE_{act}-99	4-Cl-Ph		Me	OEt
PDE_{act}-100	4-Cl-Ph		OMe-Me	OEt
PDE_{act}-101	4-Cl-Ph		2-COOH-3-Cyclohexenyl	OMe
PDE_{act}-102	4-Cl-Ph		Tetrahydrofuryl	OEt
PDE_{act}-103	2,4-Cl-Ph		2-COOH-3-Bicyclo(2,2,1)-Heptyl	1-Me-OEt
PDE_{act}-104	4-F-Ph		OMe-Me	OEt
PDE_{act}-105	4-F-Ph		Cl-Me	OEt
PDE_{act}-106	4-F-Ph		Et	OEt
PDE_{act}-107	4-F-Ph		1-Me-Et	OEt
PDE_{act}-108	4-F-Ph		Pyridine-3-yl	OEt
PDE_{act}-109	4-F-Ph		Tetrahydrofuryl	OEt
PDE_{act}-110	4-F-Ph		Isoindoline-1,3-dione	OEt
PDE_{act}-111	4-NO_2-Ph		Ph	OEt
PDE_{act}-112	4-Ph-Ph		Me	OEt
PDE_{act}-113	4-Ph-Ph		SPh-Me	OEt
PDE_{act}-114	4-Ph-Ph		1-Me-Et	OEt
PDE_{act}-115	4-Ph-Ph		4-Me-Ph	OEt

Table 14(continued). Inactive analogues of PDE$_{act}$-04.

Compound	R1	R2	R3	R4
PDE$_{act}$-116	4-Ph-Ph		Furan-2-yl	OEt
PDE$_{act}$-117	4-Ph-Ph		1-Napthyl	OEt
PDE$_{act}$-118	Ph	Me	Me	OEt
PDE$_{act}$-119	Ph	Me	SPh-Me	OEt
PDE$_{act}$-120	Ph	Me	Ph	OEt
PDE$_{act}$-121	Ph	Me	1,4-Benzodioxyl	OMe
PDE$_{act}$-122	Ph	Me	Coumaryl	OEt
PDE$_{act}$-123	Ph	Me	Pyridine-3-yl	OEt
PDE$_{act}$-124	Ph	Me-Oxyme	Me	OEt
PDE$_{act}$-125	Ph	Me-CO	Me	OEt
PDE$_{act}$-126	Ph	Me-CO	Ph	OEt
PDE$_{act}$-127		Me-CO	2-Cl-Ph	OEt
PDE$_{act}$-128	Ph	Et	(4-Cl-OPh)-Me	OEt
PDE$_{act}$-129	Ph	NO$_2$	Ph	OEt
PDE$_{act}$-130	Ph	Ph		OEt
PDE$_{act}$-131	Ph	Ph	Et	OEt
PDE$_{act}$-132	Ph	Ph	Propanyl	OEt
PDE$_{act}$-133	Ph	Ph	Ph	OEt
PDE$_{act}$-134	Ph	Ph	Anilio	OEt
PDE$_{act}$-135	4-Me-Ph	Cl	Cl-Me	OEt
PDE$_{act}$-136	2,5-di-Me-Ph	Me	2-COOH-3-Bicyclo(2,2,1)-Heptyl	OMe
PDE$_{act}$-137	3,4-di-OMe-Ph	Me		OEt
PDE$_{act}$-138	3,4-di-OMe-Ph	Me	Me	OEt
PDE$_{act}$-139	3,4-di-OMe-Ph	Me	Et	OEt
PDE$_{act}$-140	3,4-di-OMe-Ph	Me	1-Me-Et	OEt
PDE$_{act}$-141	3,4-di-OMe-Ph	Me	1,1-di-Me-Et	OEt
PDE$_{act}$-142	3,4-di-OMe-Ph	Me	Furan-2-yl	OEt
PDE$_{act}$-143	4-NO$_2$-Ph	Me-CO	Me	OEt
PDE$_{act}$-144	4-NO$_2$-Ph	NO$_2$	Ph	OEt

Ph = Phenyl, OPh = Phenoxy, SPh = Thiophenoxy, Me = Methyl, OMe = Methoxy, Et = Ethyl, OEt = Ethoxy, CO = Carbonyl, COOH = Carboxyl, Br = Bromo, Cl = Chloro, F=Fluoro, and NO$_2$ = Nitro

Characterization of aryl-3-alkoxycarbonyl-2-(acylamino)thiophenes

PDE$_{act}$-03, one of the most potent compounds in this class, inhibited a dDAVP mediated increase in chloride conductance of the FRT-V$_2$R cells in a short-circuit current measurement with IC$_{50}$ of approximately 6μM (Figure 33, left panel). Addition of forskolin after the maximal PDE$_{act}$-03 restored most but not all of the

chloride conductance. In the same cells, the IC_{50} for reduction of cytoplasmic cAMP was approximately 0.2 µM (Figure 33, right panel).
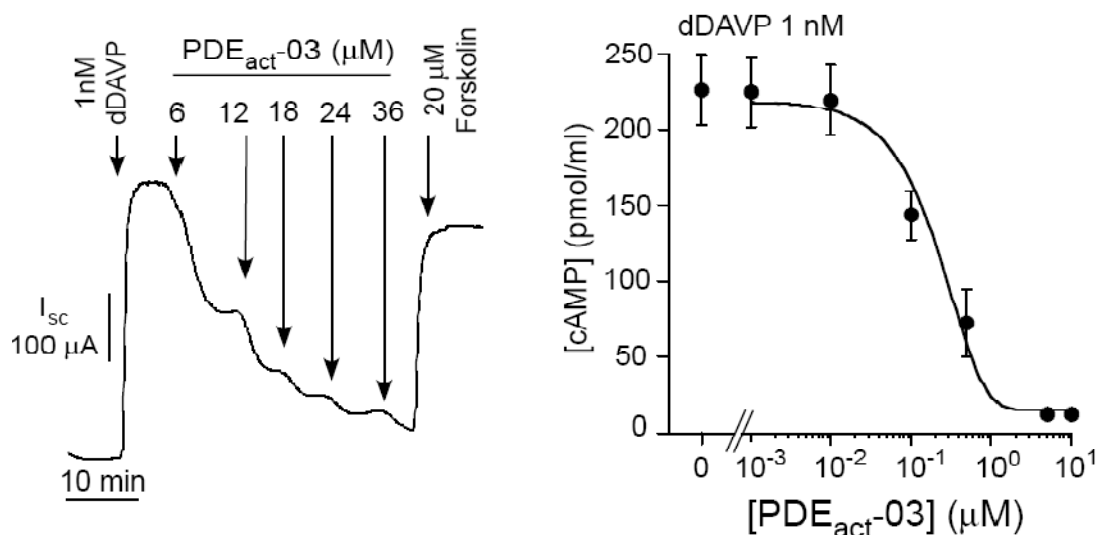
Figure 33. Inhibition of dDAVP-induced responses in FRT-V_2R cells by PDE_{act}-03. Left and right panels, are a short-circuit current measurement and a cAMP immuno-assay, respectively. In the short-circuit current measurement, dDAVP, forskolin and PDE_{act}-03 were added as indicated. The tracing shown was the representative data from 3 separate sets of experiments. For the cAMP assay, cells were incubated with dDAVP and various concentrations of PDE_{act}-03 for 20 minutes before being assayed for cAMP concentrations. Data were shown as mean ± SE, n=2.

V_2R is not a target for 2-(acylamino)-3-thiophenecarboxylates

Experiments were carried out to define a cellular target of the 2-(acylamino)-3-thiophenecarboxylates. First, cAMP measurements were done in the cells expressing different Gs-coupled receptors. Figure 34A showed that PDE_{act}-04 was as effective as propranolol in reducing cAMP after the isoproterenol stimulation in cells expressing β2-adrenergic receptors. Data for reduction of cAMP following dDAVP stimulation of the V_2R were shown as well. These results indicated that the GPCR was not the target because PDE_{act}-04 was active with different GPCRs.

To investigate the possibility that Gs was the target, cAMP was measured after an irreversible Gs-protein activation by the cholera toxin, see Figure 34B. PDE_{act}-04
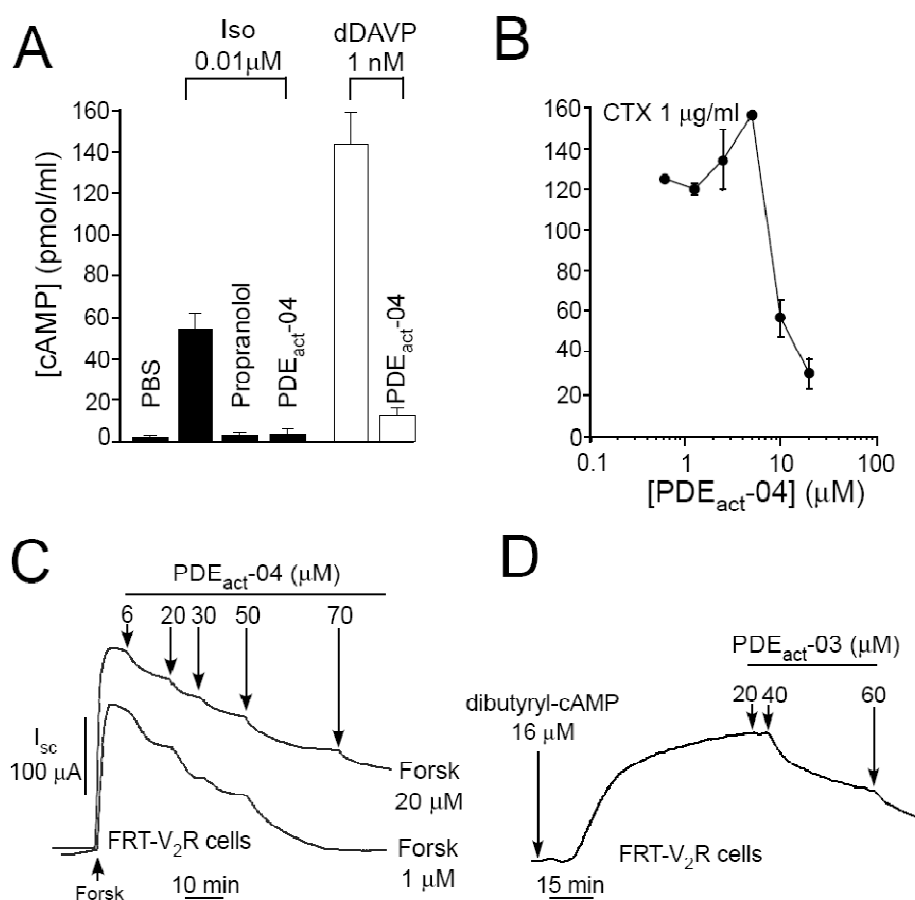
Figure 34. Identification of the PDE$_{act}$ targets. A. Inhibition of 0.01 μM isoproterenol and 1 nM dDAVP by 20 μM PDE$_{act}$-04. CHO cells transiently transfected with the human beta-2 adrenergic receptor (β$_2$AR) and the FRT-V$_2$R cells were treated for 20 minutes with isoproterenol (black bars) or dDAVP (white bars), and assayed for cAMP concentrations. Propranolol (20 μM), a β$_2$AR antagonist, and 20 μM PDE$_{act}$-04 were co-incubated with isoproterenal or dDAVP where indicated. The data were shown as mean ± SE, n=3. B. The effects of PDE$_{act}$-04 on a CTX-induced increase in cAMP levels in the CHO cells. The cells were incubated with CTX and the indicated concentrations of PDE$_{act}$-04 for 3 hours before performing the cAMP assays (mean ± SE, n=3). C. Short-circuit current measurement showing the effects of PDE$_{act}$-04 on the forskolin-induced I$_{sc}$. Forskolin at 1 and 20 μM, and PDE$_{act}$-04 were applied where indicated. D. Inhibition of the dibutyryl cAMP, a cell-permeable cAMP analogue, by PDE$_{act}$-03 in a short-circuit current measurement. The tracings shown in C and D were representative data from 3 separate sets of experiments.

was effective in reducing cAMP after the cholera toxin, indicating a Gs inhibition and/or PDE activation. Figure 34C showed the PDE_{act}-04 inhibition of the short-circuit current measurement following the stimulation by 1 or 20 μM of the AC activator forskolin. An effective inhibition was found, albeit better for 1 than 20 μM forskolin. Therefore, the primary target of PDE_{act}-04 was downstream from Gs. Together with the observation that PDE_{act}-04 inhibited dDAVP- or cholera toxin-induced increase in cAMP which indicated that PKA or CFTR could not be the primary target, these data suggested AC (cAMP production) or PDE (cAMP degradation) as the target.

To further clarify the site of action of 2-(acylamino)-3-thiophenecarboxylates, the generation of cAMP by AC was bypassed using dibutyryl-cAMP, a cell-permeable cAMP analog that was susceptible to degradation by PDE, though more slowly than unmodified cAMP. Figure 34D showed that PDE_{act}-03 inhibited a short-circuit current in the FRT cells after dibutyryl-cAMP stimulation, which together with the data above, suggested that the 2-(acylamino)-3-thiophenecarboxylates functioned as PDE activators.

The compounds reducing the cyclic nucleotide levels as a potential therapy for secretory diarrhea, and polycystic kidney disease

The pathological elevation in cAMP due to toxins, hormonal imbalance or G-protein mutations was involved in the pathogenesis of enterotoxin-mediated secretory diarrheas (Sack DA et al., 2004), polycystic kidney disease (Sweeney et al., 2006), certain adenomas and other tumors (Murakami M et al., 1999). Therefore, there were several potential clinical applications of the agents that increased cyclic nucleotide degradation, and consequently reduced the cyclic nucleotide concentrations. Secretory diarrheas were caused by enterotoxin-mediated increased concentration of the cyclic nucleotide in enterocytes, examples of which included the cholera toxin with elevated cAMP in cholera, and the STa toxin with elevated cGMP in Traveler' diarrhea (Golin-Bisello et.al., 2005). Elevated cyclic nucleotide concentration activated CFTR, resulting in chloride secretion into the lumen of the intestine, which was followed by the sodium and water secretion. T84 colonic epithelial cells were a commonly used model of the intestinal chloride secretion (Banks MR et.al., 2004 and 2005; Madara

et.al., 1993; Berschneider et.al., 1992). Figure 35A (left) shows slowed activation of CFTRs in T84 cells following the cholera toxin. The short-circuit current was fully inhibited by PDE_{act}-03. Figure 35A (right) showed an even greater potency of PDE_{act}-03 for inhibition of the short-circuit current after stimulation by the STa toxin.

The T84 cells developed large intracellular vacuoles at 3 hours following the cholera toxin exposure (Crane et.al., 2006), as shown in Figure 35B. This change in
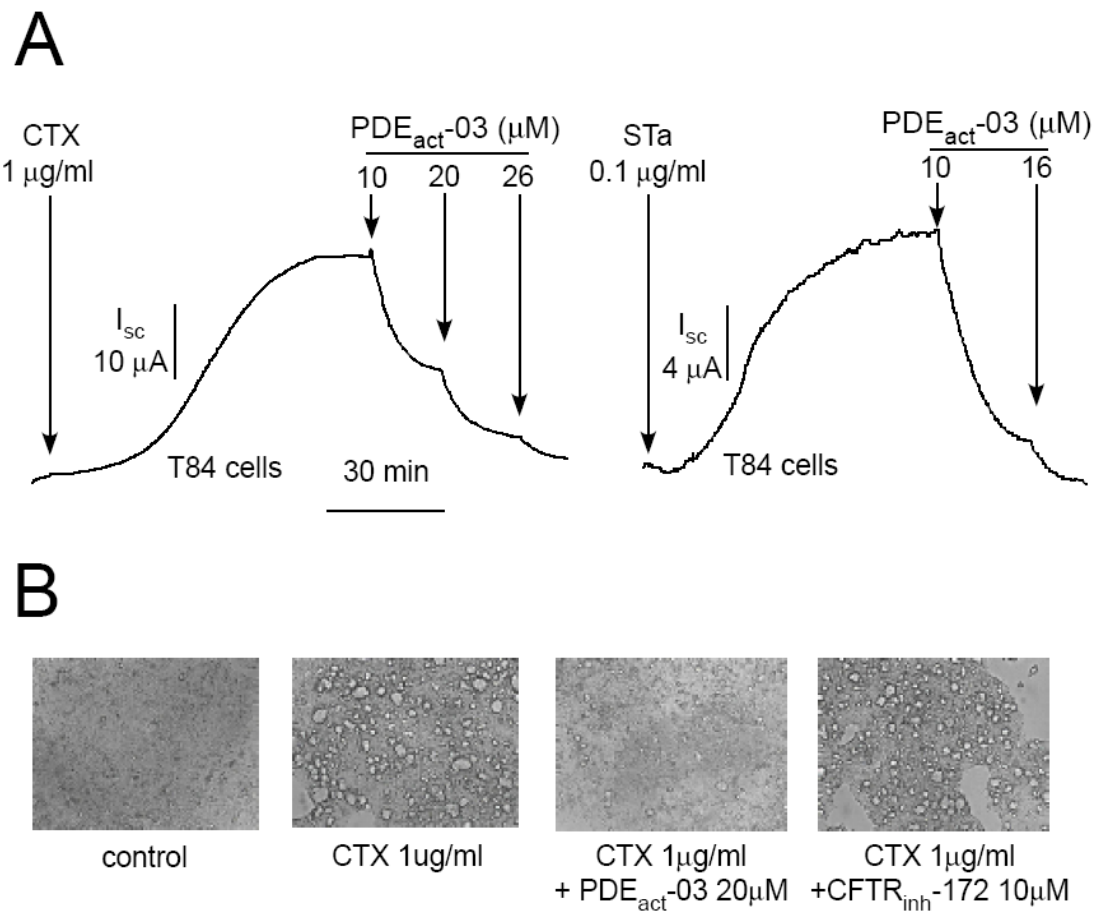
Figure 35. Effects of PDE_{act}-03 and -04 on intestinal secretion induced by the cholera toxin (CTX) and the E. Coli heat-stable toxin (STa). A. Short-circuit current measurements in T84 cells. The CTX (left), STa (right), and PDE_{act}-03 were added where indicated. The tracings shown were representative data from 3 separate sets of experiments. B. A morphological change in the T84 cells after CTX treatment (Best representation from 5 experiments). Before subjected to morphological observations, the T84 cells are incubated for 3 hours with the PBS, CTX, and CTX with PDE_{act}-03, or CTX with $CFTR_{inh}$-172 as specified.

morphology was thought to be caused by the cAMP-dependent but CFTR-independent fluid secretion into the intracellular vesicles (Crane et.al., 2006). Figure 35B showed that PDE$_{act}$-03 largely prevented the cholera toxin-induced vacuolarization of the T84 cells, whereas inhibition of the CFTR chloride channel by CFTR$_{inh}$-172 did not.

The efficacy of PDE$_{act}$-03 in reducing the intestinal fluid accumulation in a well-established closed-loop mouse model of secretory diarrhea was tested. The intestinal loops were injected with saline, cholera or STa toxin, with or without PDE$_{act}$-04. The intestinal loop fluid accumulation was quantified by loop weight-to-length ratio at 6 hours. Figure 36(left) showed that the loop fluid accumulation increased greatly with the cholera toxin, and that the fluid accumulation was partially inhibited by PDE$_{act}$-04.
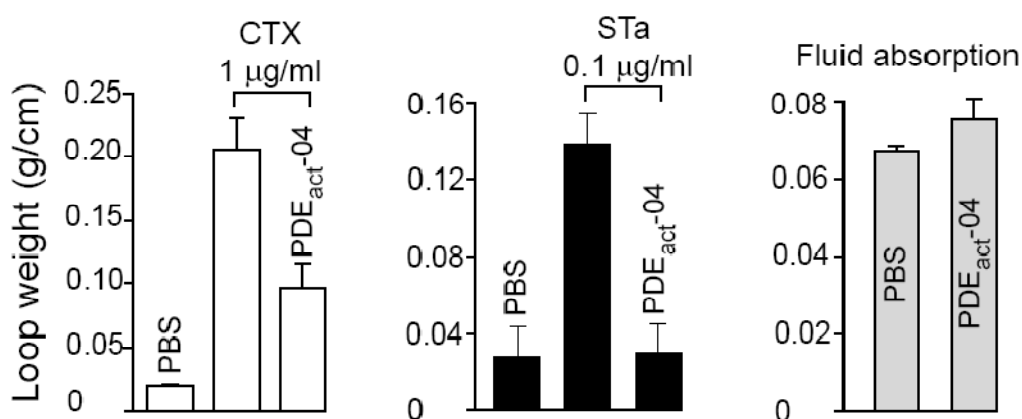
Figure 36. Intestinal secretion in a mouse closed-loop model. The mouse ileums were tightly tied at two points, 1-1.5 cm apart; injected with PBS, CTX (left graph), STa (middle graph), 20 μM PDE$_{act}$-04 and CTX, and 20 μM PDE$_{act}$-04 and STa, respectively, as indicated on the graphs. For the intestinal secretion (left and middle graphs) and the absorption (right graph) experiments, the loops were excised after 6 hours and 20 minutes, respectively. Then, the loop weight-to-length ratios were measured. The data were shown as mean ± SE, n=3.

Figure 36 (middle) showed a significant increase in the loop fluid accumulation with the STa toxin, but lower when compared with that with the cholera toxin. The PDE$_{act}$-04 fully inhibited the loop fluid accumulation with the STa toxin. Figure 36

(right) revealed that PDE$_{act}$-04 did not affect the intestinal fluid absorption, using a standardized model of fluid absorption (Maunprasat et.al., 2004). This is an important requirement for its potential application as an antidiarrheal.

Chronically elevated cAMP was thought to be responsible for progressive cyst expansion in the autosomal dominant polycystic kidney disease by increasing the cell proliferation and the CFTR-dependent fluid transport into the cyst lumen (Torres VE, 2005). An established MDCK model of in vitro cyst formation (Li et,al., 2004) was used to test whether PDE$_{act}$-04 could inhibit the cyst growth. In the initial studies, cAMP was measured in the MDCK cells following an exposure to forskolin (1, 5 or 10 µM), with and without PDE$_{act}$-04. Figure 37 showed the suppression of the forskolin-induced cAMP elevation in the MDCK cells by PDE$_{act}$-04. Figure 38 showed representative photographs of the MDCK cell cysts over time after plating in a Matrigel matrix in the presence of forskolin. PDE$_{act}$-04 remarkably reduced cyst expansion. Data from many individual cultures were summarized in Figure 39, as the ratio of the final-to-initial cyst areas. Though considerable heterogeneity in the cyst
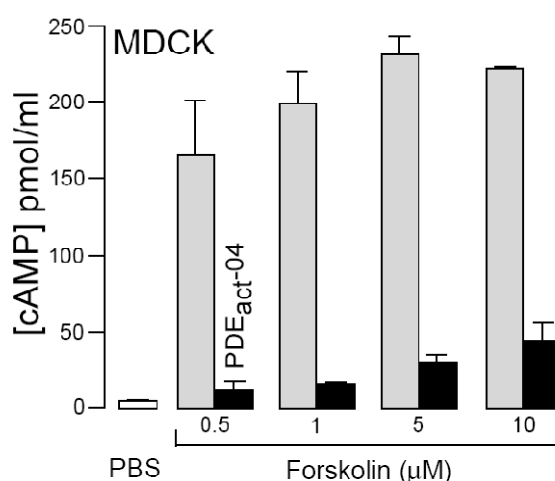
Figure 37. Inhibitions of forskolin-induced cAMP elevation by PDEact-04 in the MDCK cells. The MDCK cells grown in a 24-well plate without matrigel were treated with the indicated concentrations of Forskolin and 20µ M of PDEact-04. The data were obtained from 2 separate experiments and shown as mean ± SE.

forskolin 1 μM

forskolin 1 μM +PDE$_{act}$-04 20μM

day 1   day 3   day 5   day 7
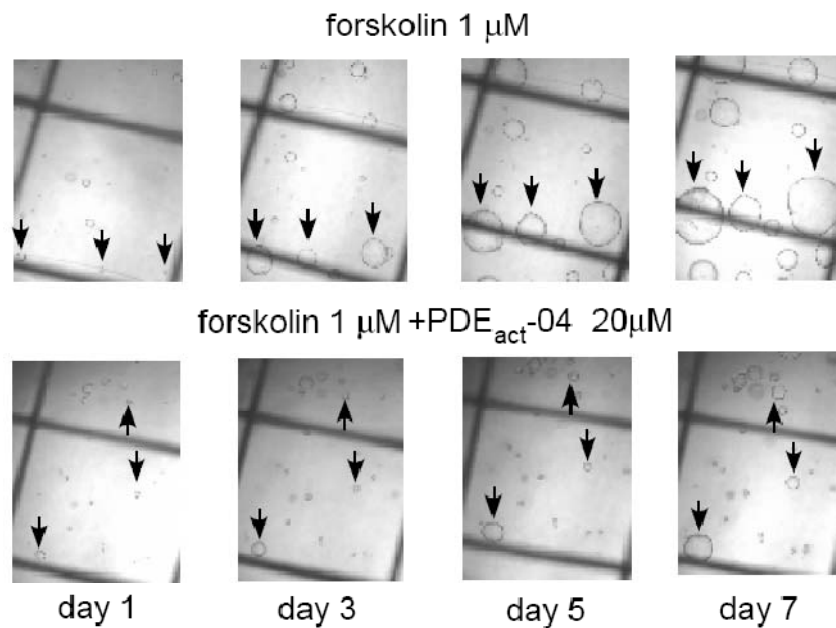
Figure 38. Development of Cysts from the MDCK cells. A. The MDCK cells were cultured in a collagen matrix and exposed for 7 days to 1μM forskolin (top panel) or 1 μM Forskolin together with 20 μM PDE$_{act}$-04 (lower panel). The arrows point to the developing cysts.
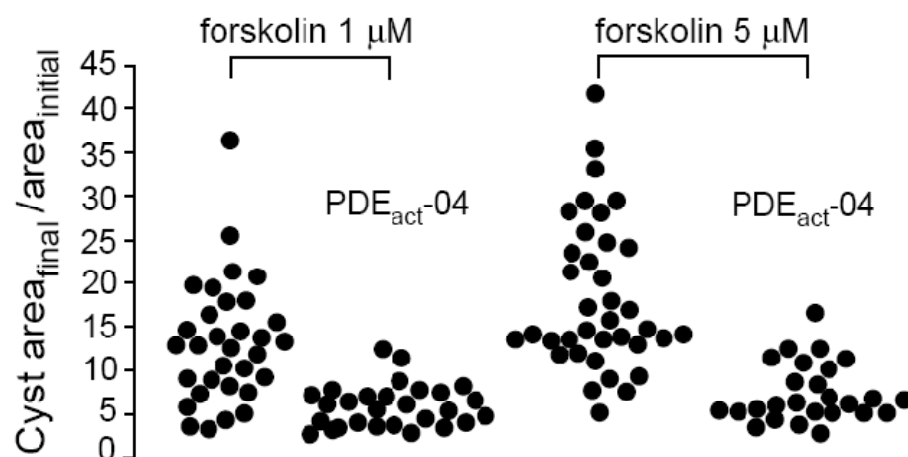
Figure 39. Cyst growth rates. From the same cyst, growth rate was calculated by dividing the final cyst area (day 7) by the initial cyst area (day 1). Each circle represents 1 cyst. Different types of treatment were indicated in the graph.

areas was observed, PDE$_{act}$-04 clearly prevented the growth of large cysts. Figure 40 summarized the data differently, as a percentage of the total number of MDCK cells
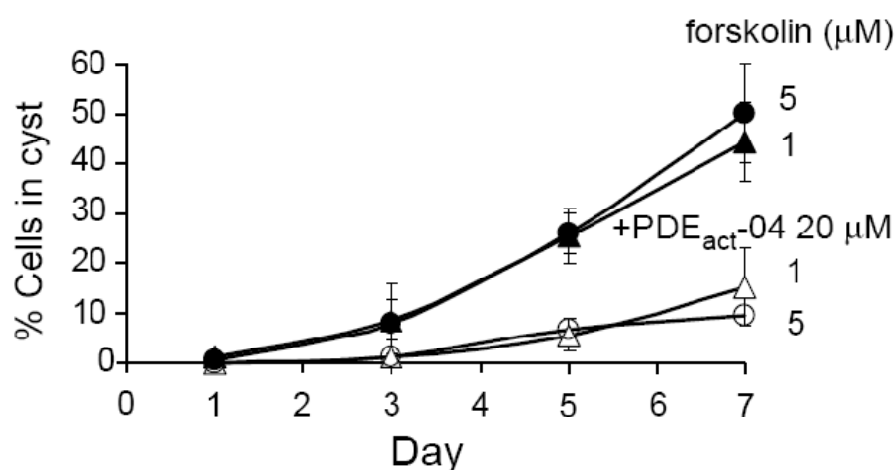
Figure 40. Percent of the cells that developed into cysts. The MDCK cells were treated for 7 days with forskolin 1 μM (indicated by filled triangles), and 5 μM(filled circles), or with 20μM PDE$_{act}$-04 in the presence of forskolin of 1 μM (open triangles), and 5 μM(open circles), respectively. The data were obtained from 2 separate experiments and shown as mean ± SE.

that formed cysts which were defined as a luminal structure with the diameter >100 μm. PDE$_{act}$-04 significantly reduced the percentage of the MDCK cells that progressed to form cysts.

CHAPTER V

DISCUSSION

A novel cell-based functional assay of Gs- or Gi-coupled GPCR modulators based on cAMP-dependent activation of the CFTR Cl$^-$ channels was reported. The assay was technically simple, inexpensive, and readily adaptable to the fluorescence-based, high-throughput screening formats. The assay employed an epithelial cell line suitable for both fluorescence and electrophysiological measurements. The cells had low basal halide conductance and cAMP concentration, excellent for stable transfection, and rapid growth on uncoated plastic. The Z'-factor for the assay was approximately 0.7, indicating very good sensitivity and specificity in single primary screening. The assay was applied to identify V$_2$R antagonists in screening of 50,000 small molecules in a 96-well plate format. The assay was designed as a 'pathway screening', so that the compounds inhibiting a CFTR I$^-$ influx could function as V$_2$R antagonists, Gs inhibitors, Gi activators, adenylyl cyclase inhibitors, phosphodiesterase activators, protein kinase A inhibitors, or CFTR inhibitors. Such a pathway screening had an advantage of identifying small-molecule modulators of multiple targets in a single screening, with the target identification done in small-scale secondary assays.

Expression of the wild -type and mutant V$_2$R in the FRT cells

Functional assays of cell responses are widely used in high-throughput screening, in part because they are technically simpler than radioligand binding assays. Binding assays are unable to distinguish between agonists and antagonists, and have low sensitivity for detection of allosteric modulators. Several functional assays have been developed based on cAMP measurement, as mentioned in Chapter II: Literature review

One objective of this study is to establish a sensitive, homogenous, non-radioactive, miniaturizable and economically feasible cell-based high throughput

screening assay for Gs-GPCR modulators. The sensitivity of the assay is dependent mainly on the level of signal detection in the signal transduction cascade and the measurement platform employed. Here, it was the first time that the CFTR was selected as a level of signal detection in a high-throughput screening assay for GPCR modulators. Because the CFTR was at the most downstream level after an increase in cAMP, where signal amplification was at its maximum, our assay yielded high sensitivity. However, there was no easy or high-throughput screening compatible way to assess the CFTR activity directly, except for the use of a high-throughput patch clamp system which required complicated instruments as an add-on to the regular high-throughput screening machinery (Sigworth et al., 2002). Therefore, the halide-sensitive YFP was employed for an indirect assessment of the CFTR activity in a fluorescence platform, one of the most widely used platforms throughout the world because it is sensitive and suitable for a 96-well plate format. The sensitivity of our assay was then also dependant on the halide sensitivity of YFP, which was shown to be in a mM level, see Appendix A. The low halide sensitivity of YFP was not a problem, because the small cellular volume resulted in a high halide concentration even when a small amount of halide entered the cells. Among all the halides, iodide was the third best YFP quencher, but it was chosen for our assay due to its low toxicity.

Besides the important characteristics required for high-throughput screening, the cells employed in the proposed model must be able to express a correctly folded and fully functional V_2R at its cell membrane. Ideally, the cells endogenously expressing the human V_2R, such as the human inner medullary duct cells, are preferred. Unfortunately, they were obtained only from a primary culture which was not suitable for high throughput screening. Animal cell lines endogenously expressing V_2R such as MDCK cells grew rapidly and were suitable for high throughput screening, but the receptors were not that of human. Rodent and humans V_2R were found to response differently to a V_2R modulator for example β-Me used in this study competitively antagonized rodent V_2R while partially agonized human V_2R. Therefore the compound identified using the animal cell line might result in a compound useless for human. Stable expression of V_2R was advantageous over its transient expression because (i) the level of the receptors in the cells, which would affect the signal

intensity and hence the assay quality, was more constant, and (ii). the stable transfection allowed selection of the best clone which expressed V_2R most evenly in all cells.

The results of stable N-terminal-cmyc-tagged humanV_2R expression in the FRT cells, already expressing CFTR and YFP, were shown in Figure 18A. The immunostaining of the living non-permeabilized FRT cells, stably transfected with cmyc-tagged wild-type humanV_2R with anti-cmyc antibody, revealed staining at the edge of the cells. Because the N-terminus of the human V_2R which containing cmyc was on the outside of the membrane, and the large antibody could not pass through the intact cell membrane, this favored the membrane over the cytoplasmic expression of the V_2R. The anti-cmyc antibody was able to stain the FRT cells stably transfected with cmyc-tagged W164S humanV_2R only when the cells were permeabilized with preceding triton-x incubation. The staining was evenly distributed throughout the cells except for the nuclear regions. These findings implied cytoplasmic expression of the W164S, a mutant human V_2R. The conclusions that could be drawn from the immunostaining experiments were (i) the expression of wild-type human V_2R was at the membrane location as expected, and (ii) the sequence of the human V_2R was an important factor in determining a target location of the cmyc-tagged receptors. The expression of the wild-type human V_2R on the cell membrane appeared to be on the basolateral side, mimicking the location of its expression in the inner medullar collecting duct cells, because the staining was prominent on the edge of the cells. It was also possible that the expression was uniformly distributed throughout the membrane except at the edge where there were receptors from the two adjacent cells, thus the staining appeared to be relatively more prominent. It was not very important where the receptors were located on the membrane (except for the strict basal expression which would be difficult for vasopressin to reach the V_2R) as long as they could function normally. However, visualization of the staining under a confocal microscope would reveal a definite receptor expression site at the cell membrane.

The immunoblot experiments confirmed that the stably expressed human wild-type V_2R was of a correct size and correlated well with those of other studies (Sadeghi et al., 1999; Innamorati et al., 1996; Sadeghi et al., 1997). The molecular weight of cmyc was only 1.26 kDa and contributed to a very small shift in the immunoblot band.

The 40 kDa band, consisting of bands ranging from approximately 33 to 40 kDa, represented the glycosylated receptors, while the 64kDa band was the aggregated receptors which correlated well to the aggregation of the two receptors of approximately 33 kDa in size. (Sadeghi et al., 1999). The human V_2R underwent both N-linked and O-linked glycosylation at its extracellular N-terminal domain. Normally, glycosylation protected the protein from being prematurely digested by the extracellular proteases, but none of the V_2R glycosylated sites were found to be important to neither V_2R membrane expression level, nor V_2R affinity to vasopressin (Sadeghi et al., 1999). The V_2Rs that did not undergo a complete glycosylation (an immature receptor) tended to aggregate to each other (Sadeghi et al., 1999). The immunoblot study showed a thick band at 64 kDa, indicating a significant amount of the receptor aggregation which could possibly be explained by the overwhelmed glycosylation machinery by a large number of over-expressed receptors resulting from the stable expression. In the membrane of a living cell, the receptors should not aggregate to each other, because the immature receptors, which tended to aggregate, remained in the endoplasmic reticulum or the Golgi complex, and were not yet presented to the membrane until they were mature or glycosylated. However, with the overwhelmed glycosylation machinery, some of the immature receptors might be able to escape to the membrane without maturation. The aggregation, if existed, could result in the difficulty of a G-protein to approach the receptor and in a reduction of the maximal response of the cell to vasopressin. However, this effect should be negligible, because the immature V_2Rs were shown to be functionally similar to the mature receptors (Sadeghi et al., 1999).

Functionally, the FRT cells stably expressing the cmyc-tagged wild-type humanV_2R, CFTR and YFP were validated using both the fluorescence plate reader and the short circuit current measurement in order to demonstrate that activation of the V_2R by dDAVP could induce the cellular responses as being proposed in the assay's principle. Treatments of the cells with dDAVP and forskolin, respectively, both resulted in quenching of YFP by the entry of iodide. The iodide entered the cells through CFTR as evidence by the ability of $CFTR_{inh}$-172, a known CFTR inhibitor, to inhibit the quenching of YFP. The short-circuit current measurement demonstrated directly the presence of a $CFTR_{inh}$-172 inhibitable chloride current running across the

apical membrane after addition of dDAVP or forskolin. The apical current, not the transcellular current, was recorded because of the need to eliminate the influence of the basolateral chloride transporters on the chloride current. The dDAVP could not induce quenching of YFP in the FRT cells stably expressing W164S V_2R, a mutant receptor previously known to be functional if rescued to the membrane. This indicated that the membrane expression was crucial for the functioning of V_2R, and also confirmed that the FRT cells with stable expression of the wild-type V_2R had to express the receptors at the cell membrane. The ability of the V_2R antagonist and the partial agonist, SR-121463 and β-Me, respectively, to inhibit dDAVP-induced quenching of YFP confirmed that the dDAVP acted through V_2R in the CFTR stimulation.

Comparing the dose-response curve of dDAVP- induced quenching of YFP to that of forskolin demonstrated that the EC_{50} of forkolin was 10,000 times more than that of dDAVP. This was due to (i) different affinity and efficacy of dDAVP and forkolin in their target activation, and (ii) signal amplification. Initiation of the signal transduction cascade by dDAVP was more upstream from that of forskolin (adenylyl cyclase), and this resulted in more pronounced signal amplification, and hence less EC_{50}. The EC_{50} was inversely related to the assay's sensitivity.   The EC_{50} of the radioactive vasopressin binding assay in the intact cells reported from other studies (Sadeghi et al., 1997; and Beckh et al., 1999) was approximately 10 times more than that of the dDAVP-induced quenching of YFP.   In fact, the EC_{50} of dDAVP in binding to a human wild-type V_2R was found to be 3 times more than that of vasopressin, therefore the actual ratio of the EC_{50} of the two assays might be more than 30 (Sadeghi et al., 1997). The EC_{50} of the dDAVP-induced increase in cAMP concentration obtained from the cAMP antibody competitive assay (Figure 29A) was 10 times more that that of the proposed assay. However, it should be noted that the cAMP antibody competitive assay used in this study was based on the colorimetric method which was the least sensitive among all the available measurement platforms. Using the bench-top double chromatography column method, the EC_{50} of the dDAVP-induced increase in a cellular cAMP concentration was approximately 0.3 nM which was not much different from the proposed assay (Sadeghi et al., 1997). In the bench-top assay, a large volume of the cellular extract containing cAMP was processed

through the chromatography column to separate and concentrate cAMP before the measurement, therefore it was not surprising that the bench-top assay yielded higher sensitivity than that of the cAMP antibody competitive assay which was designed specifically for high-throughput screening where separation and concentration of the cAMP were not convenient. This indicated that the assay platform was an important determinant of the assay's sensitivity. Invitrogen, a company that developed the reporter gene assays for GPCR using β-lactamase gene (GeneBlazer reporter technology), reported the EC_{50} of dDAVP-induced reporter gene activity to be 0.12 nM which was comparable to that of the proposed assay. Taken together, the sensitivity of the proposed, CFTR-based, YFP quenching assay was comparable to that of the β-lactamase reporter gene assay, but was more than those of a radioactive ligand binding assay and a caloricmetric cAMP antibody competitive assay. The low EC_{50} value derived from the proposed assay allowed the identification of even a weak V_2R agonist form the screening. Similarly, the assay was also sensitive for a V_2R antagonist because less concentration of dDAVP was required in order to activate the signal transduction cascade, which in turn increased [the] chance of a weak antagonist to successfully compete with dDAVP binding.

High-throughput screening

The concentration of dDAVP used in the screening was specified with due considerations of the following requirements: (i) enough signal intensity to give good quality of the assay without compromising on the chance to detect a weak antagonist, and (ii) stability of the cellular responses over the measurement period which could be influenced by a receptor desensitization (previously reviewed in Chapter II). The V_2R was endocytosed and destroyed by lysosome after binding to vasopressin, which in turn resulted in a very slow reappearing rate of the receptor to the cell membrane. The phosphorylation of the serine residues in its C-terminus by the G-protein coupled receptor kinase caused the V_2R to form a stable endocytic complex with β-arrestin in an extended period of time as compared with the other GPCRs (Barak et al., 2001). In addition, the majority of the complexes were destined to lysosomal degradation (Bouley et al., 2004). The concentration and the time-dependent nature of the cellular responses to dDVP were shown in Figure 21. At a dDAVP concentration of 1 μM, the

cellular responses degraded significantly over the period of 45 minutes. This finding correlated well with the study by Bouley et al. in 2004, who observed a 70% decrease in the vasopressin binding sites in the LLC-PK1 cells stably expressing a hybrid V_2R-GFP after incubation of the cells with 1μM vasopressin for 1 hour. The deterioration of the cellular responses could also be a result of an alteration of the activity of the other downstream targets in the signal transduction cascade such as an increase in the activity of PDE. However, the one-hour incubation of the cells with various concentrations of forskolin ranging from 5 to 20 uM did not produce any deterioration of the cellular responses, therefore the most likely explanation for the deterioration was desensitization of the V_2R. Finally, the dDAVP concentration of 1nM, the least possible concentration giving good and stable responses, was chosen for further characterization of the assay's quality. The Z' factor of the proposed assay was within an excellent range and was not significantly different from those of the commercially available radioactive-based and fluorescence-based cAMP antibody competitive assays, namely FlashPlate^{TM}, Fluorescence polarization, and HitHunter^{TM}, but was less than that of the GeneBlazer reporter gene assay. The GeneBlazer assay gave rise to the best Z' factor because it employed the chemiluminescence platform with a ratiometric read out which yielded a very high signal-to-noise ratio.

A good high-throughput screening assay should contain the least possible number of steps without complicated handling processes. The classic cAMP assay for high-throughput screening required long incubation time and multiple handling steps, including complicated washing processes; therefore it was clearly a disadvantage and would not be compared to the proposed assay. Instead, the comparison will be made between the proposed assay and the improved version of the cAMP antibody competitive assays such as FlashPlate^{TM} and AlphaScreen^{TM}. The proposed assay was composed of only 2 steps, namely, (i) co-incubation of the test compound and dDAVP with the cells for 20 minutes per plate, and (ii) detection of the fluorescence signal in the fluorescence plate reader for 20 minutes per plate, whereas the cAMP antibody competitive assays were composed of 4 steps, i.e. (i) co-incubation of the test compound, and dDAVP with the cells for 20 minutes, (ii) incubation of the lysed cells with anti-cAMP acceptor beads for 30 minutes, (iii) incubation with biotinylated-cAMP/streptavidin donor beads for 1 hour, and (4) signal detection. The total time

consumed per plate for the proposed assay was at least 70 minutes less that that of the cAMP antibody competitive assays. For the reporter gene assay, such as GeneBlazer technology, the rate limiting step was at the co-incubation of the test compound and dDAVP with the cells, which consumed at least 6 hours per plate in order to allow transcription and translation of the reporter. However, the signal detection step was simple, requiring only addition of the substrate without a cell lysis step. A long incubation time could be a deadly drawback for the reporter gene assay in the screening for V_2R modulators, because the majority of the V_2Rs might disappear from the cell membrane, and thus the cellular responses could be reduced.

Assuming that the same type of cells, the same cell culture media and the same basic high-throughput machinery were used, the operating cost of each high-throughput screening assay was compared as follows. For the cAMP antibody competitive assay, there were many commercially available kits for high-throughput screening and the approximate cost of the kit was 200-300 dollars per one 96-well plate (the price indicated here was obtained directly from the manufacturer's product webpage). The proposed assay cost 9 dollars per 96-well plate including the reagents. However, in the proposed assay as well as in the reporter gene assay, one needed to take in to account the cost of the cell line development which in turn comprised of the plasmid construction and expansion, cell transfection and selection, and the reagents necessary for cell line validation. According to the materials actually used in this study (see the section 'material and method'), the approximate cost of the cell line development was 2,000-3,000 dollars which was roughly equal to the screening cost of the cAMP antibody competitive assay of about ten 96-well plates or 960 test wells, including the control and the standard wells. And the time consumed for developing a cell line, including trial and error, was approximately 3-4 months. Therefore, in view of a cost-effective high-throughput screening, the proposed assay would be more suitable for a long-term project with more than one thousand test compounds to be screened.

In order to demonstrate a proof of concept of CFTR-based HTS assay we screened a small-molecule compound library for a V_2R antagonist. Twenty seven of four-in-one compound groups out of the total 12,500 groups, or 0.21% of the total, were identified as strong V_2R inhibitors at 20 μM. The hits could be identified as the

compounds that yielded the percent dDAVP inhibition of more than 60%, approximately two standard deviations away from the mean. However, the concentration of the test compound at 20 μM was already high; therefore the compounds with the percent dDAVP inhibition of less than 90 % were likely to be a very weak antagonist and were not further characterized in this study. There were three false positive four-in-one compound groups, amounting to 11%, found from the twenty seven strong hits. The compound precipitation, interference of the YFP fluorescence by the test compounds that emitted the yellow fluorescence light, and the abnormally low signal from the wells with dead cells caused the identification of the false positive compounds. Compound precipitation was commonly encountered in almost every high-throughput screening. The automated liquid dispensing system sometimes failed to aspirate the precipitated compound that was tightly packed to the bottom of the well, even though the compound was thoroughly mixed before the aspiration. This led to a false negative result when the test compound was actually a hit. When a clump of the precipitated compound was successfully aspirated and transferred to the cells by the liquid dispensing system, the final compound concentrations were dependent on the compound's solubility in the phosphate buffer, a solution in which the cells were incubated. For the compound with low solubility, the final compound concentration would be lower than expected. On the contrary, the concentration of the highly soluble compound would be very high which in turn resulted in the cellular toxicity, detachment of the cells from the bottom of the wells, a low YFP fluorescent signal, respectively. Some of the yellow fluorescence compounds from the library gave rise to high fluorescence read-outs, sometimes exceeding the signal detection window, and thus quenching of YFP could not be demonstrated. This resulted in a false positive hit identification. The false positive compound, identified from the wells with dead cells or with the yellow fluorescence compound, could be easily isolated by a revision of the fluorescence tracing in a search for the abnormally low and the high fluorescence baselines. A manual revision of the tracing was not a practical approach when a large-scale compound screening, such as that of a pharmaceutical company, was carried out. However, a data analysis program could be easily designed to report wells with abnormal fluorescence baseline.

        In summary, the proposed newly developed assay is homogeneous and sensitive,

and requires only 2 handling steps including the measurement step. It does not require lysis or reagent addition steps. However, the proposed assay does require a specialized cell line expressing CFTR, YFP and GPCR of interest. To the best of our knowledge, the only assay assessing the activation of GPCR by measuring the activity of a downstream effector protein, similar to that of the proposed assay, was developed by Atto Bioscience (Rich et al., 2005), where the calcium influx was used as a read-out of the cyclic nucleotide-sensitive ion channels.

An analysis of the V_2R_{inh} structure-activity relationship (SAR)

In this study, the GPCR pathway screening was applied to identify inhibitors of the vasopressin- stimulated cAMP acting through the V_2R. Clinical indications of the V_2R antagonists included the treatment of hyponatremias associated with the increased or normal total body water, such as congestive heart failure, cirrhosis, and the syndrome of inappropriate ADH secretion (Paranjape et al., 2001). Water retention is a common clinical problem that increases the mortality and morbidity of the underlying cardiovascular and hepatic diseases. The current main strategy in treating water retention is the use of hypertonic normal saline and diuretics, which increase excretion of both electrolytes and water. V_2R antagonism causes an increase in water excretion without a significant electrolyte loss, and so is a superior treatment strategy. Early attempts to develop V_2R antagonists focused on the peptide analogs of vasopressin (Allison et al., 1988), though they had very low bioavailability. The first small molecule V_2R antagonist, OPC 31260, was a derivative of the vasopressin V_{1a} receptor antagonist, OPC 21268 (Thibonnier et al., 2001). The second V_2R antagonist was SR 121463 (Serradeil-Le Gal et al., 1996). These V_2R antagonists were originally identified by Otsuka Pharmaceutical Co. (Japan) and Sanofi Recherche (Toulouse, France), respectively. Both of the V_2R antagonists had a diuretic effect in the humans (Ohnishi et al., 1995; Serradeil-Le Gal et al., 2001), with IC_{50} values in the nano-molar range. Subsequently, several pharmaceutical companies modified the structures of the original V_2R antagonists to obtain more potent V_2R antagonists (Yamamura et al., 1998; Gunnet et al., 2006), a dual $V_2R/V_{1a}R$ antagonist (Tahara et al., 1997), and a $V_{1b}R$ antagonist (Serradeil-Le Gal et al., 2002). Recently, only Conivaptan (YM 087), a dual $V_2R/V_{1a}R$ antagonist, was approved for treatment of euvolemic hyponatremia

(Lemmens-Gruber et al., 2006).   SR 121463, Tolvaptan (OPC 41061), and Lixivaptan(VPA 985) were in the third phase of clinical trials (Wong et al., 2003; Ghali et al., 2006; Schrier et al., 2006).   However, the tricyclic antagonists are quite hydrophobic (logP > 4) and have limited aqueous solubility (< 1 mg/ml) (Matthews et al., 2004), which are potentially problematic in further development for therapeutic purposes.   New classes of V_2R antagonists can provide useful lead compounds that may overcome these concerns.

After small-molecule screening of 50,000 compounds, a novel chemical class of V_2R antagonists was identified that were unrelated to other known V_2R antagonists. After confirming that   a class of 5-aryl-4-benzoyl-3-hydroxy-1-(2-arylethyl)-2H-pyrrol-2-one was bona fide V_2R antagonists, small-scale screening of commercially available structural analogs was carried out, identifying 4-benzoyl-5-(4-fluorophenyl)-1,5-dihydro-3-hydroxy-1-[2-(4-hydroxyphenyl)ethyl]-2H-pyrrol-2-one (V_2R_{inh}-02) as the most potent compound of 3-hydroxy-2-pyrrolones. Comparing the structures of the active and the inactive compounds gives an insight into the structural determinants of the compound activity.   In general, R_1 tolerates various substituted phenyl rings, R_2 is more limited in the fact that primarily 4-halophenyl and 4-nitrophenyl derivatives give the active compounds, and R_3 tolerates phenyl and 4-hydroxyphenyl substitution. A more focused 3-hydroxy-2-pyrrolone library, incorporating the functional groups of the most active V_2R_{inh}-02 antagonists and having more diversity in R_1 and R_3, should yield more potent V_2R antagonists as well as the compounds with different V_2R-versus- V_1R selectivity.

V_2R_{inh}-02 is a competitive V_2R antagonist

While V_2R_{inh}-02 successfully inhibited dDAVP-induced cellular responses, its failure to inhibit the cellular responses induced by isoproterenol clearly indicated that V_2R_{inh}-02 was a V_2R antagonist. The β_2AR was chosen for the experiment, because it employed the same signal transduction cascade as that of the V_2R, and the two receptors were from different sub-family groups with low similarity. V_2R_{inh}-02 was found to be a competitive antagonist, as demonstrated by the cAMP measurements following cell incubation with different V_2R_{inh}-02/dDAVP concentrations, and by direct displacement assays of the radiolabeled vasopressin.   The existing chemically

unrelated V_2R antagonists, OPC 31260 and SR 121463, were also the competitive antagonists (Serradeil-Le Gal et al., 1996; Thibonnier et al., 2001). The value of K_i of V_2R_{inh}-02 was approximately 70 nM, as estimated from the competition data. V_2R_{inh}-02 was approximately 70 times more selective for V_2R than V_{1a}, as demonstrated by the radioactive binding assay.

Identification of 2-(acylamino)-3-thiophenecarboxylates from the pathway screening

The 2-(acylamino)-3-thiophenecarboxylates reported herein are discovered for the first time ever to be possible small-molecule PDE activators. They suppressed the basal and the agonist-induced elevations in cytoplasmic cAMP. The effect was quite robust as demonstrated by using multiple cell types, tissues and agonists. Small-molecule PDE activators are useful research tools in probing the cyclic nucleotide signaling mechanisms, and notwithstanding the specificity concerns, they are also potentially useful for the therapy of secretory diarrheas, polycystic kidney disease, and cAMP-dependent tumor growth.

The 2-(acylamino)-3-thiophenecarboxylates inhibited the cellular responses induced by activation of V_2R and β_2AR, forskolin and CTX, through modification of cAMP levels. This suggested possible sites of action at cAMP synthesis or degradation. To inhibit the cAMP synthesis which resulted from the hydrolysis of ATP by adenylyl cyclase enzyme, the 2-(acylamino)-3-thiophenecarboxylates could directly inhibit the enzyme or cause depletion of ATP. The 2-(acylamino)-3-thiophenecarboxylates were able to inhibit the responses induced by dibutyrly cAMP, a cell-permeable man-made cAMP, thus the most likely site of action was at cAMP degradation, see Figure 34D. Also, the observation that it was more potent in inhibiting low concentrations of forskolin than the higher ones supported the conclusion. The only enzyme that degraded the cyclic nucleotide was PDE, which could be the target of our compound (Beavo, 1995; Mongillo et.al., 2006). PDE_{act}-03 was able to inhibit STa, as evidenced by an increase in the cGMP level; thus a target PDE isoform should be able to degrade both cAMP and cGMP. However, a direct evidence showing inhibition of PDE activity in vitro by the compound is still needed. Another possible action of the 2-(acylamino)-3-thiophenecarboxylates were through

depletion of ATP. The opening of CFTR was ATP dependent, therefore depletion of ATP could inhibit the responses induced by dibutyrly cAMP through inhibition of CFTR. The depletion of ATP was not the most likely mode of action because it should be deleterious to the cellular function resulting in cell death, but the toxicity of the compound was not demonstrated at the concentrations used in this study.

Synthesis and structure-activity analysis of 2-(acylamino)-3-thiophenecarboxylates

To understand the possible requirements of functionality on 2-(acylamino)-3-thiophenecarboxylates, almost 144 small molecule analogues of this series were screened for their ability to inhibit the dDAVP responses in FRT-V$_2$R cells. Among these analogues, the compounds with typical functionality with 4-substitute aryl-3-alkoxycarbonyl-thiophen-2-ylcarbamoyl bicyclo[2.2.1]heptane-2-carboxylic acid were found to be most potent PDE activators. Figure 31 shows the structure and the pharmacological profile of the two most active compounds in the series.

Retro-synthetic analysis of PDE$_{act}$-3 and PDE$_{act}$-4 clearly revealed two important synthons as Bicyclo[2.2.1]heptane-2,3-dicarboxylic anhydride (5 or 6) and 5-methyl-4-substituted aryl-3-alkoxycarbonyl-2-aminothiophene (4) as depicted in a representative synthetic scheme in Figure 31. The Gewald synthesis was probably the most versatile method for synthesis of the key synthon, 5-methyl-4-substituted aryl-3-alkoxycarbonyl-2-aminothiophene (4) which was generated by a two-step procedure which involved isolation of α,β-unsaturated nitriles (3) from Knoevenagel condensation between (1) & (2). Subsequent conversion of these olefins 3 to the corresponding 2-aminothiophenes (4) by treatment with sulfur and diethylamine. Further, condensation of 5-methyl-4-substituted aryl-3-alkoxycarbonyl-2-aminothiophene(4) with either *endo*(5) or *exo* bicyclo[2.2.1]heptane-2,3-dicarboxylic anhydride (6) to get the respective 3-(3-(alkoxycarbonyl)-5-methyl-4-substituted arylthiophen-2-ylcarbamoyl) *endo* or *exo* bicyclo[2.2.1]heptane-2-carboxylic acid as *endo* PDE$_{act}$-3 (7) or *exo* PDE$_{act}$-03 (8) respectively. Similar *exo* or *endo*, PDE$_{act}$-04 was synthesized with the same strategy.

Possible applications of 2-(acylamino)-3-thiophenecarboxylates, **a compound that reduces the cyclic nucleotide levels**

Proof-of-concept experiments supported the potential utility of 2-(acylamino)-3-thiophenecarboxylates in reducing the intestinal fluid accumulation in secretory diarrheas, and in slowing the renal cyst growth and fluid accumulation in PDK. After the CTX or STa treatments, PDEact-03 inhibited the trans-epithelial current in the T84 cells, a commonly used model of the intestinal chloride secretion. This was also confirmed in an in vivo model. By reducing the intestinal secretion, PDEact-04 reduced fluid accumulation in the mouse closed-intestinal-loops after 6-hour treatments with CTX or STa. PDEact-04 also successfully slowed the cyst growth and fluid accumulation in an in vitro model for a polycystic kidney disease (MDCK cells treated with forskolin). Both actions of 2-(acylamino)-3-thiophenecarboxylates were through the reduction in the c ellular cyclic nucleotide level.

CHAPTER VI
CONCLUSION

1. Having been established is a novel high-throughput screening 'pathway' assay for identification of modulators of Gs- or Gi-coupled GPCRs. The assay is very sensitive, technically simple and inexpensive when compared with the existing cell-based GPCR assays. Based on the EC_{50} of the dDAVP-induced cellular response, the sensitivity of the proposed assay is comparable to that of the β-lactamase reporter gene assay, but it is more than those of the radioactive ligand binding assay and the calorimetric cAMP antibody competitive assay, respectively. The proposed assay consists of only two steps, namely (i) co-incubation of the cell with dDAVP and a test compound, and (ii) the fluorescence reading. Therefore, the assay is the least complex comparing with the cAMP antibody competitive assay, and the reporter gene assay, respectively. In view of economy, the assay costs only 9 dollars per one 96-well plate, the cheapest among the cAMP antibody competitive assay and the β-lactamase reporter gene assay. However, the requirement of a cell line with the developmental cost of approximately 2,000-3,000 dollars causes the proposed assay to be cost-effective only for a long-term project with more than one thousand test compounds to be screened. Since the proposed assay is based on the detection of the yellow fluorescence signal, a yellow fluorescence compound was observed to give a false positive result.

2. The proposed assay, a high-throughput screening with the cell-based assay, was successfully applied for the first time in screening for the non-peptide V_2R antagonists. The 5-aryl-4-benzoyl-3-hydroxy-1-(2-arylethyl)-2H-pyrrol-2-one was identified as a new competitive V_2R antagonist of structurally unrelated to the previously identified antagonists. Also, the small-molecule 2-(acylamino)-3-thiophenecarboxylates, compounds that suppressed the cyclic nucleotide concentration in cells and tissues, was for the first time discovered from the screening. These successful hit identifications proved the validity, practicality, and advantage of the

proposed assay where the modulators of multiple targets can be identified with one screening..

   For the future perspective, the proposed assay can be used for screening of the V_2R agonists and modulators of Gi-coupled receptors. The latter requires further optimization of the assay; because pre-activation of adenylyl cyclase with forskolin is required to elevate the cAMP level before the screening. The 5-aryl-4-benzoyl-3-hydroxy-1-(2-arylethyl)-2H-pyrrol-2-one and 2-(acylamino)-3-thiophenecarboxylates have several therapeutic potentials, therefore the future research on their properties based on the analysis of the structure-activity relationship may be worthwhile.

REFERENCES

Abraham, W.T., Shamshirsaz, A.A., McFann, K., Oren, R.M., and Schrier, R.W. (2006). Aquaretic effect of lixivaptan, an oral, non-peptide, selective V2 receptor vasopressin antagonist, in New York Heart Association functional class II and III chronic heart failure patients. *J Am Coll Cardiol, 47,* 1615-1621.

Albright, J.D., Reich, M.F., Santos, E.G.D., Dusza, J.P., Sum, F.W., Venkatesan, A,M., Coupet, J., Chan, P.S., Ru, X., Mazandarani, H., and Bailey,T. (1998)**.** 5-Fluoro-2-methyl-*N*-[4-(5*H*-pyrrolo[2,1-*c*]-[1,4]benzodiazepin-10(11*H*)-ylcarbonyl)-3-chlorophenyl]benzamide (VPA-985): An orally active arginine vasopressin antagonist with selectivity for V2 receptors. *J Med Chem, 41,* 2442-2444.

Allison, N.L., Albrightson-Winslow, C.R., Brooks, D.P., Stassen, F.L., Huffman, W.F., Stote, R.M., and Kinter, L.B. (1988). Species heterogeneity and antidiuretic hormone antagonists: what are the predictors? In Vasopressin: Cellular and Integrative Functions. (Allen W, Cowley Jr, Jean-Francois L, and Dennis A, eds) New York, USA: *Raven Press Ltd.*, 207-214.

Andersen-Beckh, B., Dehe, M., Schülein, R., Wiesner, B., Rutz, C., Liebenhoff, U., Rosenthal, W., and Oksche, A. (1999). Polarized expression of the vasopressin V2 receptor in Madin-Darby canine kidney cells. *Kidney. Int, 56,* 517-527.

Angrogue, H.J., Madias, N.E. (2000). Hyponatremia. *N Engl J Med, 342,* 1581-1589.

Aridor, M., and Balch, W.E. (1999). Integration of endoplasmic reticulum signaling in health and disease. *Nat Med, 5,* 745-751.

Bankir, L. (2001). Antidiuretic action of vasopressin: quantitative aspects and interaction between V1a and V2 receptor-mediated effects. *Cardiovasc Res, 51,* 372-390.

Banks, M.R., Farthing, M.J., Robberecht, P., and Burleigh, D.E. (2005). Antisecretory actions of a novel vasoactive intestinal polypeptide (VIP) antagonist in human and rat small intestine. *Br J Pharmacol, 144,* 994-1001.

Banks, M.R., Golder, M., Farthing, M.J., and Burleigh, D.E. (2004). Intracellular potentiation between two second messenger systems may contribute to cholera toxin induced intestinal secretion in humans. *Gut, 53,* 50-57.

Barak, L.S., Oakley, R.H., Laporte, S.A., and Caron, M.G. (2001). Constitutive arrestin-mediated desensitization of a human vasopressin receptor mutant associated with nephrogenic diabetes insipidus. *PNAS, 98,* 93-98.

Barberis, C., Brossard, G., Soubrie, P., Nisato, D., Pascal, M., Pruss, R., Scatton, B., Maffrand, J.P., and Le Fur, G. (2002). Characterization of (2S,4R)-1-[5-Chloro-1-[(2,4-dimethoxyphenyl)sulfonyl]-3-(2-methoxy-phenyl)-2-oxo-2,3-dihydro-1H-indol-3-yl]-4-hydroxy-N,N-dimethyl-2-pyrrolidinecarboxamide (SSR149415), a selective and orally active vasopressin V_{1b} receptor antagonist. *J Pharmacol Ex, Ther, 300,* 1122-1130.

Barberis, C., Mouillac, B., and Durroux, T. (1998). Structural bases of vasopressin / oxytocin receptor function. *J Endocrinol, 156,* 223–229.

Baylis, P.H. (1989). Regulation of vasopressin secretion. *Baillieres ClinEndocrinol. Metab, 3,* 313–330.

Beavo, J.A. (1995). Cyclic nucleotide phosphodiesterases: functional implications of multiple isoforms. *Physiol Rev, 75,* 725-748.

Beckh, B.A., Dehe, M., Schulien, R., Wiesner, B., Rutz, C., Liebenhoff, V., Rosenthal, W., and Oksche, A. (1999). Polarized expression of the vsopressin V2 receptor in Madin-Darby canine kidney cells. *Kidney international, 56,* 517-527.

Berne, R.M., Levy, M.N. (1998). Physiology: Membrane receptors, second messengers and signal transduction pathways. USA: *Mosby*.

Bens, M., Van Huyen, J.P., Cluzeaud, F., Teulon, J., and Vandewalle, A. (2001). CFTR disruption impairs cAMP-dependent Cl(-) secretion in primary cultures of mouse cortical collecting ducts. *Am J Physiol Renal Physiol, 28,* F434-F442.

Berschneider, H.M., and Powell, D.W. (1992). Fibroblasts modulate intestinal secretory responses to inflammatory mediators. *J Clin Invest, 89,*: 484-489.

Bertuccio, C.A., Ibarra, F.R., Toledo, J.E., Arrizurieta, E.E., and Martin, R.S. (2002). Endogenous vasopressin regulates Na-K-ATPase and Na(+)-K(+)-Cl(-) cotransporter rbsc-1 in rat outer medulla. *Am J Physiol Renal Physiol, 282,* F265-F270.

Billington, C.K., and Penn, R.B. (2003). Signaling and regulation of G protein-coupled receptors in airway smooth muscle. *Respir Res, 4,* 2.

Borroni, G., Maggi, A., Sangiovanni, A., Cazzaniga, M., and Salerno, F. (2000). Clinical relevance of hyponatremia for the hospital outcome of cirrhotic patients. *Dig Liver Dis, 32,* 605-610.

Bouley, R., Lin, H.Y., Raychowdhury, M.K., Marshansky, V., Brown, D., and Ausiello, DA. (2005). Down regulation of the vasopressin type 2 receptor (V2R) after vasopressin-induced internalization: involvement of a lysosomal degradation pathway. *Am J Physiol Cell Physiol, 288,* C1390-1401.

Bourque, C.W., and Oliet, S.H. (1997). Osmoreceptors in the central nervous system. *Annu Rev Physiol, 59,* 601–619.

Boyle, W.A. 3rd , and Segel, L.D. (1999). Attenuation of vasopressin-mediated coronary constriction and myocardial depression in hypoxic heart. *Circ Res, 66,* 710-721.

Bremnes, T., Paasche, J.D., Mehlum, A., Sandberg, C., Bremnes, B., and Attramadal, H. (2000). Regulation and intracellular trafficking pathways of the endothelin receptors. *J Biol Chem, 275,* 17596–17604.

Burnier, M., Fricker, A.F., Hayoz, D., Nussberger, J., and Brunner, H.R. (1999). Pharmacokinetic and pharmacodynamic effects of YM087, a combined V1/V2 vasopressin receptor antagonist in normal subjects. *Eur J Clin Pharmacol, 55,* 633-637.

Burrell, L.M., Phillips, P.A., Rolls, K.A., Buxton, B.F., Johnston, C.I., and Liu JJ. (1994). Vascular responses to vasopressin antagonists in man and rat. *Clin Sci (Lond), 87,* 389-395.

Bylund D, Deupree JD, and Toews ML. (2004). Radioligand-binding methods for membrane preparations and intact cells. *Methods Mol Biol, 259,* 1-28.

Chalmers, D.T. and Behan, D.P. (2002). The use of constitutively active GPCRs in drug discovery and functional genomics. *Nat Rev Drug Discov,1,* 599-608.

Carrasquillo, M.M., McCallion, A.S., Puffenberger, E.G., Kashuk, C.S., Nouri, N., and Chakravarti, A. (2002). Genome-wide association study and mouse model identifying interaction between RET and EDNRB pathways in Hirschsprung disease. *Nat Genet, 32,* 237-244.

Carman, C.V., Lisanti, M.P., and Benovic, J.L. (1999). Regulation of G protein-coupled receptor kinases by caveolin. *J Biol Chem, 274,* 8858–8864.

Cheng, S.H., Rich, D.P., Marshall, J., Gregory, R.J., Welsh, M.J., and Smith, A.E. (1991). Phosphorylation of R domain by cAMP-dependent protein kinase regulates the CFTR chloride channel. *Cell, 66,*1027-1036.

Chang, C.T., Bens, M., Hummler, E., Boulkroun, S., Schild, L., Teulon, J., Rossier, B.C., and Vandewalle, A. (2005). Vasopressin-stimulated CFTR Cl⁻ currents are increased in the renal collecting duct cells of a mouse model of Liddle's syndrome. *J Physiol, 562,* 271-284.

Cho, H., Murakami, K., Nakanishi, H., Fujisawa, A., Isoshima, H., Niwa, M., Hayakawa, K., Hase, Y., Uchida, I., Watanabe, H., Wakitani, K., and Aisaka, K. (2004). Synthesis and structure-activity relationships of 5,6,7,8-tetrahydro-4H-thieno[3,2-b]azepine derivatives: novel arginine vasopressin antagonists. *J Med Chem, 47,* 101-109.

Cowley, A.W. Control of the renal medullary circulation by vasopressin V1 and V2 receptors in the rat. *Exp Physiol, 85,* 223S–231S.

Crane, J.K., Choudhari, S.S., Naeher, T.M., Duffey, M.E. Mutual enhancement of virulence by enterotoxigenic and enteropathogenic Escherichia coli. *Infect Immun, 74,* 1505-1515.

Dale, L.B., Bhattacharya, M., Seachrist, J.L., Anborgh, P.H., and Ferguson, S.S. (2001). Agonist-stimulated and tonic internalization of metabotropic glutamate receptor 1a in human embryonic kidney 293 cells: agonist-stimulated endocytosis is beta-arrestin1 isoform-specific. *Mol Pharmacol, 60,* 1243–1253.

De Lapp, NW. (2004). The antibody-capture [^{35}S]GTPγS scintillation proximity assay: a powerful emerging technique for analysis of GPCR pharmacology. *Trends in Pharmacological Sciences, 25,* 400-401.

Dessy, C., Kelly, R.A., Balligand, J.L., and Feron, O. (2000). Dynamin mediates caveolar sequestration of muscarinic cholinergic receptors and alteration in NO signaling. *EMBO J, 19,* 4272–4280.

DeVita, M.V., Gardenswartz, M.H., Konecky, A., and Zabetakis, P.M. (1990). Incidence and etiology of hyponatremia in an intensive care unit. *Clin Nephrol, 34,* 163-166.

Devuyst, O., and Guggino, W.B. (2002). Chloride channels in the kidney: lesson learned from knockout animals. *Am J Physiol Renal Physiol, 283,* F1176-F1191.

De Wet, J.R., Wood, K.V., DeLuca, M., Helinski, D.R., and Subramani, S. (1987). Firefly luciferase gene: structure and expression in mammalian cells. *Mol Cell Biol, 7,* 725-737.

Dove, A. (2007). Technology feature: High-throughput screening goes to school. *Nature Methods, 4,* 523-532.

Engelmann, M., Landgraf, R., Wotjak, C.T. (2004). The hypothalamic–neurohypophysial system regulates the hypothalamic–pituitary–adrenal axis under stress: An old concept revisited. *Front Neuroendocrinol, 25,* 132–149.

Fan, F., and Wood, K.V. (2007). Bioluminescent assays for high-throughput screening. *Assay Drug Dev Technol, 5,* 127-136.

Fujiwara, T.M., Morgan, K., and Bichet, D.G. (1995). Molecular biology of diabetes insipidus. *Annu Rev Med, 46,* 331-343.

Gabow, P.A. (1993). Autosomal dominant polycystic kidney disease. *N Engl J Med, 329,* 332-342.

Gabriel, D., Vernier, M., Pfeifer, M.J., Dasen, B., Tenaillon, L.,and Bouhelal, R. (2003). High throughput screening technology for direct cAMP measurement. *Assay Drug Dev Technol, 1,* 291-303.

Galietta, L.J., Jayarama, S., and Verkman, A.S. (2001). Cell based assay for high throughput quantitative screening of CFTR chloride transport agonists. *Am J Physiol, 281,* C1734-C1742.

Gerbes, A,L,, Gulberg, V., Gines, P., Decaux, G., Gross, P., Gandjini, H., Djian, J., and

VPA Study Group. (2003). Therapy of hyponatremia in cirrhosis with a

vasopressin receptor antagonist: a randomized double-blind multicenter trial.

Gastroenterology, 124, 933-939.

Ghali, J.K., Koren, M.J., Taylor, J.R., Brooks-Asplund, E., Fan, K., Long, W.A., and

Smith, N. (2006). Efficacy and safety of oral conivaptan: a V1A/V2

vasopressin receptor antagonist, assessed in a randomized, placebo-controlled

trial in patients with euvolemic or hypervolemic hyponatremia. *J Clin

Endocrinol Metab, 91,* 2145-2152.

Gheorghiade, M., Gattis, W.A., O'Connor, C.M., Adams, K.F. Jr, Elkayam, U.,

Barbagelata, A., Ghali, J.K., Benza, R.L., McGrew, F.A., Klapholz, M.,

Ouyang, J., and Orlandi, C. (2004). Acute and Chronic Therapeutic Impact of a

Vasopressin Antagonist in Congestive Heart Failure (ACTIV in CHF)

Investigators. Effects of tolvaptan, a vasopressin antagonist, in patients

hospitalized with worsening heart failure: a randomized controlled trial. *JAMA,

291,* 1963-1971.

Gheorghiade, M., Gottlieb, S.S., Udelson, J.E., Konstam, M.A., Czerwiec, F., Ouyang,

J., Orlandi, C., and Tolvaptan Investigators. (2006). Vasopressin V(2) receptor

blockade with tolvaptan versus fluid restriction in the treatment of

hyponatremia. *Am J Cardiol, 97,* 1064-1067.

Gheorghiade, M., Niazi, I., Ouyang, J., Czerwiec, F., Kambayashi, J., Zampino, M.,

Orlandi, C., and Tolvaptan Investigators. (2003). Vasopressin V2-receptor

blockade with tolvaptan in patients with chronic heart failure: results from a

double-blind, randomized trial. *Circulation, 107,* 2690-2696.

Gheorghiade, M., Orlandi, C., Burnett, J.C., Demets, D., Grinfeld, L., Maggioni, A.,

Swedberg, K., Udelson, J.E., Zannad, F., Zimmer, C., and Konstam, M.A.

(2005). Rationale and design of the multicenter, randomized, double-blind,

placebo-controlled study to evaluate the Efficacy of Vasopressin antagonism in Heart Failure: Outcome Study with Tolvaptan (EVEREST). *J Card Fail, 11,* 260-269.

Goh, K.P. (2004). Management of hyponatremia. *Am Fam Physician, 69,* 2387–2394.

Goldsmith, S.R. (2006). Is there a cardiovascular rationale for the use of combined vasopressin V_{1a}/V_2 receptor antagonists? *Am J Med, 119,* S93-S96.

Golin-Bisello, F., Bradbury, N., and Ameen, N. (2005). STa and cGMP stimulate CFTR translocation to the surface of villus enterocytes in rat jejunum and is regulated by protein kinase G. *Am J Physiol Cell Physiol, 289,* C708-C716.

Grantham, J.J. (1993). Polycystic kidney disease. *Adv Intern Med, 38,* 409-420.

Gullans, S.R., and Verbalis. J,G. (1993). Control of brain volume during hyperosmolar and hypoosmolar conditions. *Annu Rev Med, 44,* 289-301.

Gunnet, J.W., Matthews, J.M., Maryanoff, B.E., Garavilla, L.D., Andrade-Gordon, P., Damiano, B., Hageman, W., Look, R., Stahle, P., Streeter, A.J., Wines, P.G., and Demarest, K.T. (2006). Characterization of RWJ-351647, a novel, nonpeptide vasopressin V_2 receptor antagonist. *Clin Exp Pharmacol Physiol, 33,* 320-326.

Guyader, D., Patat, A., Ellis-Grosse, E.J., and Orczyk, G.P. (2002). Pharmacodynamic effects of a nonpeptide antidiuretic hormone V2 antagonist in cirrhotic patients with ascites. *Hepatology, 36,* 1197-1205.

Haskal, R. (2007). Current issues for nurse practitioners: hyponatremia. *J Am Acad Nurse Pract, 19,* 563-579.

Hausmann, H., Richters, A., Kreienkamp, H., Meyerhof, W., Mattei, H., Lederis, K., Zwiers, H., and Richter, D. (1996). Mutational analysis and molecular modeling of the nonapeptide hormone binding domains of the [Arg8] vasotocin receptor. *Proc Natl Acad Sci USA, 93,* 6907–6912.

Head, J.F., Inouye, S.,Teranishi, K., and Shimomura, O. (2000). The crystal structure of the photoprotein aequorin at 2.3 Å resolution. *Nature, 405,* 372–376.

Hill, S.J. (2006). G-protein-coupled receptors: past, present and future. *Br J Pharmacol, 147,* S27-S37.

Hill. S.J. (2001). Reporter-gene systems for the study of GPCRs. *Curr Opin Pharmacol, 1,* 526-532.

Hitotsubashi, S., Fujii, Y., Yamanaka, H., and Okamoto, K.. (1992). Some properties of purified Escherichia coli heat-stable enterotoxin II. *Infect. Immun, 60,* 4468-4474.

Holmes ,C., Landry, D.W., and Granton, J.T. (2004). Science review: Vasopressin and the cardiovascular system part 2-clinical physiology. *Crit Care, 8,* 15-23.

Hopkins, A.L., Groom, C.R. (2002). The druggable genome. *Nat Rev Drug Discov, 1,* 727-730.

Innamorati, G., Sadeghi, H., and Birnbaumer, M. (1996). A fully active non glycosylated V2 vasopressin receptor. *Mol Pharmacol, 50,* 476-473.

Ishikawa, S., and Schrier, R.W. (2003). Pathophysiological roles of arginine vasopressin and aquaporin-2 in impaired water excretion. *Clin Endocrinol (Oxf), 58,* 1-17.

Iversen, P.W., Eastwood, B.J., Sittampalam, G.S., and Cox, K.L. (2006). A comparison of assay performance measures in screening assays: signal window, Z' factor, and assay variability ratio. *J Biomol Screen, 11,* 247-252.

Jacoby, E., Bouhelal, R., Gerspacher, M., and Seuwen, k. (2006). The 7-TM G-protein coupled receptor target family. *ChemMedChem, 1,* 760-783.

Jayaraman, S., Haggie, P.M., Wachter, R.M., Remington, S.J., and Verkman, A.S. (2000). Mechanism and cellular applications of a green fluorescent protein-based halide sensor. *J Biol Chem, 275,* 6047-6050.

Kasper, C.K. (1984). Desmopressin acetate (DDAVP). Good news. *JAMA, 251,* 2564-2565.

Kaufmann, J.E., Oksche, A., Wollheim, C.B., Gunther, G., Rosenthal, W., and Vischer, U.M. (2000). Vasopressin-induced von Willebrand factor secretion from endothelial cells involves V2 receptors and cAMP. *J Clin Invest, 106,* 107-116.

Kaufmann, J.E., and Vischer, U.M. (2003). Cellular mechanisms of homeostatic effects of desmopressin (DDAVP). *J Thromb Haemost, 1,* 682-689, 2003.

Kearney, M.T., Fox, K.A., Lee, A.J., Prescott, R.J., Shah, A.M., Batin, P.D., Baig, W., Lindsay, S., Callahan, T.S., Shell, W.E., Eckberg, D.L., Zaman, A.G.,

Williams, S., Neilson, J.M., and Nolan, J. (2002). Predicting death due to progressive heart failure in patients with mild-to-moderate chronic heart failure. J Am Coll Cardiol, *40,* 1801–1808.

Kenakin, T. (1997). Pharmacologic analysis of drug receptor interaction, third edition. *Lippincott Raven*, 331-373.

Kirk, K.L. (2000). New paradigms of CFTR chloride channel regulation. *Cell Mol Life Sci, 57,* 623-634.

Klabunde, T., and Hessler, G. (2002). Drug design strategies for targeting G-protein-coupled receptors. *ChemBioChem, 3,* 928-944.

Lam, K.S. (2007). New aspects of natural products in drug discovery. *Trends Microbiol, 15,* 279-289.

Landry, D.W., and Oliver, J.A. (2001). The pathogenesis of vasodilatory shock. *N Engl J Med, 345,* 588-595.

Lee, D.S., Austin, P.C., Rouleau, J.L., Liu, P.P., Naimark, D., and Tu, J.V. (2003). Predicting mortality among patients hospitalized for heart failure: Deviation and validation of a clinical model. *JAMA, 290,* 2581-2587.

Lefkowitz, R.J. (1998). G protein-coupled receptors. III. New roles for receptor kinases and beta-arrestins in receptor signaling and desensitization. *J Biol Chem, 273,* 18677–18680.

LeJemtel, T.H., and Serrano, C. (2007). Vasopressin dysregulation: Hyponatremia, fluid retention and congestive heart failure. *Int J Cardiol, 120,* 1-9.

Lemmens-Gruber, R., Kamyar, M. (2006). Drugs of the future: Review. *Cell Mol Life Sci, 63,* 1766-1779.

Li, H., Findlay, I.A., and Sheppard, D.N. (2004). The relationship between cell proliferation, Cl^- secretion, and renal cyst growth: a study using CFTR inhibitors. *Kidney Int, 66,* 1926-1938.

Lipinski, C., Lomberdu, F., Dominy, B., and Feeney, P. (1997). Experimental and computational approaches to estimate soluability and permeability in drug discovery and development setting. *Adv. Drug Deliv. Rev, 23,* 3-25.

Liu, J.J., Hartman, D.S., and Bostwick, J.R. (2003). An immobilized metal ion affinity absorption and scintillation proximity assay for receptor-stimulated phosphoinositide hydrolysis. *Anal Biochem, 318,* 91-99.

Lorenz WW, McCann RO, Longiaru M, and Cormier MJ. (1991). Isolation and expression of a cDNA encoding *Renilla reniformis* luciferase. *Proc Natl Acad Sci USA, 88,* 4438-4442.

Ma, T., Thiagarajah, J.R., Yang, H., Sonawane, N.D., Folli, C., Galietta, L.J., and Verkman, A.S. (2002). Thiazolidinone CFTR inhibitor identified by high throughput screening blocks cholera toxin-induced intestinal fluid secretion. *J Clin Invest, 110,* 1651-1658.

Madara, J.L., Patapoff, T.W., Gillece-Castro, B., Colgan, S.P., Parkos, C.A., Delp, C., and Mrsny, R.J. (1993). 5'-adenosine monophosphate is the neutrophil-derived paracrine factor that elicits chloride secretion from T84 intestinal epithelial cell monolayers. *J Clin Invest, 91,* 2320-2325.

Manning, M., Cheng, L.L., Stoev, S., Klis, W., Nawracka, E., Olma, A., Sawyer, W.H., Wo, N.C., and Chan, W.Y. (1997). Position three in vasopressin antagonist tolerates conformationally restricted and aromatic amino acid substitutions: a striking contrast with vasopressin agonists. *J Pept Sci, 3,* 31-46.

Mannucci, P.M., Ruggeri, Z.M., Pareti, F.I., and Capitanio, A. (1977). A 1-deamino-8-D-arginine vasopressin: a new pharmacological approach to the management of haemophillia and von Willebrand diseases. *Lancet, 1,* 869-872.

Marchese, A., and Benovic, J.L. (2001). Agonist-promoted ubiquitination of the G protein-coupled receptor CXCR4 mediates lysosomal sorting. *J Biol Chem, 276,* 45509–45512.

Matthews, J.M., Hoekstra, W.J., Dyatkin, A.B., Hecker, L.R., Hlasta, D.J., Poulter, B.L., Andrade-Gordon, P., de Garavilla, L., Demarest, K.T., Ericson, E., Gunnet, J.W., Hageman, W., Look, R., Moore, J.B., Reynolds, C.H., and Maryanoff, B.E. (2004). Potent nonpeptide vasopressin receptor antagonists based on oxazino- and thiazinobenzodiazepine templates. *Bioorg Med Chem Lett, 14,* 2747-2752.

Milligan, G. (2003). Principles: extending the utility of [^{35}S]GTPγS binding assays. *Trends Pharmacol Sci, 24,* 87-90.

Milligan, G., Feng, G.J., Ward, R.J., Sartania, N., Ramsay, D., McLean, A.J., and Carrillo, J.J. (2004). G protein-coupled receptor fusion proteins in drug discovery. *Curr Pharm Des, 10,* 1989-2001.

Mongillo, M., and Zaccolo, M. (2006). A complex phosphodiesterase system controls β-adrenoceptor signalling in cardiomyocytes. *Biochem. Soc. Trans, 34,* 510–511.

Morello, J.P., Salahpour, A., Laperrière, A., Bernier, V., Arthus, M.F., Lonergan, M., Petaja-Repo, U., Angers, S., Morin, D., Bichet, D.G., and Bouvier, M. (2000). Pharmacological chaperones rescue cell-surface expression and function of misfolded V2 vasopressin receptor mutants. *J Clin Invest, 105,* 887-895.

Mouillac, B., Chini, B., Balestre, MN., Elands, J., Trumpp-Kallmeyer, S., Hoflack, J., Hibert, M., Jard, S., and Barberis, C. (1995). The binding site of neuropeptide vasopressin V1a receptor. Evidence for a major localization within transmembrane regions. *J Biol Chem, 270,* 25771–25777.

Muanprasat, C., Sonawane, N.D., Salinas, D., Taddei, A., Galietta, L.J., and Verkman, A.S. (2004). Discovery of glycine hydrazide pore occluding CFTR inhibitors: mechanism, structure-activity analysis, and in vivo efficacy. *J Gen Physiol, 124,* 125-137.

Murakami, M., Kamiya, Y., Yanagita, Y., and Mori, M. (1999). Gs alpha mutations in hyperfunctioning thyroid adenomas. *Arch Med Res, 30,* 514-521.

Naito, A., Ohtake, Y., Hasegaw, H., Fukaya, A.Y., Kurasawa, T., Naito, K., Matsukawa, H., Oguma, T., Ezure, Y., Tsuriya, Y., Tanaka, H., Koike, K., and Shigenobu, K. (2000). Pharmacological profile of VP-343, a novel selective vasopressin V2 receptor antagonist, in rats. *Biol Pharm Bull, 23,* 182-9.

Newman, D.J., Cragg, G.M., and Snader, K.M. (2003). Natural products as sources of new drugs over the period 1981–2002. *J Nat Prod, 66,* 1022–1037.

Nguyen, M.K., and Kurtz, I. (2005). An analysis of current quantitative approaches to the treatment of severe symptomatic SIADH with intravenous saline therapy. *Clin Exp Nephrol, 9,* 1–4.

Nouel, D., Gaudriault, G., Houle, M., Reisine, T., Vincent, J.P., Mazella, J., and Beaudet, A. (1997). A differential internalization of somatostatin in COS-7 cells transfected with SST1 and SST2 receptor subtypes: a confocal microscopic study using novel fluorescent somatostatin derivatives. Endocrinology, *138,* 296-306.

Ohnishi, A., Orita, Y., Takagi, N., Fujita, T., Toyoki, T., Ihara, Y., Yamamura, Y., Inoue, T., and Tanaka, T. (1995). Aquaretic effect of a potent, orally active, non-peptide V2 antagonist in man. *J Pharmacol Exp Ther, 272,* 546-551.

Oi, H., Matsuura, D., Miyake, M., Ueno, M., Takai, I., Yamamoto, T., Kubo, M., Moss, J., and Noda, M. (2002). Identification in traditional herbal medications and confirmation by synthesis of factors that inhibit cholera toxin-induced fluid accumulation. *Proc Natl Acad Sci U S A, 99,* 3042-3046.

Oksche, A., Schulein, R., and Rutz, C. (1996). Vasopressin V2 receptor mutants that cause x-linked nephrogenic diabetes insipidus: analysis of expression, processing, and function. *Mol Pharmacol, 50,* 820-828.

Ozgonenel, B., Paipurkar, M., Lusher, J.M. (2007). How do you treat bleeding disorders with desmopressin? *Postgrad Med J, 83,* 159-163.

Paranjape, S.B., and Thibonnier, M. (2001). Development and therapeutic indications of orally active non-peptide vasopressin receptor antagonists. *Expert Opin Invest Drugs, 10,* 825-834.

Pedemonte, N., Lukacs, G.L., Du, K., Caci, E., Zegarra-Moran, O., Galietta, L.J., Verkman, A.S. (2005). Small molecule correctors of defective ΔF508-CFTR cellular processing identified by high-throughput screening. *J Clin Invest, 115,* 2564-2571.

Pereira, D.A., and Williams, J.A. (2007). Review: Historical perspectives in pharmacology origin and evolution of high throuput screening. *Br J Pharmacol, 152,* 53-61.

Praetorius, H.A., Praetorius, J., Nielsen, S., Frokiaer, J., and Spring, K.R. (2004). Beta1-integrins in the primary cilium of MDCK cells potentiate fibronectininduced Ca2+ signaling. *Am J Physiol Renal Physiol,* 287, F969–F978.

Praetorius, H.A., and Spring, K.R. (2001). Bending the MDCK cell primary cilium increases intracellular calcium. *J Membr Biol, 184,* 71–79.

Rees, S. (2002). Functional assay systems for drug discovery at G-protein coupled receptors and ion channels. *Receptors Channels*, 8, 257-259.

Reinscheid, R.K., Kim, J., Zeng, J., and Civelli, O. (2003) High throughput real-time monitoring of Gs-coupled receptor activation in intact cells using cyclic nucleotide-gated channels. *Eur J Pharmacol, 478,* 27-34.

Rich, T.C. and Karpen, J.W. (2005). High-throughput screening of phosphodiesterase activity in living cells. *Methods Mol Biol, 307,* 45-61.

Robben, J.H., Knoers, N.V., and Deen, P.M. (2004). Regulation of the vasopressin V_2 receptor by vasopressin in polarized renal collecting duct cells. *Mol Biol Cell, 15,* 5693-5699.

Russell, S.D., Selaru P, Pyne DA, Ghazzi MM, Massey KD, Pressler M, Serikoff A, and Coats AJ. (2003). Rationale for use of an exercise end point and design for the ADVANCE (A Dose evaluation of a Vasopressin Antagonist in CHF patients undergoing Exercise) trial. *Am Heart J, 145,* 179-186.

Sack, D.A., Sack, R.B., Nair, G.B., and Siddique, A.K. (2004). Cholera. *Lancet, 363,* 223-233.

Sadeghi, H.M., Innamorati, G., Dagarag, M., and Birnbaumer, M. (1997). Palmitoylation of the V2 vasopressin receptor. *Mol Pharmacol, 52,* 21–29.

Sadeghi, H.M., Robertson, G.L., Bichet, D.G., Innamorati, G., and Birnbaumer, M. (1997). Biochemical basis of partial NDI phenotype. *Molecular endocrinology, 11,* 1806-1813.

Sadeghi, H.M., and Birnbaumer, M. (1999). O-glycosylation of the V2 vasopressin receptor. *Glycobiology, 9,* 731-737.

Saito, M., Tahara, A., and Sugimoto, T. (1996). 1-desamino-8-arginine vasopressin (dDAVP) as an agonist on V_1b vasopressin receptor. *Biochem Pharmacol, 53,* 1711-1717.

Sands, J.M., and Bichet, D.G. (2006) Nephrogenic Diabetes Insipidus. *Ann Intern Med, 144,* 186-194.

Schrier, R.W., Briner, V., and Caramelo, C. (1993). Cellular Action and Interactions of Arginine Vasopressin in Vascular Smooth Muscle: Mechanisms and Clinical Implications. *J Am Soc Nephrol, 4,* 2-11.

Schrier, R.W., Gross, P., Gheorghiade, M., Berl, T., Verbalis, J.G., Czerwiec, F.S., Orlandi, C., and SALT Investigators. (2006). Tolvaptan, a selective oral vasopressin V2-receptor antagonist, for hyponatremia. *N Engl J Med, 355,* 2099-2112.

Seethala, R., and Fernandes, B. (2001). Handbook of drug screening. *Marcel Dekker,* 550-553.

Serradeil-Le Gal, C. (2001). An overview of SR121463, a selective non-peptide vasopressin V2 receptor antagonist. *Cardiovasc Drug Review, 19,* 201-214.

Serradeil-Le Gal, C., Lacour, C., Valette, G., Garcia, G., Foulon, L., Galindo, G., Bankir, L., Pouzet, B., Guillon, G., Barberis, C., Chicot, D., Jard, S., Vilain, P., Garcia, C., Marty, E., Raufaste, D., Brossard, G., Nisato, D., Maffrand, J.P., and Le Fur, G. (1996). Characterization of SR 121463A, a highly potent and selective, orally active vasopressin V2 receptor antagonist. *J Clin Invest, 98,* 2729-2738.

Serradeil-Le Gal, C., Wagnon, J., Garcia, C., Lacour, C., Guiraudou, P., Christophe, B., Villanova, G., Nisato, D., Maffrand, J.P., and Le Fur, G. (1993). Biochemical and pharmacological properties of SR 49059, a new, potent, non peptide antagonist of rat and human V1a receptors. *J Clin Invest, 92,* 224-231.

Serradeil-Le Gal, C., Wagnon, J., Simiand, J.,Griebel, G., Lacour, C., Guillon, G., Barberis, C., Brossard, G., Soubrie, P., Nisato, D., Pascal, M., Pruss, R., Scatton, B., Maffrand, J.P., and Le Fur, G. (2002). Characterization of (2S,4R)-1-[5-Chloro-1-[(2,4-dimethoxyphenyl)sulfonyl]-3-(2-methoxy-phenyl)-2-oxo-2,3-dihydro-1H-indol-3-yl]-4-hydroxy-N,N-dimethyl-2-pyrrolidinecarboxamide (SSR149415), a selective and orally active vasopressin V_{1b} receptor antagonist. *J Pharmacol Ex, Ther, 300,* 1122-1130.

Shenoy, S.K., McDonald, P.H., Kohout, T.A., and Lefkowitz, R.J. (2001). Regulation of receptor fate by ubiquitination of activated β2-adrenergic receptor and β-arrestin. *Science, 294,* 1307–1313.

Shimada, Y., Taniguchi, N., Matsuhisa, A., Sakamoto, K., Yatsu, T., and Tanaka, A. (2000). Highly potent and orally active non-peptide arginine vasopressin antagonists for both V1A and V2 receptors: synthesis and pharmacological properties of 4'-[(4,4-difluoro-5-methylidene-2,3,4,5-tetrahydro-1H-1-benzoazepin-1-y l)carbonyl]-2-phenylbenzanilide derivatives. *Chem Pharm Bull (Tokyo), 48,* 1644-51.

Shimomura, O., Johnson, F.H., and Saiga, Y. (1962). Extraction, purification and properties of aequorin, a bioluminescent protein from the luminous hydromedusan, *Aequorea*. *J Cell Comp Physiol, 59,* 223-239.

Sigworth, F.J., Klemic, K.G., (2002). Patch clamp on a chip. *Biophys J*, 82, 2831-2832.

Snyder, P.M. (2005). Minireview: regulation of epithelial Na+ channel trafficking. Endocrinology, *146,*5079-5085

Soupart, A., Gross, P., Legros, J.J., Alföldi, S., Annane, D., Heshmati, H.M., and Decaux, G. (2006). Successful long-term treatment of hyponatremia in syndrome of inappropriate antidiuretic hormone secretion with satavaptan (SR121463B), an orally active nonpeptide vasopressin V2-receptor antagonist. *Clin J Am Soc Nephrol, 1,* 1154-1160.

Sterns, R.H., Riggs, J.E., and Schochet, S.S. Jr. (1986). Osmotic demyelination syndrome following correction of hyponatremia. *N Engl J Med, 314,* 1535-1542.

Sweeney, W.E. Jr, and Avner, E.D. (2006). Molecular and cellular pathophysiology of autosomal recessive polycystic kidney disease (ARPKD). *Cell Tissue Res, 326,* 671-685.

Tahara, A., Tomura, Y., Wada, K.I., Kusayama, T., Tsukada, J., Takanashi, M., Yatsu, T., Uchida, W., and Tanaka, A. (1997). Pharmacological profile of YM087, a novel potent non-peptide vasopressin V_{1a} and V_2 receptor antagonist, in vitro and in vivo. *J Pharmacol Exp Ther, 282,* 301-308.

Terrillon, S., Barberis, C., Bouvier, M., and Bourne, H.R. (2004). Heterodimerization of V1a and V2 Vasopressin Receptors Determines the interaction with b-

Arrestin and Their Trafficking Patterns. *Proc Natl Acad Sci USA, 101,* 1548-1553.

Thibonnier M, Coles P, Thibonnier A, and Shoham M. (2001). The basic and clinical pharmacology of nonpeptide vasopressin receptor antagonists. *Annu Rev Pharmacol Toxicol, 41,* 175-202.

Thibonnier, M., Conary, D.M., Preston, J.A., Plesnicher, C.L., Dweik, R.A., and Erzurum, S.C. (1999). Human vascular endothelial cells express oxytocin receptors. *Endocrinology, 140,* 1301-1309.

Thibonnier, M., Preston, J.A., Dulin, N., Wilkins, P.L., Berti-Mattera, L.N., and Mattera, R. (1997). The human V3 pituitary vasopressin receptor: ligand binding profile and density-dependent signaling pathways. *Endocrinology, 138,* 4109-4122.

Torres, V.E., and Harris, P.C. (2005). Mechanisms of disease: autosomal dominant and recessive polycystic kidney diseases. *Nat Clin Pract Nephrol, 2,* 40-55.

Treschan, T.A., and Peters, J. (2006). The vasopressin system: physiology and clinical strategies. *Anesthesiology, 105,* 599-612.

Udelson, J.E., Smith, W.B., Hendrix, G.H., Painchaud, C.A., Ghazzi, M., Thomas, I., Ghali, J.K., Selaru, P., Chanoine, F., Pressler, M.L., and Konstam, M.A. (2001). Acute hemodynamic effects of conivaptan, a dual V(1A) and V(2) vasopressin receptor antagonist, in patients with advanced heart failure. *Circulation, 104,* 2417-2423.

Verbalis, J.G. (2003). Disorders of body water homeostasis. *Best Pract Res Clin Endocrinol Metab, 17,* 471-503.

Vischer, U.M., and Moerloose, P.D. 1999 Von Willebrand factor: from cell biology to the clinical management of Von Willebrand's disease. *Hematology, 30,* 93-109.

Walker, B.R., Childs, M.E., and Adams, E.M: (1988). Direct cardiac effects of vasopressin: role of V1- and V2-vasopressinergic receptors. *Am J Physiol, 255,* H261-H265.

Wang, S., Luo, Y., Wilson, P.D., Witman, G.B., and Zhou, J. (2004). The autosomal recessive polycystic kidney disease protein is localized to primary cilia, with concentration in the basal body area. *J Am Soc Nephrol, 15,* 592-602.

Wang, X., Gattone, V. 2nd, Harris, P.C., and Torres, V.E. (2005). Effectiveness of vasopressin V2 receptor antagonists OPC-31260 and OPC-41061 on polycystic kidney disease development in the PCK rat. *J Am Soc Nephro, 16,* 846–851.

Williams, C. (2004). cAMP detection methods in HTS: selecting the best from the rest. *Nat Rev Drug Discov, 3,* 125-135.

Williams, S., Neilson, J.M., and Nolan, J. (2002). Predicting death due to progressive heart failure in patients with mild-to-moderate chronic heart failure. *J Am Coll Cardiol, 40,* 1801–1808.

Wise, A., Jupe, S.C., and Rees, S. (2004). The identification of ligands at orphan G protein coupled receptors. *Annu Rev Pharmacol Toxicol, 44,* 43-66.

Wong, F., Blei, A.T., Blendis, L.M., and Thuluvath, P.J. (2003). A vasopressin receptor antagonist (VPA-985) improves serum sodium concentration in patients with halide sensor. *J Biol Chem, 275,* 6047-6050.

Wong, L.L., and Verbalis, J.G. (2002). Systemic diseases associated with disorders of water homeostasis. *Endocrinol Metab Clin North Am, 31,* 121–140.

Wong, L.L., and Verbalis, J.G. (2001). Vasopressin V2 receptor antagonists. *Cardiovasc Res, 51,* 391-402.

Wysolmerski, J.J., Cormier S, Philbrick, W.M., Dann, P., Zhang, J.P., Roume, J., Delezoide, A.L., and Silve, C. (2001). Absence of functional type 1 parathyroid hormone (PTH)/PTH related protein receptors in humans is associated with abnormal breast development and tooth impaction. *J Clin Endocrinol Metab, 86,* 1487-1488.

Xu, Y., Hopfner, R.L., McNeill, J.R., and Gopalakrishnan, V. (1999). Vasopressin accelerates protein synthesis in neonatal rat cardiomyocytes. *Mol Cell Biochem, 195,* 183-190.

Yamamura, Y., Ogawa, H., Chihara, T., Kondo, K., Ongawa, T., Nakamura, S., Mori, T., Tominaga, M., and Yabuuchi, Y. (1991). OPC-21268, an orally effective, nonpeptide vasopressin V1 receptor antagonist. *Science, 252,* 572-557.

Yamamura, Y., Ogawa, H., Yamashita, H., Chihara, T., Miyamoto, H., Nakamura, S., Onogawa, T., Yamashita, T., Hosokawa, T., Mori, T., Tominaga, M., and Yabuuchi, Y. (1992). Characterization of a novel aquaretic agent, OPC-31260, as an orally effective, nonpeptide vasopressin V_2 receptor antagonist. *Br J Pharmacol, 105,* 787-791.

Yamamura, Y., Nakamura, S., Itoh, S., Hirano, T., Onogawa, T., Yamashita, T., Yamada, Y., Tsujimae, K., Aoyama, M., Kotosai, K., Ogawa, H., Yamashita, H., Kondo, K., Tominaga, M., Tsujimoto, G., and Mori, T. (1998). OPC-41061, a highly potent human vasopressin V2-receptor antagonist: pharmacological profile and aquaretic effect by single and multiple oral dosing in rats. *J Pharmacol Exp Ther, 287,* 860-867.

Zeltser, D., Rosansky, S., van Rensburg, H., Verbalis, J.G., Smith, N., and Conivaptan Study Group. (2007). Assessment of the efficacy and safety of intravenous conivaptan in euvolemic and hypervolemic hyponatremia. *Am J Nephrol, 27,* 447-457.

APPENDIX

APPENDIX A
YELLOW FLUORESCENT PROTEIN (YFP)

Four-points mutation of a green fluorescent protein (GFP), a fluorophore commonly found in variety of bioluminescence organisms, yields YFP which is a fluorescent protein with a red fluorescent protein shifted in excitation and emission spectra, improved fluorescent intensity, and photo-stability. The YFP structure is composed of 11 β-sheets surrounding the central α-helix core which contains a fluorophore. It emits yellow fluorescent light at the spectral maximum of 535nm, when excited at 500 nm. YFP fluorescence is sensitive to pH and several anions, therefore with some modifications to optimize the sensitivity, YFP can be a valuable pH or anion indicator.

Developed by Jayaraman et.al. in 2000, YFP-H148Q was a mutant YFP with replacement of histidine by glutamine at amino acid position 148. Sensitivities to the anions of YFP-H148Q in the order of magnitude were as follows: $F^->ClO_4^->I^->SCN^->NO_3^->Br^->Cl^->$formate>acetate; and insensitivity to sulfate, glutamate, isothionate, phosphate, and other cations was also detected. It was found to have good halide sensitivity (K_{Cl} = 197mM, K_I = 20 mM) at a normal cytoplasmic pH. YFP-H148Q was also tested as a cellular halide sensor in Swiss 3T3 fibroblasts expressing CFTR chloride channels and YFP-H148Q. The fluorescent intensity of YFP-H148Q found in the cytoplasm and nucleus was inversely related to the extracellular halide concentrations and the cellular halide conductance mediated by CFTR. Taken together, YFP-H148Q could be used as a cellular halide sensor.

In the subsequent year, the halide sensitivity of YFP-H148Q was improved further by adding one more mutation, I152L (Galietta et.al., 2001). The YFP-H148Q/I152L was much more sensitive to chloride and iodide (K_{Cl} = 88mM, K_I = 3 mM) compared with YFP-H148Q at the cytoplasmic pH. The fluorescent intensity of this latest mutant YFP was also shown to be dependent on the CFTR-mediated halide transport and the extralcellular halide concentration in Swiss 3T3 fibroblasts.

Therefore, YFP-H148Q/I152L, a sensitive cellular halide sensor, is superior to its predecessors in detection of the halide influx mediated by CFTR. In fact, it has already been used successfully in HTS for CFTR modulators in the Fischer rat thyroid cells stably expressing YFP-H148Q/I152L and human CFTR (Pedemonte et al., 2005; Ma et al., 2002a; Muanprasat et al., 2004). Because YFP-H148Q/I152L has a higher sensitivity to iodide, the screening in those studies utilized iodide instead of chloride in the assessment of the CFTR mediated quenching of YFP fluorescence.

APPENDIX B

INTRODUCTION OF cmyc SEQUENCE TO HUMAN V$_2$R cDNA

The coding sequence for cmyc was incorporated into the human wild type and the mutant V$_2$R cDNA sequences by a PCR reaction using the primers and the conditions shown below. The size of the PCR products was verified by agarose gel electrophoresis (1% agarose). Then, parts of the gel containing the products were excised, and purified by a QIAquick Gel Extraction Kit.

Materials

Table 15.   Materials necessary for PCR, agarose gel electrophoresis, and PCR product purification.

Reagents and Equipments	Sources
Plasmids encoding human wild type and mutant (W164S) V$_2$Rs	Dr. Daniel Bichet (University of Montreal)
Taq polymerase enzyme	Invitrogen
Custom PCR primers	UCSF cell culture facility
10mM dNTP mix	Invitrogen
Thermocycler GeneAmp PCR System 9700	Applied Biosystems
Certified^{TM} Molecular Biology agarose	Bio-Rad
TAE buffer (tris/ acetic acid/ EDTA)	Bio-Rad
Lambda DNA/*Hin*dIII Markers	Promega
UltraPure^{TM} 10mg/ml Ethidium Bromide	Invitrogen
FisherBiotech Horizontal Electrophoresis Systems	Fisher Scientific
QIAquick Gel Extraction Kit	Qiagen
Microcentrifuge tubes	

Method

1. The cmyc coding sequence was introduced to the human V_2R cDNA by a PCR reaction.

    1.1 PCR primers

Forward primer (with cmyc)	5′ CCG CTC GAG ATG GAG CAG AAA CTC ATC TCT GAA GAG GAT CTG CTC ATG GCG TCC ACC ACT TCC 3′
Reverse primer	5′ ATG GCG GCC AAG CTT CTGC 3′

    1.2 PCR reaction mixture

Reagents	Volume (µl)
Distilled water	33.00
PCR buffer	5.00
dNTP (10 mM)	8.75
Forward primer	1.00
Reverse primer	1.00
Taq polymerase	0.75
Plasmid containing human V_2R	0.50
Total volume	50.00

    1.3 PCR condition

Condition	Temperature (^{o}C)	Time (min)	Cycle
Denature	94	5	1
Denature	94	0.5	
Annealing	60	2	
Extension	72	1	30
Extension	72	7	1

2. For agarose gel electrophoresis, the PCR products and a DNA marker were loaded into the gel (1% agarose in TAE buffer and ethidium bromide 1µl/100ml), run for 30 minutes at 100 volts, and visualized under the UV light. The expected size of

cmyc-tagged V_2R cDNA was approximately 1500 base pairs. The gel parts containing the PCR products were excised with a clean scalpel.

3. The cmyc-tagged V_2R PCR products were purified from agarose by using a gel extraction kit.

    3.1 The QG buffer of 300 μl was added to each 100 mg of the excised gel, and the mixture was incubated at 50^oC until the gel was completely dissolved.

    3.2 To bind the DNA products, the solution was applied to a spin column, and centrifuged for 1 minute at 13,000 RPM.

    3.3 The flow-through was discarded, and 0.75 ml of PE buffer was added to the spin column, and centrifuged at 13,000 RPM for 1 minute.

    3.4 To get rid of the traces of the PE buffer, the flow-through was discarded and centrifuged again at the same speed for 1 minute

    3.5 To elute the DNA products, the spin column was placed on top of a clean microcentrifuge tube, the EB buffer of 50 μl was added to the spin column, incubated at the room temperature for 1 min, centrifuged at 13,000 RPM for 1 minute, and the flow-through containing the purified PCR products was collected.

APPENDIX C

SUBCLONING AND EXPANSION OF PLASMIDS

The cmyc-tag V_2R PCR products and pCDNA3.1Hyg+ plasmids were restricted with the indicated restriction enzymes, separated by agarose gel electrophoresis, purified with a gel purification kit (see APPENDIX B for details), and ligated together by T4 DNA ligase. The competent *E Coli*. was transformed with the ligation product, and selected with Ampicillin (100 μg/ml) on LB agar plates. The surviving colonies were propagated separately in the LB broth containing 100 μg/ml Ampicillin. The plasmids were extracted from each culture by a plasmid extraction kit, and run in comparison with pCDNA3.1Hyg+ in agarose gel electrophoresis. The plasmids incorporating cmyc-tag V_2R cDNA were identified by an increase in size relative to that of pCDNA3.1Hyg+. The presence of cmyc-tag V_2R cDNA was finally confirmed by DNA sequencing (the Fisher lab, University of California, San Francisco).

Materials

Table 16. Materials for plasmid subcloning and expansion.

Reagents and Equipments	Sources
pCDNA3.1 Hyg$^+$	Invitrogen
PCR product	
XhoI, XbaI, HindIII	New England Biolab
T4 DNA ligase	Invitrogen
One shot® chemically competent E Coli.	Invitrogen
Ampicillin	Roche
LB Amp plates	Teknova
S.O.C. medium	Invitrogen
QIAspin miniprep plasmid extraction kit	Qiagen

Table 16(continued). Materials for plasmid subcloning and expansion (continue).

Reagents and Equipments	Sources
QIAquick Gel Extraction Kit	
Water bath,	
Incubator-shaker	
Spectrophotometer	

Method

1. The pCDNA3.1Hyg+ plasmid was restricted with HindIII and XbaI in the reaction mixture indicated below overnight at 37°C.

Reagents	Volume (µl)
Distilled water	9.5
Buffer 2	2.0
Bovine serum albumin	0.5
HindIII	1.0
XbaI	1.0
pCDNA3.1Hyg$^+$ (6 µg/µl)	6.0
Total volume	20.0

2. The cmyc-tag V$_2$R PCR product was restricted with XhoI and XbaI overnight at 37°C, the reaction mixture as follows.

Reagents	Volume (µl)
Distilled water	
Buffer 2	4.0
Bovine serum albumin	1.0
XhoI	2.0
XbaI	2.0
PCR products	31.0
Total volume	40.0

3. The restricted plasmid in number 1 and the PCR product in number 2 were run separately in an agarose gel (0.5% w/v in TAE buffer) electrophoresis for 45

minutes at 100 volts. Then, under the UV light, parts of the gel containing the DNA bands of interest were excised.

4. Using a QIAquick Gel Extraction Kit, parts of the gel containing the restricted plasmid and the PCR product were purified, and ligated together with T4 ligase at 4^oC overnight.

Reagents	Volume (μl)
Distilled water	9.0
Buffer	8.0
T4 ligase	2.0
Restricted pCDNA3.1Hyg$^+$	1.0
Restricted PCR products	10.0
Total volume	30.0

5. Bacterial transformation of the ligated product.

5.1 On ice, twenty-five μl of competent *E Coli* was incubated with 2 μl of the mixture from the ligation reaction in number 4 for 30 minutes.

5.2 The mixture was then briefly incubated in a 42^oC water bath for 45 seconds, and was immediately placed on ice.

5.3 The S.O.C. medium of 250 μl was added, and the transformed *E coli*. was cultured in a 37^oC incubator-shaker at 250 RPM for 60 minutes.

5.4 The *E Coli* was selected on the LB agar with 100 μg/ml ampicillin at 37^oC overnight.

5.5 The surviving colonies were isolated and cultured individually in 5 ml LB broth containing 100 μg/ml Ampicillin in a 37^oC incubator-shaker at 250 RPM overnight.

6. Plasmids yielded from the overnight bacterial culture were extracted using a QIAspin miniprep plasmid extraction kit.

6.1 The bacterial culture of 5ml was centrifuged at 3,000 rpm for 10 minutes. The pelleted bacterial cells were resuspended in 250 μl Buffer P1 and transferred to a microcentrifuge tube. RNase A was to be added to Buffer P1 before use and no cell clumps should be visible after resuspension of the pellets.

6.2 Buffer P2 of 250 μl was added, and the tube was gently inverted 4–6 times to mix. Vortexing was not allowed, as this would result in shearing of the genomic DNA. If necessary, inverting of the tube could be continued until the solution became viscous and slightly clear. Do not allow the lysis reaction to proceed for more than 5 minutes.

6.3 Buffer N3 of 350 μl was added, and the tube was inverted immediately but gently 4–6 times. To avoid localized precipitation, the solution was mixed gently but thoroughly, immediately after addition of Buffer N3. The solution should become cloudy.

6.4 The tube was centrifuged for 10 minutes at 13,000 rpm (~17,900 x g) in a table-top micro-centrifuge. A compact white pellet would form.

6.5 The supernatants from step 5.4 was applied to the QIAprep spin column by decanting or pipetting.

6.6 After being centrifuged for 30–60 seconds, the flow-through was discarded.

6.7 The QIAprep spin column was washed by adding 0.5 ml Buffer PB and centrifuging for 1 minute. The flow-through was discarded. This step was necessary to remove the trace nuclease activity.

6.8 The QIAprep spin column was washed by adding 0.75 ml Buffer PE and centrifuging for 1 minute.

6.9 After discarding the flow-through, centrifugation was carried out for an additional 1 minute to remove the residual wash buffer.

6.10 The QIAprep column was placed in a clean 1.5 ml micro-centrifuge tube. To elute the DNA, 50 μl Buffer EB (10 mM Tris·Cl, pH 8.5) or water was added to the center of each QIAprep spin column, let stand for 1 minute, and centrifuged for 1 minute.

7. Measurement of DNA concentrations. The plasmid DNA concentrations were measured with a spectrophotometer at 260 and 280 nm. The DNA concentration was calculated as a 50 x OD_{280} x dilution factor. Normally, the extracted plasmid was diluted 60 times with distilled water. The quality of the DNA was assessed with the ratio of OD_{280} to OD_{260}. A purified DNA should have a ratio between 1.8-2.0.

APPENDIX D
RECIPES FOR CELL CULTURE MEDIA

The cell culture media of the cells used in the study were summarized in the table below.

Table 17. Cell culture media.

FRT	Calu-3/MDCK	T84	CHO-K1
F-12 Modified Coon's	MEM Eagle's with Earle's BSS	1:1 mixture of DMEM high glucose and F-12 medium	F-12 Ham's Nutrient mix
10% FBS	10% FBS	10% FBS	10% FBS
2mM glutamine	2mM glutamine		
1.5g/l NaHCO$_3$	1.5g/l NaHCO$_3$		
	0.11 mg/ml sodium pyruvate,		
	Non essential amino acids		
100 units/ml Penicillin	100 units/ml Penicillin	100 units/ml Penicillin	100 units/ml Penicillin
100 μg Streptomycin	100 μg Streptomycin	100 μg Streptomycin	100 μg Streptomycin

Table 18. Sources of the ingredients for cell culture media

Ingredients	Sources
F-12 Modified Coon's medium	Sigma-Aldrich
MEM Eagle's with Earle's BSS	UCSF cell culture facility
1:1 mixture of DMEM high glucose and F-12 medium	UCSF cell culture facility
F-12 Ham's Nutrient mix	UCSF cell culture facility
FBS	Hyclone
Glutamine	UCSF cell culture facility
Sodium pyruvate	UCSF cell culture facility
$NaHCO_3$	UCSF cell culture facility
Non essential amino acids	UCSF cell culture facility
Penicillin/Streptomycin	UCSF cell culture facility

APPENDIX E
CELL TRANSFECTION

The objectives of trasfection were to establish (1) a stable FRT cell line expressing CFTR, YFP-H148Q/I152L, and cmyc-tagged wild type or mutant human V_2R; (2) a stable FRT cell line expressing HA-tagged human $V_{1a}R$; and (3) CHO-K1 cells transiently expressing human β_2AR. The indicated plasmids were delivered to the nucleus of the specific cells by using liposome-based technology (Lipofectamine™ 2000). Unlike the transient expression in which the cells could be utilized 48 hours after the transfection, the stable expression required further antibiotic selection.

Materials.

Table 19. Materials for transient and stable transfections.

Reagents and Equipments		Sources
Cell related	FRT cells	UCSF cell culture facility
	FRT cells expressing CFTR, and YFP-H148Q/I152L	
	CHO-K1 cells	UCSF cell culture facility
	Cell culture media	
	0.05% Trypsin with 0.5mM EDTA	UCSF cell culture facility
	24 well plates	Fisher scientific

Table 19 (continued). Materials for transient and stable transfections.

Reagents and Equipments		Sources
Plasmids	Plasmids	
	wV$_2$R-Hyg	
	mV$_2$R-Hyg	
	HA-tagged human V$_{1a}$R	UMR cDNA Resource Center
	HA-tagged human β$_2$AR	UMR cDNA Resource Center
Transfection reagents	Lipofectamine™ 2000	Invitrogen
	Opti-MEM I medium	Invitrogen
Selective antibiotics	Zeocin	Invitrogen
	Geneticin	Gibco
	Hygromycin	Roche
Equipment	CO$_2$ incubator	

Method

1. One day before transfection, 10^5 cells were placed in a 24-well plate so that the cells would be 80% confluent at the time of transfection.

2. On the transfection day, the cell culture media was replaced at least 30 minutes before transfection with 500 µl of Opti-MEM I

3. For each transfection sample, the complexes were prepared as follows:

   3.1 The plasmid of 0.8 µg was diluted in 50 µl of Opti-MEM I Reduced Serum Medium without serum (or other medium without serum). And they were mixed together gently.

   3.2 Lipofectamine™ 2000 was gently mixed before use, then an appropriate amount of it was diluted in 50 µl of Opti-MEM I Medium, and incubated for 5 minutes at the room temperature.

   3.3 Then, the diluted DNA was combined with the diluted Lipofectamine™ 2000 (total volume = 100 µl). They were mixed together gently and

incubated for 20 minutes at the room temperature (solution may appear cloudy). The DNA-lipofectamine complexes were stable for 6 hours at the room temperature.

4. The complexes of 100 μl was added to each well containing the cells and the medium. They were mixed gently by rocking the plate back and forth.

5. The cells were incubated at $37^{o}C$ in a CO_2 incubator for 6 hours, then the medium was changed to that of the cell-specific type.

6. For transient expression, the CHO-K1 cells were used at 48 hours after the transfection.

7. For stable expression, together with their non-transfected counterpart, the FRT cells and the FRT cells expressing CFTR, and YFP-H148Q/I152L underwent antibiotic selections which were 750 μg/ml geneticin, and a combination of 500 μg/ml zeocin, 500 μg/ml geneticin, and 350 μg/ml hygromycin, respectively, at 24 hours after the transfection.

8. Two weeks after the beginning of the antibiotic selections, all of the non-transfected cells died, and the surviving colonies from the transfected groups were isolated.

9. After verifications with immunocytochemistry, immunoblot and the functional assays, several vials of successfully established cell lines were frozen in liquid nitrogen by the UCSF cell culture facility.

APPENDIX F
IMMUNOBLOT

It was required to verify that the stably transfected FRT cells successfully expressed cmyc-tagged human V_2R with correct molecular weight. The protein was extracted from the FRT cells with or without human V_2R expression, separated by electrophoresis, transferred to a PVDF membrane, and finally stained for V_2R with the rabbit anti-cmyc antibody.

Materials.

Table 20. Materials for immunobloting.

Reagents and Equipments		Sources
Cell culture	FRT cells stably transfected with cmyc-tagged human V_2R	
	PBS	UCSF cell culture facilirty
Homogenizing buffer	250 mM sucrose,	Sigma-Aldrich
	1 mM EDTA	Sigma-Aldrich
	1% protease inhibitor cocktail from	Sigma-Aldrich
	Homogenizer	
Protein concentration	Bio-Rad DC kit	Bio-Rad
	BSA	Sigma-Aldrich
Electrophoresis	SeeBlue® Pre-stained standard	Invitrogen
	Electrophoresis apparatus and a power supply	

Table 20 (continued). Materials for immunobloting.

Reagents and Equipments		Sources
Electrophoresis (continue)	NuPAGE® Novex Bis-Tris (4-12%) Pre-Cast Gels	Invitrogen
	NuPAGE® LDS Sample Buffer	Invitrogen
	NuPAGE® Reducing Agent	Invitrogen
	NuPAGE® MOPS-SDS Running Buffer	Invitrogen
	NuPAGE® Transfer Buffer	Invitrogen
Membrane transfer	PVDF membrane	Invitrogen
	Methanol	Fisher Scientific
	Filter paper	Invitrogen
	Skim milk	Sigma-Aldrich
	Blotting apparatus and a power supply	
Immunostaining	PBS	UCSF cell culture facility
	PBS-T (PBS plus 1% tween-20)	
	Tween-20	Sigma-Aldrich
	Anti-cmyc antibody	Roche
	HRP-conjugated anti-rabbit IgG	Cell Signaling Technology
	ECL Plus™ Western Blotting Detection	Amersham
	Hyperfilm^{TM}	Amersham

Method

1. The FRT cells were cultured with and without cmyc-tagged human V_2R expression in a 6-well plate till confluence. Both types of the FRT cells were processed

separately.

2. After being washed twice with ice-cold PBS, 0.5 ml of the ice-cold homogenizing buffer was added to the cells, and the cells were scraped with a cell scraper.

3. After the homogenized buffer containing the cell suspension was transferred to a micro-centrifuge tube placed on ice, it was homogenized with a small hand-held homogenizer for 3 minutes.

4. After the homogenate was centrifuged at 5,000g for 10 minutes at 4°C, the supernatant was collected which was to be assayed for protein concentration using a Bio-Rad DC kit.

5. Several concentrations of BSA (2, 1, 0.5, and 0.25 mg/ml) with homogenizing buffer to be used as a standard for the protein concentration assay were prepared.

6. After 20 μl of each of the samples in number 4, the standards in number 5, and the homogenizing buffer was pipetted into each clean disposable plastic cuvette, 200 μl of solution A was added to each cuvette and mixed thoroughly, 800 μl of solution B was in a similar manner added and mixed thoroughly, and each was let stand for 10 minutes.

7. Using the cuvette containing the homogenizing buffer as a blank, the absorbance was measured at 595 nm, and the sample protein concentrations were calculated from the standard curve constructed from the absorbance of BSA.

8. Preparation for gel electrophoresis.

    8.1 The samples were denatured by mixing 20 μg of the samples with the other reagents shown below, and then they were heated in the boiling water for 5 minutes.

Reagents	Voulume (μl)
Sample	X (20 ug)
NuPAGE® LDS Sample buffer (4X)	2.5
NuPAGE® Reducing Agent (10X)	1.0
Deionized water	6.5
Total volume	10.0

    8.2 The SeeBlue® Pre-stained standard was ready for use and did not need any

denaturing step.

8.3   The NuPAGE® MOPS running buffer was prepared by mixing 50 ml of the 20X buffer to 950 ml of de-ionized water.

8.4   The NuPAGE® Novex Bis-Tris pre-cast gels were unpacked, the comb was removed in one stroke, the wells were washed twice with the running buffer, and the tape was peeled off from the bottom of the plastic cassette.

8.5   The gel with its cassette was fixed to an electrophoresis apparatus, and the running buffer was poured until the wells were completely below the liquid surface.

9. Five micro-litres of the SeeBlue® pre-stained standard and 10 μl of the samples were loaded to the gel, and the electrophoresis was run at 200 Volts, 100mA for 50 minutes. Upon completion of the electrophoresis, the gel was left in the apparatus until preparation for the membrane transfer was completed in order to prevent the gel from drying.

10. Preparation for a membrane transfer.

10.1   The NuPAGE® transfer buffer was prepared by mixing 50 ml of the 20X buffer with 100 ml of methanol and 850 ml of de-ionized water.

10.2   A gel sized PVDF membrane was excised, soaked in methanol for 30 seconds, washed with deionized water, and soaked together with two pieces of the filter paper in the transfer buffer.

11. Bring The gel from the electrophoresis apparatus was brought, liberated from the plastic cassette by insertion of the gel blade in between the cassette plates, and the blade was moved in a perpendicular fashion to the plates. This process was repeated with all four sides of the cassette until the top plate could be removed from the gel.

12. One piece of the soaked filter paper was placed on the exposed side of the gel, getting rid of all the bubbles. The gel was removed from the remaining plates, and the pre-soaked PVDF membrane was placed on top of the newly exposed gel surface, again all the forming bubbles were to be expelled.

13. Another piece of the soaked filter paper was placed on top of the PVDF membrane, the whole stack was placed in between two pieces of a thin sponge, the assembly was placed in a cassette that came with the blotting apparatus, and

the cassette was fitted into a blotting tank.

14. The transferring buffer was poured until the assembly was completely under the liquid surface, the electrodes were connected making sure that the cathode (+) was on the PVDF membrane side while the anode (-) was on the gel side, the power supply of 30 volts and 100 mA was turned on, and run for 6 hours.

15. The PVDF membrane was disassembled from the transferring apparatus, and the presence of the color band on the PVDF membrane indicated a successful protein transfer.

16. Staining the PVDF membrane with the anti-cmyc antibody.

    16.1 The excess part of the membrane, which did not contain the transferred protein, was excised in order to minimize the amount of the antibody used on the membrane.

    16.2 The membrane was blocked overnight in the PBS containing 5% skimmed milk at $4^{o}C$

    16.3 The membrane from 16.2 was washed for 10 minutes, three times with PBS-T on a shaker.

    16.4 The anti-cmyc antibody was diluted with the PBS-T containing 1% BSA (1:1000) and incubated the dilution with the membrane using the least possible volume at the room temperature for 2 hours.

    16.5 The membrane from 16.5 was washed for 10 minutes, three times with PBS-T on a shaker.

    16.6 The membrane was incubated with HRP-conjugated anti-rabbit IgG diluted to 1:500 in PBS-T containing 1% BSA for 1 hour at the room temperature.

    16.7 The membrane was washed for 10 minutes, three times with PBS-T on a shaker.

    16.8 An ECL Plus™ Western Blotting Detection Kit was brought to the room temperature, 2ml of the solution of A:B in 40:1 mix was prepared and added to the membrane, and the resulting mixture was incubated in the dark for 5 minutes.

    16.9 To prevent air drying, both sides of the membrane were covered with a plastic wrap. The covered membrane was taped to a film box, and in the

dark the film was exposed to the membrane for 1 minute. Then the film was developed.

APPENDIX G
CELL CULTURE FOR HTS

A large-scale cell culture with 175-cm^3 flasks and the automated cell dispenser ensured a sufficient cell supply for HTS. One round of HTS utilized twenty 96-well plates, 6,400 test compounds, and approximately 10 hours to finish. To reduce the operating costs, the cell culture medium used for HTS cell-preparation purpose contained no antibiotic selection (Zeocin, Geneticin, and Hygromycin). However, the cells were to be grown in a selective environment once every month in order to maintain the transgene expression.

Materials

Table 21. Materials for HTS cell culture.

Reagents and Equipments	Sources
The FRT cells expressing human wild type V$_2$R, CFTR, and YFP-H148Q/I152L	
FRT cell medium	
0.05% Trypsin with 0.5mM EDTA	UCSF cell culture facility
PBS	UCSF cell culture facility
CMF-PBS	UCSF cell culture facility
175 cm^2 cell culture flasks	Corning-Costar
50 ml centrifuge tubes	Corning-Costar
LabSystems Multidrop Dispenser	ThermoLabsystems
Clear-bottom black twenty 96 well plates	Corning-Costar

Method

1. The cells were cultured to confluency in four 175-cm^3 cell culture flasks, each with 50 ml. of the cell culture medium.

2. The cells were washed once with CMF-PBS.

3. For each of the flasks, the cells were trypsinized with 10 ml of trypsin, and incubated it at 37^oC for 15 minutes in a CO_2 incubator

4. When all of the cells detached, all of the cell suspensions were combined into one 50-ml centrifuge tube, centrifuged at 5,000g for 10 minutes, and the resulting pellets were collected.

5. Five milli-litres of the fresh growth culture medium was added to the pellets, and they were mixed together thoroughly by pipetting.

6. The cell suspensions of 1ml were transferred to each of the four new 50-ml centrifuge tubes. The remaining 1 ml of the cell suspensions was further passaged into another set of four 175-cm^3 flasks supplying the cells for next round of HTS.

7. After 49 ml of the fresh growth medium was added to each of the four centrifuge tubes in number 6, it was mixed thoroughly by tube inversion. Twenty clear-bottom 96-well black plates were unpacked, and the automated cell dispenser was primed with ethanol, followed by PBS, fresh growth medium, and the cell suspension in number 7, respectively.

8. Place a 96-well plate, one at a time, on the cell dispenser and dispense 100 μl of cells per well.

9. The plates were returned to the CO_2 incubator. The cells should be ready for use in the next day.

APPENDIX H
PBS/I⁻ PREPARATION

All of the chemicals, except NaI, were prepared as stock solutions which were subsequently used to mix the PBS/I⁻. The table below showed a recipe for mixing a 250 ml solution.

Table 22. Recipes for 250 ml PBS/I⁻

Chemicals	MW	Stock (M)	250 ml preparation		
			Stock (ml)	Chemical (g)	Final (mM)
NaI	149.88			5.4	144.00
KCl	74.55	1	0.675		2.70
$Na_2H_2PO_4$	142.82	1	0.890		3.55
KH_2PO_4	136.10	1	0.375		1.50
$CaCl_2$	111.00	1	0.238		0.95
$MgCl_2$	95.00	1	0.123		0.49

The PBSI⁻ solution was light sensitive and should be kept away from the light at the room temperature. The pH and the osmolality of the prepared solution were 7.4, and 290-300mOSM, respectively. The $Na_2H_2PO_4$ stock solution required heating in order to be completely dissolved. Sodium- and Potassium-phosphate should be added after $CaCl_2$ to prevent precipitation.

APPENDIX I
SHORT-CIRCUIT CURRENT MEASUREMENT

The transcellular currents were measured in a Ussing chamber system. One unit of the Ussing chamber was composed of two clear glass chambers separated by a layer of specially grown cells, or tissue mucosa. Both chambers contained a solution with different chloride concentrations (Ringer and Half Ringer) in order to establish an electrochemical gradient across the cell layer. By clamping the voltage across the cell layer to zero, the transcellular current was directly related to the cellular chloride conductance. Therefore, the transcellular currents measured in this setting represented the cellular chloride conductance resulting from various treatment conditions.

Materials

Table 23. Materials for short-circuit current measurements in the Ussing chamber system.

Reagents and Equipments		Sources
Cell related	Different types of FRT cells	
	Calu cells	UCSF cell culture facility
	T84 cells	UCSF cell culture facility
	Cell culture media	
	Digital volt meter	MilliQ
	SnapWell filters	Costar 3801

Table 2(continued). Materials for short-circuit current measurements in the Ussing chamber system.

Reagents and Equipments		Sources
Compounds and chemicals	dDAVP	Ferring Pharmaceuticals
	Forskolin	Sigma-Aldrich
	Cholera toxin	Sigma-Aldrich
	E Coli. heat stable toxin	Sigma-Aldrich
	SR-121463B	Sanofi-Aventis
	Isoproterenol	Sigma-Aldrich
	Propanolol	Sigma-Aldrich
Ussing chamber systems	Vertical diffusion chamber	Costar
	DVC-1000 voltage-clamp apparatus	World Precision Instruments
	Current and voltage electrodes	Harvard apparatus
	An O_2 and CO_2 mixture tank	
	Chart 5 software for PC	
	Ringer's and half Ringer's solution	

Method

1. The cells were grown on the Snapwell filters with the media changed everyday until the transcellular resistance $\geq 500 m\Omega$. Since T84 cells grew very slowly, it was recommended to plate a large number of the cells at the beginning.

2. The Ussing chamber apparatus was set up, the chambers were placed on a holder, a dummy membrane (Snapwell filter with no cell) was placed in between the chambers, and the holder was tightened and locked.

3. The current and the voltage electrodes were attached to the chambers. If the electrodes contained air bubbles, more 3M KCl was to be filled before use. For the electrode maintenance, the agarose gel at the electrode tips was kept from drying by storing the tips in 3M KCl solution.

4. The electrodes were correctly connected to the voltage clamp apparatus.

5. Three millilitres of Ringer's and Half Ringer's solutions were added, in one-to-one correspondence, to the chambers facing the basolateral and the apical surfaces of the cells, respectively. For T84 cells, 3ml of Ringer's solution was added to both chambers. The system was checked for any leakage.

6. After the gas valve was opened, bubbles would appear in the chambers. One hundred micro-litres of the glucose stock solution (54 g/l) was added to both chambers.

7. The DVC-1000 voltage-clamp apparatus was turned on, and switched from 'Groud' to 'On'.

8. The voltage and the resistance were adjusted to zero until the values were stabilized (approximately 30 minutes).

9. The DVC-1000 voltage-clamp apparatus was switched back from 'On' to 'Ground', and the dummy membrane was replaced with the cells in number 1. The same chambers were filled again with the Ringer's and the Half Ringer's solutions, and glucose as before.

10. Optional. In case where the apical membrane current (Iap) was measured, 250 μg/ml of Amphotericin B was added to the chamber facing basolateral side of the cell for membrane permeabilization, and twenty minutes should be allowed before starting the experiment. If Isc or the transcellular current was measured, step 10 should be skipped.

11. The computer was turned on, the Chart 5 program was open, the DVC-1000 was switched back to "On", and the current was recorded. The experiment should be started after the current was stabilized.

APPENDIX J

RINGER'S AND HALF RINGER'S SOLUTIONS

All of the chemicals, except NaCl, Na-glutamate, and Na-HEPES, were prepared as stock solutions which were subsequently used to prepare Ringer's and Half Ringer's solutions (pH 7.3 and 290-300 mOsm) as shown in the table below. One hundred microlitres of glucose per 3ml of the solutions (54 g/l) were to be added directly into the vertical chamber when starting the short-circuit current measurement. This was to prevent bacterial overgrowth which woould decrease the shelf-life of the solutions. After being prepared, the solutions should be kept at $4^{o}C$

Table 24. Ringer's solution**.**

Chemicals	MW	Stock (M)	1 L preparation		
			Stock (ml)	Chemical (g)	Final (mM)
NaCl	58.5			7.605	130
KCl	74.55	1	2.7		2.7
KH_2PO_4	136.1	1	1.5		1.5
$CaCl_2$	111	1	1		1
$MgCl_2$	95	1	0.5		0.5
Na-HEPES	260.29			2.603	10

Table 25. Half Ringer's solution**.**

Chemicals	MW	Stock (M)	1 liter preparation		
			Stock (ml)	Chemical (g)	Final (mM)
NaCl	58.5			7.605	65
Na-glutamate	218.1			14.177	65
KCl	74.55	1	2.7		2.7
KH_2PO_4	136.1	1	1.5		1.5
$CaCl_2$	111	1	2		2
$MgCl_2$	95	1	0.5		0.5
Na-HEPES	260.29			2.603	10

APPENDIX K
CYCLIC AMP MEASUREMENT

The intracellular cAMP was measured using a kit from the R&D Systems. It was a simple ELISA where cAMP in the samples was competing against the alkaline phosphatase conjugated cAMP in binding with an anti-cAMP antibody fixed to the bottom of a 96-well plate. In the presence of the alkaline phosphatase conjugated cAMP, addition of the enzyme substrate yielded a product which could be measured by a spectrophotometer at 405nm.

Materials

Table 26. Materials for ELISA-based cAMP measurements.

	Reagents and Equipments	Sources
Cell related	FRT	
	CHO-K1	UCSF cell culture facility
	MDCK	UCSF cell culture facility
	Cell culture media	
	Hank BSS buffer	UCSF cell culture facility
	24 well plates	
Chemicals	dDAVP	Ferring Pharmaceuticals
	SR-121463	Sanofi-Aventis
	Isoproterenol	Sigma-Aldrich
	Propanolol	Sigma-Aldrich
	Forskolin	Sigma-Aldrich
Kit	R&D cAMP kit	R&D
Equipments	Probe sonicator	
	FluoStar Optima	BMG Lab Technologies

Method

1. Samples preparation.

    1.1 The CHO-K1 cells were grown in a 24-well plate. The cells transiently expressing human β_2AR were used 48 hours after the transfection.

    1.2 Each well was washed twice with PBS, and the medium was replaced with the Hank BSS buffer.

    1.3 The cells from 1.2 were treated with compounds to be tested for the indicated period of time.

    1.4 The treatment solutions in 1.3 were replaced with 200µl of the cell lysis buffer provided with the kit (the lysis buffer provided was in 5X concentration, and had to be diluted)

    1.5 Within 10 minutes, if the cells in 1.4 were not lysed sufficiently, each well was sonicated for 10 seconds with a probe-type sonicator set at the lowest strength.

    1.6 The lysate was transferred to 1.5-ml micro-centrifuge tubes, and centrifuged at 9,000 rpm for 10 minutes to remove the debris. The supernatant was collected which could be kept in a -70°C freezer for up to 1 week.

    1.7 If the samples had very low cAMP levels, acetylation of the samples would increase the sensitivity of the assay. Acetylation was done by adding 10 µl of the acetylating reagent (1:2; acetic anhydride: triethylamine) to 200 µl of the samples. Acetylation should be done in the hood because triethylamine possessed a very strong odour. In the situation where the samples had very high cAMP levels, they should be diluted with 1X cell lysis.

2. Preparation of the standard cAMP solutions.

    2.1. Standard cAMP was prepared at 200, 100, 50, 25, 12.5, 6.25, and 3.125 pmol/ml, using a serial dilution method with the cell lysis buffer as a solvent.

    2.2. If the samples were acetylated, cAMP standards were prepared at 50, 25, 12.5, 6.25, 3.125, 1.5 and 0.625 pmol/ml. The standards had to be acetylated as well as the samples.

3. The assay procedure:

    3.1   The assay reagents were brought to the room temperature.

3.2   One hundred micro-litres of the samples and the standards were added to each well of the anti-IgG coated 96-well plate provided with the kit. Then, the samples and the standards were assayed in triplicate.

3.3   One hundred and fifty microlitres of the 1X cell lysis buffer was added to one of the wells for a non-specific binding control.

3.4   One hundred microlitres of the 1x cell lysis buffer was added to one of the wells for a maximal binding control.

3.5   Fifty microlitres of the conjugated cAMP was added to every well.

3.6   Fifty microlitres of the anti-cAMP antibody was added to every well except the non-specific binding control. These mixtures were incubated for 3 hours at the room temperature on the rotator at 300rpm.

3.7   The excess cAMP was washed off with the 1X washing buffer.

3.8   Fifty microlitres of the substrate (a 1:1 mixture of reagents A and B) was added to every well, and they were incubated at the room temperature for 30 minutes. Blue color should start to develop.

3.9   Fifty microlitres of the top solution was added to each well. The color should change to yellow. The samples were measured with a spectrophotometer (FluoStar Optima) at 405nm, and the OD_{450} was corrected with OD_{514}.

4. Calculation.

   The corrected OD_{450} could be converted to cAMP concentrations (pmol/ml) using a standard curve constructed from the standard cAMP.

APPENDIX L
TRIBROMOETHANOL (AVERTIN®)

Materials.

Table 27. Avertin ingredients**.**

Chemicals	Weight/Volume	Sources
2,2,2 Tribromoethanol	2.5 g	Sigma-Aldrich
2-methyl-2-butanol (amylene hydrate, tertiary amyl alcohol)	5 ml	Sigma-Aldrich
distilled water	200 ml	

Method

1. Tribromoethanol of 2.5 g was dissolved in 5 ml of amylene hydrate. This required heating to approximately 40° C and stirring vigorously.
2. Distilled water was added to the final volume of 200 ml, and stirred continuously.
3. The contents from 2 were filtered through a 5-micron Millipore filter for sterilization (optional).
4. The final solution was aliquoted into appropriate containers.
5. The aliquots were refrigerated and protected them from light. The material degraded in to toxic metabolites rapidly in the presence of heat or light. Even refrigerated and wrapped in foil, the material was stable for only about two weeks.

Dosage: Avertin was given by IP injection at a dose of 250 mg/Kg. Induction required only 1-2 minutes and the righting reflex returned in approximately 40-90 minutes.

APPENDIX M

MOUSE INTESTINAL LOOP EXPERIMENTS

The mouse intestinal loop experiment was an in vivo model used to study intestinal fluid secretion or absorption. The mouse intestine was surgically exteriorized. A segment of the intestine was then tied at both ends to form a closed intestinal loop. The compound in question was injected into the loop. Then the intestine loop was returned to the mouse abdominal cavity, and at the indicated time, the mouse was sacrificed, the intestinal loop was excised and quantified for a loop-weight to length ratio.

Animals

Adult CD1 mice weighing between 25-30g were deprived of food for 24 hours, but given 5% dextrose water. The mice were housed in the UCSF animal facility.

Materials

Table 28. Materials for mouse intestinal loop experiment.

Reagents and Equipments	Sources
Avertin	
Surgical set	
Silk suture no. 3	Harvard apparatus
Syringe	BD Bioscience
Gauze	Fisher Scientific
Alchohol pad	Fisher Scientific
Cholera toxin	Sigma-Aldrich
STa	Sigma-Aldrich
Compound	
PBS	UCSF cell culture facility
Heat pad	

Method

1. Avertin was injected (see the appropriate dose in Appendix L) to the mouse intraperitoneally. The mouse was left in the cage for approximately 10 minutes for Avertin to take effects.

2. All four limbs of the mouse were fixed with a plastic tape to the heat pad that was set at an appropriate temperature to keep the mouse warm through out the surgery.

3. After the incision area was shaved and wiped with an alcohol pad, a vertical incision along the midline of the mouse abdomen was made. It was not necessary to employ a strict sterile technique because the mouse would be sacrificed at 6 hours after the surgery.

4. After the intestine was exteriorized, the jejunum was located by tracing for a transition in the intestinal appearance, and three jejunal loops of 10-15 mm in length were made with sutures.

5. PBS, 1 μg/ml of Cholera toxin (CTX) in PBS or 0.1 μg/ml of the E coli heat-stable toxin (STa) in PBS, and the mixture of CTX or Sta and PDE_{act}-04 were injected to the first, second and third loops, respectively. The volume of each injection was 100 μl.

6. The intestine was placed back to the abdominal cavity, the abdominal wall was sutured, and the mouse was left to recover in a cage warmed with a lamp.

7. Six hours later the mouse was sacrificed with an overdose of Avertin, the intestinal loops were excised and weighed, and their lengths were measured.

APPENDIX N

MDCK CYST DEVELOPMENT

The objective of the study was to observe the effects of PDE_{act}-04 on cyst formation in a cellular model of the polycystic kidney disease or MDCK cells, (Li H et.al., 2004). MDCK cells could form cysts or a tubule-like structures provided that the cells were grown in a three dimensional fashion which could be easily created by culturing the cells in matrigel (a mixture of cell culture media and Purecol, a purified collagen). Forskolin was an important inducer of MDCK cyst formation (Li H et.al., 2004). The cells were treated twice daily with forkolin at 1 or 5 μM concentration until small cysts developed, at which t ime PDE_{act}-04 was added and the culture continued for 7 more days. Phase-contrast light micrographs of the cysts were obtained on a confocal microscope at 10X magnification every two days. Cyst growth was quantified using the NIH-Image J software.

Materials.

Table 29. Materials for MDCK cyst development.

Reagents and Equipments	Sources
MDCK cells	UCSF cell culture facility
MDCK culture media (with only 5% FBS)	
Purecol	Inamed Corporation
10X MEM with Earl's salts	Gibco
HEPES buffer	UCSF cell culture facility
NaOH	UCSF cell culture facility

Table 29 (continued). Materials for MDCK cyst development.

Reagents and Equipments	Sources
Forskolin	Sigma-Aldrich
0.05% Trypsin with 0.5mM EDTA	UCSF cell culture facility
CMF-PBS	UCSF cell culture facility
24-well plates	
15 ml centrifuge tube	
Confocal microscope	
Hemocytometer	

Method

1. After the cells were washed twice with CMF-PBS , trypsin was added just enough to cover the culture surface of the flask (approximately 5 mL), and the flask was returned to a CO_2 incubator until all of the cells detached from the flask culture surface (10-15 min).

2. The MDCK cell suspension was transferred to a 15 ml centrifuge tube, centrifuged at 3,000 g for 10 minutes, pellets were collected, and fresh culture media were added to the pellets in order to obtain the cell density of 1 cells/µl.

3. A mixture of the cell culture media and Purecol was prepared according to the table below. The volume presented in the table was intended for the total volume of 13 ml which was tailored for the experiments using all of the wells of a 24-well plate.

Table 30. Matrigel.

Ingredients	Volume (ml)	Final concentration
Ice cold Purecol	9.47	73% V/V
10X MEM	1.3	1X
HEPES (1M)	0.13	10 mM
Penicillin/Streptomycin	0.13	100 units/ml/ 100 µg/ml
NaOH (0.1M)	0.60	5 mM

4. After 300 ml of the cell suspension in number 2 was added to the matrigel in
    number 3, they were mixed gently in order to minimize the bubble formation.

5. The mixture in number 4 was transferred, 500μl/well, to a 24-well plate, and the
    plate was incubated for 2 hours at $37^{o}C$ in a CO_2 incubator until the mixture became
    solid.

6. The forskolin containing the MDCK culture media was added on top of the solid
    gel, and the plate was returned to the CO_2 incubator. The media was changed twice
    daily in order to ensure constant presence of forkolin during the experimental
    period. The progression of cyst development was visualized and photographed
    under a confocal microscope at 10x magnification every two days. Growth of the
    MDCK cysts was followed and quantified individually by measuring their cross
    sectional areas with the NIH-Image J software.

7. After the small cysts developed which was on the forth day after the forkolin
    treatment, PDE_{act}-04 was added together with forkolin for another 7 days. The
    culture media were changed twice daily as usual.

BIBIOGRAPHY

NAME	Miss Buranee Yangthara
DATE OF BIRTH	July 13, 1981
PLACE OF BIRTH	Bangkok, Thailand
INSTITUTION ATTENDED	Mahidol University, 1998:

B.Sc. (Medical Science) with

First Class Honours

Mahidol University, 2002:

Ph.D. (Physiology)

HOME ADDRESS   85 Soi Prachachuen 41

Prachachuen Rd.

Bangsue District

Bangkok 10800, Thailand

Tel. 02 589-5967, 02 951-7883

Email: buraneeyangthara@gmail.com

PUBLICATION:

Yangthara, B., Mills, A., Chatsudthipong, V., Lukmanee, T., and Verkman, A.S. (2007). Small-Molecule Vasopressin-2 Receptor Antagonist Identified by a G-Protein Coupled Receptor " Pathway" Screen. *Mol Pharmacol, 72,* 86-94.